



401 N. Lindbergh Blvd.
St. Louis, MO 63141
Tel.: 314.993.1700, #546
Toll Free: 800.424.2841, #546
Fax: 800.708.1364
Cell: 314.283.1983

Send via email to: jbode@aaortho.org and cyoung@aaortho.org

AAO Foundation Final Report Form (a/o 6/30/2019)

In an attempt to make things a little easier for the reviewer who will read this report, please consider these two questions before this is sent for review:

- Is this an example of your very best work, in that it provides sufficient explanation and justification, and is something otherwise worthy of publication? (We do publish the Final Report on our website, so this does need to be complete and polished.)*
- Does this Final Report provide the level of detail, etc. that you would expect, if you were the reviewer?*

Please prepare a report that addresses the following:

Type of Award Orthodontic Faculty Development Fellowship Award

Name(s) of Principal Investigator(s)

Institution

Title of Project

Period of AAOF Support (e.g. 07-01-20 to 06-30-21):

Amount of Funding

Summary/Abstract

Detailed results and inferences:

1. If the work has been published please attach a pdf of manuscript OR
2. Describe in detail the results of your study. The intent is to share the knowledge you have generated with the AAOF and orthodontic community specifically and other who may benefit from your study. Table, Figures, Statistical Analysis and interpretation of results should be included.

Hyeran Helen Jeon

2019 The Orhan C. Tuncay Teaching Fellowship Award

Summary/Abstract

The objective of this proposal is to support Dr. Hyeran Helen Jeon for her successful academic career development as an Assistant professor in the Department of Orthodontics at the University of Pennsylvania School of Dental Medicine. Dr. Jeon's long-term goal is to become a clinician-scientist in translational research, educator and practicing orthodontist. The AAOF OFDFA has been used mainly for Dr. Jeon's research support, allowing her to produce the preliminary data and present her findings at professional meetings. Dr. Jeon's primary research mentor is Dr. Shuying Yang, the well-established bone biologist and the Associate Professor at the Department of Basic and Translational Sciences at Penn Dental Medicine. In addition, Dr. Dana Graves, the Vice Dean for Scholarship and Research and Director in Doctor of Science in Dentistry (DScD) at Penn Dental Medicine, co-mentors Dr. Jeon's research progress. Dr. Chun-Hsi Chung, the Chauncey M. F. Egel Endowed Chair and Program Director at the Department of Orthodontics at Penn Dental Medicine mentors Dr. Jeon's overall educational, clinical research, teaching and clinical development. With the distinguished mentors' guidance, this AAOF OFDFA grant has been essential in Dr. Jeon's academic career.

AAOF OFDFA supports mainly those two research projects as below.

1. The Effect of Intraflagellar Transport Protein IFT80 in Mesenchymal Stem Cells during Maxillary Expansion: I established the mouse maxillary expansion model and generated the experimental transgenic mice. Based on the preliminary data, I submitted the grant proposal for the NIH/NIDCR R03 this month, June 2021.
2. The Role of NF- κ B in Osteoblast lineage cells and Periodontal ligament fibroblasts during Orthodontic tooth movement: We published this study in the Angle Orthodontist last April 2021. In addition, my student (Min Kyung Shin) presented our study at the 2021 Penn Dental Medicine (PDM) Research Day and got an award for the PDM AADR Travel Award. In addition, she participates in the 2021 IADR/AADR/CADR Hatton Competition and IADR Innovation Award for Excellence in Orthodontics Research as one of the finalists.

Detailed results and inferences:

1. If the work has been published, please attach a pdf of manuscript.
 - i. **Hyeran Helen Jeon***, Hellen Teixeira, Andrew Tsai. Mechanistic Insight Into Orthodontic Tooth Movement Based on Animal Studies. J Clin Med. 2021 Apr 16;10(8):1733. PMID: 33923725. *AAOF support was acknowledged*
 - ii. **Hyeran Helen Jeon***, Chia-Ying Yang*, Min Kyung Shin, Jingyi Wang, Juhin Hiren Patel, Chun-Hsi Chung, Dana T. Graves. Osteoblast lineage cells and periodontal ligament fibroblasts regulate orthodontic tooth movement that is dependent on Nuclear Factor-kappa B (NF- κ B) activation. Angle Orthod. 2021 Apr 14. doi: 10.2319/031520-182.1. Online ahead of print. PMID: 33852725. *AAOF support was acknowledged*
 - iii. **Hyeran Helen Jeon***, Quan Yu*, Lukasz Witek*, Yongjian Lu, Tianshou Zhang, Olga Stepanchenko, Victoria Jeyoun Son, Evelyn Spencer, Temitope Oshilaja, Min Kyung Shin, Faizan Alawi, Paulo G. Coelho, Dana T. Graves. Clinical application of a FOXO1 inhibitor improves connective tissue healing in the diabetic minipig model. Am J Transl Res. 2021; 13(2): 781–791. PMID: 33594326
 - iv. Cassie Truong*, **Hyeran Helen Jeon* (Co-First author)**, Puttipong Sripinun, Ann Tierney, Normand S. Boucher. Short- and long-term effect of rapid maxillary expansion on the nasal soft and hard tissue: A CBCT study. Angle Orthod. 2021 Jan 1;91(1):46-53. PMID: 33289784. *AAOF support was acknowledged*

Hyeran Helen Jeon

2019 The Orhan C. Tuncay Teaching Fellowship Award

Respond to the following questions:

1. Were the original, specific aims of the proposal realized? YES

i. Educational Plan

As I proposed, I attended the 2020 AAO Winter Conference in Austin, TX (in person) and the 2020 and 2021 AAO Annual Session (virtual). In addition, I plan to attend the 2021 Angle East Annual Meeting this September in New Hampshire. I also have participated in the Penn Faculty Pathways Program, which is designed to enhance the personal and professional development of faculty members in STEMM (Science, Technology, Engineering, Math & Medicine) fields in the first phase of their careers at Penn for the last two years. I have the Mentoring Committee of the renowned clinician-scientists and educators at Penn and have met with them every semester. I have taught both predoctoral and postdoctoral courses. I led the monthly orthognathic surgery seminars with the oral surgery department and attended the weekly orthodontics case presentation seminars, TMJ lecture series (bimonthly), and continuing education (CE) courses at PDM. Lastly, I completed the Program for Advanced Standing Students (PASS)-faculty program at Penn and got my DMD degree last May 2021.

ii. Research Plan

For the last two years, I have published four papers and submitted one paper. Currently I am actively working on two manuscripts. Most importantly, I could submit my first grant proposal for NIH/NIDCR R03 this month, based on the preliminary data with strong support from the AAOF OFDFA.

2. Were the results published?

a. If so, cite reference/s for publication/s including titles, dates, author or co-authors, journal, issue and page numbers

- i. **Hyeran Helen Jeon***, Hellen Teixeira, Andrew Tsai. Mechanistic Insight Into Orthodontic Tooth Movement Based on Animal Studies. *J Clin Med.* 2021 Apr 16;10(8):1733. PMID: 33923725. *AAOF support was acknowledged*
- ii. **Hyeran Helen Jeon***, Chia-Ying Yang*, Min Kyung Shin, Jingyi Wang, Juhin Hiren Patel, Chun-Hsi Chung, Dana T. Graves. Osteoblast lineage cells and periodontal ligament fibroblasts regulate orthodontic tooth movement that is dependent on Nuclear Factor-kappa B (NF-kB) activation. *Angle Orthod.* 2021 Apr 14. doi: 10.2319/031520-182.1. Online ahead of print. PMID: 33852725. *AAOF support was acknowledged*
- iii. **Hyeran Helen Jeon***, Quan Yu*, Lukasz Witek*, Yongjian Lu, Tianshou Zhang, Olga Stepanchenko, Victoria Jeyoun Son, Evelyn Spencer, Temitope Oshilaja, Min Kyung Shin, Faizan Alawi, Paulo G. Coelho, Dana T. Graves. Clinical application of a FOXO1 inhibitor improves connective tissue healing in the diabetic minipig model. *Am J Transl Res.* 2021; 13(2): 781–791. PMID: 33594326
- iv. Cassie Truong*, **Hyeran Helen Jeon* (Co-First author)**, Puttipong Sripinun, Ann Tierney, Normand S. Boucher. Short- and long-term effect of rapid maxillary expansion on the nasal soft and hard tissue: A CBCT study. *Angle Orthod.* 2021 Jan 1;91(1):46-53. PMID: 33289784. *AAOF support was acknowledged*

b. Was AAOF support acknowledged? YES

Hyeran Helen Jeon

2019 The Orhan C. Tuncay Teaching Fellowship Award

c. If not, are there plans to publish? If not, why not?

- Based on the preliminary data, I submitted my proposal for the R03 as a PI this month. I plan to submit at least two publications from this study. One will be submitted for publication by early 2022 and AAOF support will be acknowledged in the manuscripts.

3. Have the results of this proposal been presented?

a. If so, list titles, author or co-authors of these presentation/s, year and locations

- Hyeran Helen Jeon***. Mechanistic Insight Into Orthodontic Tooth Movement Based on Animal Studies (Oral presentation). Penn Dental Medicine (PDM) Crosstalk, 2021
- Hyeran Helen Jeon, Chia-Ying Yang, **Min Kyung Shin (PRESENTER)**, Jingyi Wang, Juhin Hiren Patel, Chun-Hsi Chung, Dana T. Graves. Osteoblast lineage cells and periodontal ligament fibroblasts regulate orthodontic tooth movement that is dependent on Nuclear Factor-kappa B (NF-kB) activation. *2021 PDM Research Day [PDM AADR Travel Award Recipient] and 2021 IADR/AADR/CADR [Hatton Competitor and IADR Innovation Award for Excellence in Orthodontics Research Finalists]*

b. Was AAOF support acknowledged? YES

c. If not, are there plans to do so? If not, why not?

4. To what extent have you used, or how do you intend to use, AAOF funding to further your career?

This AAOF OFDFA funding has been used entirely for Dr. Jeon's research support, allowing her to produce the preliminary data for extramural grant proposals and present her findings at professional meetings. This generous funding from the AAOF has greatly helped Dr. Jeon's academic and scientific growth.

Accounting for Project;

All of the funding has been used for this proposal.

Review

Mechanistic Insight into Orthodontic Tooth Movement Based on Animal Studies: A Critical Review

Hyeran Helen Jeon * , Hellen Teixeira and Andrew Tsai

Department of Orthodontics, School of Dental Medicine, University of Pennsylvania, 240 South 40th Street, Philadelphia, PA 19104-6030, USA; hellen@dental.upenn.edu (H.T.); andrewts@dental.upenn.edu (A.T.)

* Correspondence: hjeon@upenn.edu; Tel.: +1-215-898-5792

Abstract: Alveolar bone remodeling in orthodontic tooth movement (OTM) is a highly regulated process that coordinates bone resorption by osteoclasts and new bone formation by osteoblasts. Mechanisms involved in OTM include mechano-sensing, sterile inflammation-mediated osteoclastogenesis on the compression side and tensile force-induced osteogenesis on the tension side. Several intracellular signaling pathways and mechanosensors including the cilia and ion channels transduce mechanical force into biochemical signals that stimulate formation of osteoclasts or osteoblasts. To date, many studies were performed in vitro or using human gingival crevicular fluid samples. Thus, the use of transgenic animals is very helpful in examining a cause and effect relationship. Key cell types that participate in mediating the response to OTM include periodontal ligament fibroblasts, mesenchymal stem cells, osteoblasts, osteocytes, and osteoclasts. Intercellular signals that stimulate cellular processes needed for orthodontic tooth movement include receptor activator of nuclear factor- κ B ligand (RANKL), tumor necrosis factor- α (TNF- α), dickkopf Wnt signaling pathway inhibitor 1 (DKK1), sclerostin, *transforming growth factor* beta (TGF- β), and bone morphogenetic proteins (BMPs). In this review, we critically summarize the current OTM studies using transgenic animal models in order to provide mechanistic insight into the cellular events and the molecular regulation of OTM.

Keywords: orthodontic tooth movement; animal studies; mechanosensing; osteoclastogenesis; osteogenesis



Citation: Jeon, H.H.; Teixeira, H.; Tsai, A. Mechanistic Insight into Orthodontic Tooth Movement Based on Animal Studies: A Critical Review. *J. Clin. Med.* **2021**, *10*, 1733. <https://doi.org/10.3390/jcm10081733>

Academic Editors: Letizia Perillo, Vincenzo Grassia and Fabrizia d'Apuzzo

Received: 9 March 2021

Accepted: 13 April 2021

Published: 16 April 2021

Publisher's Note: MDPI stays neutral with regard to jurisdictional claims in published maps and institutional affiliations.



Copyright: © 2021 by the authors. Licensee MDPI, Basel, Switzerland. This article is an open access article distributed under the terms and conditions of the Creative Commons Attribution (CC BY) license (<https://creativecommons.org/licenses/by/4.0/>).

1. Introduction

Alveolar bone remodeling in orthodontic tooth movement (OTM) requires the coordinated action of different cell types, including periodontal ligament (PDL) fibroblasts, mesenchymal stem cells, inflammatory cells, osteoblasts, osteocytes, and osteoclasts. Generally, OTM is composed of three stages on the compression side; (i) a gradual compression of the PDL, which may last from about 4–7 days, (ii) the hyalinization period, when cell death due to lack of blood supply in the compressed area of the PDL occurs, which may last from 7–14 days or more, and (iii) the secondary period, which is characterized by direct bone resorption so that the tooth will continue to move [1–3]. On the tension side, the PDL is stretched and blood flow is activated, stimulating osteoblastic activity and osteoid deposition and mineralization. On mechanical force loading, cells around the tooth sense either compression or tension and release multiple cytokines and growth factors that stimulate subsequent biological responses. The process by which cells transmit mechanical forces and generate biological responses is essential for bone remodeling in OTM [4].

On the compression side, multinucleated osteoclasts initiate bone resorption to allow tooth movement to occur in the direction of the applied force, which is a rate limiting step in OTM. In addition, a sterile inflammatory response is induced by the generation of proinflammatory cytokines such as tissue necrosis factor (TNF), interleukin-1 (IL-1), prostaglandins, and IL-6, along with matrix metalloproteinases (MMPs) within a short time after the application of pressure [5–10]. The response to mechanical stress induces transitory inflammation that is pathogen-free. In addition, prostaglandins are secreted when cells are mechanically deformed and focal adhesion kinase, the mechanosensor in PDL cells,

is known to be related with this process [11]. Therefore, both sterile inflammation and mechano-transduction are important for OTM [12]. Cells experiencing compressive forces induce osteoclastogenesis through up-regulation of receptor activator of nuclear factor kappa-B ligand (RANKL) [13]. Proinflammatory cytokines induce RANKL expression to stimulate osteoclastogenesis, further contributing to bone resorption in OTM [14]. On the tension side, PDL cells are stretched and proliferate with increased PDL width, followed by new bone formation, eventually returning to a normal PDL width [15]. Progenitor cells in the PDL and alveolar bone proliferate and differentiate into osteoblasts to produce new bone. The osteogenic transcription factor Runx2 and bone matrix proteins osteocalcin and osteopontin are significantly up-regulated by tension forces [7]. The mechano-response, osteoclastogenesis and osteogenesis are important components of OTM as they represent simultaneous bone remodeling processes in response to mechanical loading.

Human studies examining changes induced by orthodontic forces have frequently examined gingival crevicular fluid after orthodontic force loading. While important, these studies do not establish the cause and effect relationships. Transgenic mouse models are ideal in delineating the molecular actions of specific genes, as they facilitate lineage-specific gene deletion to well-defined cell types [16]. In addition, inducible transgenic mice models are available, allowing the induction of a transgene or the deletion of an endogenous gene in a time- and tissue-specific manner to address limitations of global constitutive germ-line deletion [17].

In this review, we focus on the roles of various mechanosensory cells, cytokine expression and signaling pathways in OTM that have been identified by animal models and summarize the possible cellular mechanosensors. A better understanding of the cellular processes in OTM may one day benefit our patients by expediting tooth movement, preventing relapse and improving treatment stability through the modification of specific genes which are critical for the orthodontic bone remodeling.

2. Cytokines, Mechanosensory Cells, and Intracellular Signaling Pathways in OTM

2.1. Cytokines in OTM

2.1.1. RANKL

RANKL is a member of the TNF cytokine family and is critical for osteoclastogenesis [18]. During OTM, RANKL is highly expressed in periodontal tissue on the compression and tension side [13,19]. Numerous cell types in OTM have been shown to express RANKL including PDL fibroblasts, mesenchymal stem cells, lymphocytes, osteoblasts, and osteocytes, particularly in response to inflammatory cytokines [9,13,20–22].

Human gingival crevicular fluid (GCF) samples have been used for cytokine analysis during OTM as it is non-invasive and convenient. Human GCF isolated from the tooth 24 h after orthodontic forces application, the early phase of OTM, had shown a significant increase in the levels of RANKL, IL-1 β , IL-6, and TNF- α , while the levels of osteoprotegerin (OPG) had remained significantly lower when compared to the control teeth [7,23–25]. Furthermore, Garlet et al. examined the cytokine expression on the PDL of extracted human teeth after OTM [7]. After 7 days of OTM, teeth were extracted and PDL cells on both compression and tension sides were collected for real-time PCR analysis. On the compression side, tumor necrosis factor alpha (TNF- α), RANKL, and matrix metalloproteinases (MMPs) were highly expressed. On the tension side, IL-10, tissue inhibitors of metalloproteinase 1 (TIMP-1), type I collagen, OPG, and osteocalcin were highly expressed. The same author tested chemokine expression on the extracted teeth after OTM and found that the compression side exhibited higher expression of monocyte chemoattractant protein-1 (MCP-1/CCL2), macrophage inflammatory protein-1 α (MIP-1 α /CCL3) and RANKL, which predominate bone resorption activity, while the tension side presented higher expression of osteocalcin.

Consistent with human studies, animal models demonstrated bone resorption activity with proinflammatory cytokines and osteoclastic markers on the compression side and bone formation activity with the osteogenic markers on the tension side. To further

apply the findings to clinical orthodontics, several animal studies have examined the modulation of RANKL to accelerate OTM [26–28]. Injection of RANKL during OTM increases osteoclastogenesis and the rate of tooth movement [26]. Indeed, the rate of OTM is increased by 130% with RANKL injection [28]. Local RANKL gene transfer in animals with OTM increases RANKL protein expression and osteoclastogenesis without any systemic effects, accelerating the amount of tooth movement [27]. The authors proposed that local RANKL gene transfer might be a useful tool to accelerate orthodontic tooth movement, even the ankylosed teeth. Conversely, daily local RANKL antibody injection reduces the rate OTM by 70% [22]. In a comparison of RANKL gene transduction compared to periodontal accelerated osteogenic orthodontics, gene transduction led to more prolonged osteoclastogenesis and a greater rate of tooth movement during OTM [29].

In vitro compressive force causes an increase of RANKL expression and a decrease of OPG expression in human PDL cells, consistent with the human GCF and animal studies results. PDL fibroblasts are distorted under compressive force and express higher amounts of RANKL, TNF- α , MMPs, IL-1 β and prostaglandins on the compression side [30]. Experimental compressive forces on the PDL resulted in a 16.7-fold increase in RANKL secretion and a 2.9-fold decrease in OPG secretion when compared to the control [23].

Taken together, studies with RANKL indicate that this cytokine is a central pro-osteoclastogenic factor that is expressed in response to mechanical forces. Interestingly, RANKL is also expressed on the tension side [19]. Thus, early induction of RANKL and osteoclastogenesis in response to tension may initiate a formation of bone remodeling that leads to increased bone formation on the tension side. This concept warrants further investigation.

2.1.2. Sclerostin

Sclerostin, encoded by the SOST gene and is primarily produced by mature osteocytes in response to OTM, promotes bone resorption and inhibits new bone formation [31,32]. Sclerostin stimulates RANKL expression by osteocytes, negatively regulates expression of BMP proteins and prevents canonical Wnt signaling [33,34]. Sclerostin expression is initially induced on the compression side in OTM models and gradually diminishes after 5–7 days, demonstrating their effect in the early phase of OTM [31,35]. During OTM, sclerostin KO mice have a 20% reduction in osteoclasts and reduced RANKL expression on the compression side with a reduced rate of tooth movement [35]. Local injection of sclerostin on the compression side doubles RANKL expression, reduces OPG expression by 30%, increases osteoclastogenesis by 150% and accelerates tooth movement [36]. In addition, in vitro studies showed that rhSCL-supplement enhanced the expression of RANKL and the RANKL/OPG ratio in osteocytes, supporting the in vivo finding. In addition, the intensity of sclerostin expression is closely related with the force magnitude [37]. On the tension side, sclerostin expression is immediately decreased and maintained at low levels during OTM, negating their negative effect on new bone formation [31]. These studies suggest that sclerostin can be a key factor in OTM by regulating both bone resorption and formation.

2.1.3. Bone Morphogenetic Proteins (BMPs)

It is well known that BMPs induce new bone formation and that the expression of BMPs increases on the tension side during OTM, stimulating the differentiation of mesenchymal stem cells to osteoblasts [30,38]. Noggin, an inhibitor of several bone morphogenetic proteins (BMPs), prevents mechanical force-induced osteoblast differentiation. BMP-3 expression is gradually increased on the tension side until 14 days in rodent models of OTM, the mid-stage in OTM [39]. One study examined the effect of BMP2 injection on tension side and found that local injection of BMP-2 on the tension side did not accelerate OTM, indicating that new bone formation per se is not a rate limiting step in OTM [40].

2.1.4. Transforming Growth Factor (TGF)- β

TGF- β signaling is involved in many cellular processes, including cell migration, proliferation, differentiation, and cellular homeostasis [41]. A previous study with extracted human teeth after OTM showed that TGF- β expression was similarly increased in both the compression and tension sides [7]. In OTM, its role on the compression side is complex as TGF- β has both positive and negative effects on osteoclastogenesis [42]. In some studies, TGF- β has been reported to inhibit osteoclastic activity. However, other studies found that TGF- β actually induces bone resorption, depending on the cell types involved, TGF- β concentration, and inducing mechanism [42,43]. Its expression on the tension side is significantly greater than that on the compression side [7,44–46]. TGF- β is generally known for its anabolic activity, regulating osteoblast differentiation from progenitors on the tension side [47]. Pretreatment with a TGF- β receptor inhibitor inhibits mechanical force-induced bone mineralization in vitro, suggesting that TGF- β could play a role in osteogenesis in response to tension forces during OTM.

Combining all, the findings from the animal studies could be the base foundation for the studies to expedite the OTM in humans. For example, RANKL or sclerostin can be given on the compression side to accelerate the osteoclastogenesis or BMPs can be given on the tension side to support the new bone formation. As previously mentioned, the new bone formation itself on the tension side cannot make the tooth movement faster while their effects are more important in the late phase in OTM. Therefore, many studies to speed up the velocity of OTM have been focused on the osteoclastogenic markers on the compression side.

2.2. The Mechanosensory Cells in OTM

PDL cells, osteocytes, and osteoblasts are the principal mechanosensory cells that produce various cytokines to regulate alveolar bone remodeling in OTM, by converting mechanical force into intracellular signals [48–51] (Figure 1). The role of mechanosensors in these cells during OTM will be reviewed later in this paper.

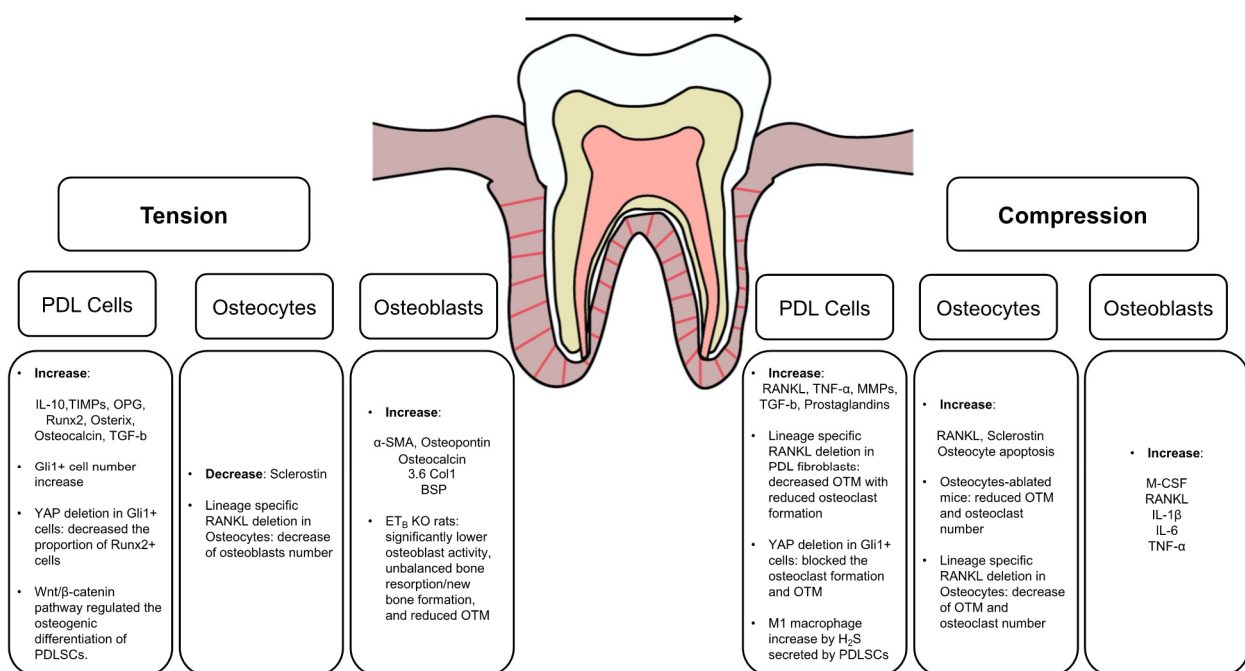


Figure 1. Cytokines and Mechanosensory cells in OTM.

2.2.1. Periodontal Ligament Cells

Periodontal Ligament Fibroblasts

The periodontal ligament (PDL) is a fibrous tissue that connects teeth with alveolar bone and transmits mechanical stimuli [52]. The PDL comprises of heterogeneous cell types including fibroblasts, progenitor cells, bone-lining cells, osteoclasts, endothelial cells, nerve cells and others [53]. PDL fibroblasts constitute 50–60% of the total PDL cellularity and contribute to bone resorption in OTM as a main source of RANKL [21]. Interestingly, PDL fibroblasts have some characteristics similar to those of osteoblasts, expressing a 2.3 kb regulatory unit of Col1 α 1 promoter typical of osteoblasts and osteocytes [54,55] and bone-associated proteins such as alkaline phosphatase [56]. Indeed, PDL fibroblasts are more similar to tendon cells than skin fibroblasts in many respects [30,57].

On the compression side, the experimental mice with RANKL deletion in PDL fibroblasts showed significantly less osteoclast formation with narrower PDL space compared to control mice, leading to severely impaired OTM [21]. In addition, our recent study found that this up-regulation of RANKL depends on NF- κ B activation [58]. NF- κ B inhibition in PDL fibroblasts blocked the OTM with significantly reduced osteoclastogenesis, narrower PDL width, higher bone volume fraction and reduced RANKL expression compared to wild type mice. Both studies support the critical role of PDL fibroblasts via NF- κ B activation in OTM.

Periodontal Ligament Stem Cells

Mesenchymal stem cells reside in the PDL, giving rise to PDL, alveolar bone, and cementum during alveolar bone remodeling. Gli1+ cells have been identified as the multipotent stem cells in adult mouse PDL [59]. Complete removal of Gli1+ cells using the inhibitors or by the genetic ablation significantly reduce OTM by 60% and diminish osteoclast formation by more than 80% [60]. On the tension side, Gli1+ increases its cell number and differentiate into osteoblasts with increased Runx2 expression during OTM [60].

Mesenchymal stem cells reside in the PDL, giving rise to PDL, alveolar bone, and cementum function as mechanosensory cells during OTM [60]. Yes-associated protein (YAP) and the paralogue transcriptional coactivator with PDZ-binding motif (TAZ), the downstream effectors of the Hippo signaling pathway, have been identified as important regulators during mechanotransduction [61]. Recent rodent OTM studies showed that YAP and TAZ expression were up-regulated with nuclear translocation in the PDL cells on both compression and tension side [62,63]. Moreover, YAP and TAZ expression were proportional to the applied orthodontic force. A recent study investigated the role of Gli1+ cells through Yes-associated protein (YAP) activation in mouse OTM models [60]. Lineage-specific deletion of the YAP in Gli1+ cells significantly reduced OTM by 50% with decreased osteoclast formation by more than 80% on compression side. On the tension side, the same transgenic mice with the YAP deletion in Gli1+ cells showed a significantly decreased proportion of Runx2+ cells by more than 80%. In vitro cyclic stretch promoted the osteogenic differentiation of human PDL cells [62]. Moreover, the nuclear translocation of YAP was significantly increased with increased expression of connective tissue growth factor (CTGF) and cysteine-rich angiogenic inducer 61 (CYR61) mRNA, the target gene of YAP. Furthermore, knockdown of YAP suppressed the cyclic stretch induced osteogenesis in human PDL cells, while overexpression of YAP enhanced osteogenesis. Both in vivo and in vitro data support the role of YAP as the mechanical sensor and important regulator of the osteogenic differentiation in PDL cells under tensile force. In addition, the level of tension is important in the osteogenic differentiation as the magnitude of tension differentially regulates osteogenic and osteoclastic process [64]. Tension with a magnitude of 12% could increase osteogenic differentiation and proliferation of mesenchymal stem cells whereas tension above 12% would up-regulate the function of mesenchymal stem cells to regulate osteoclast differentiation, demonstrating the impor-

tance of the light force during OTM especially for the patients with poor bony support such as periodontitis [65,66].

Mechanical force-induced hydrogen sulfide (H₂S), produced by PDL mesenchymal stem cells, supports macrophage polarization toward an inflammatory, M1 phenotype and promotes osteoclast activity in OTM [67,68]. These cells express cystathionine- β -synthase that generates H₂S. Treatment with an inhibitor of H₂S reduces osteoclast formation and OTM by almost half. The generation of M1 macrophages is increased 5.6-fold after orthodontic force loading. An H₂S blocker reduces M1 macrophage formation by 70%, and an H₂S donor enhances it 1.4-fold. This shows that PDL mesenchymal stem cells can increase the expression of M1-macrophages, which are main source of several proinflammatory cytokines such as IL-1 β , IL-6, and TNF- α , leading to the RANKL stimulation.

2.2.2. Osteocytes

Osteocytes are terminally differentiated from osteoblasts and embedded in the bone matrix. They are the most abundant cells in the adult skeleton, comprising 90–95% of all bone cells [12,51]. They are the primary mechanosensory cells in bone and regulate both osteoclast and osteoblast formation and function during mechanical force-induced bone remodeling [69,70]. They have dendritic processes that interact with other osteocytes and bone-lining cells. Mechanical loading stimulates dentin matrix protein 1 (DMP1) expression in osteocytes *in vivo*, which is a key molecule in regulating osteocyte formation, maturation, phosphate regulation and regulating mineralization [71,72]. In addition to RANKL, osteocytes produce sclerostin, M-CSF, OPG, and other cytokines during OTM.

As the early findings in OTM, osteocyte apoptosis peaks at 24 h on the compression side in mouse OTM models, as measured by TUNEL and caspase-3 immunofluorescence stain [73]. Osteoclastogenesis was evident after 72 h and continued to increase up to 7 days. Apoptotic osteocytes were preferentially located close to osteoclasts, suggesting that dying osteocytes produce active signaling to recruit osteoclasts [73–75].

Osteocytes can be also an important source of RANKL in OTM mouse models [22,76,77]. Osteocyte-deleted mice have a 60% reduction in osteoclasts and a 50% reduction in tooth movement compared to normal controls [78]. Under basal conditions osteocyte ablation negatively affects bone quality by increasing intracortical porosity, osteoblastic dysfunction, and adipose tissue proliferation in the marrow space [79]. These mice showed a severe osteopetrotic phenotype due to a lack of osteoclasts. The mice with lineage-specific RANKL deletion in osteocytes decreased OTM by 40% and osteoclast number by 60% compared with WT mice [22]. *In vitro*, osteocytes express a higher amount of RANKL and have a greater capacity to support osteoclastogenesis than osteoblasts and bone marrow stromal cells [77]. Interestingly, the osteoblast number on the tension side was significantly reduced in the same transgenic mice, possibly through a coupling mechanism.

2.2.3. Osteoblasts

Osteoblasts are bone forming cells, accounting for the 4–6% of total bone cells and differentiate from mesenchymal stem cells [80]. Runx2 and osterix are transcription factors that promote osteoblastic differentiation from mesenchymal stem cells. The fate of osteoblasts includes: (1) apoptosis, (2) become bone-lining cells or (3) form osteocytes. Bone-lining cells maintain homeostasis of bone and contain osteoblast progenitors [81]. Osteoblasts are mechanosensory cells and convert the mechanical signals into biological responses, producing various cytokines such as prostaglandin, OPG, RANKL and BMPs [82,83]. In OTM, bone-lining cells and osteoblasts express M-CSF and RANKL and produce other factors that positively influence osteoclastogenesis, including IL-1 β , IL-6 and TNF- α [84–86].

Osteoblast differentiation is an important process on the tension side during OTM. The initial response to OTM on the tension side is a proliferation of osteoblast progenitors that express α -SMA, which peaks at 2 days after initiating OTM while osteoid formation in mice peak at 4 days, the early phase of OTM, represented by osteopontin, osteocalcin,

and bone sialoprotein in mouse OTM models [87,88]. Endothelin B receptors (ET_B) play an important role in alveolar bone modeling in the late stage of OTM in the rat animal model [89]. To examine the role of osteoblasts in OTM, ET_B knockout rats (ET_B-KO) exhibited decreased OTM after 35 days, a late stage in OTM, by 27% compared to the ET_B-WT mice. The alveolar bone volume in the ET_B-KO appliance group was significantly less due to diminished osteoblast activity, but osteoclast volume was not significantly different compared to the ET_B-WT appliance group. In addition, the expression levels of osteocalcin and DMP1, the osteoblast activity markers, were significantly down-regulated by 70% in the ET_B-KO appliance group compared to the ET_B-WT appliance group. However, the expression of cathepsin K, an osteoclast activity marker, did not show any statistical difference. In summary, ET_B knockout rats (ET_B-KO) have significantly lower osteoblast activity, unbalanced bone resorption/new bone formation, and reduced OTM with increased tooth mobility compared with control group, explaining the role of osteoblasts in the late stage of OTM.

Taken together, identifying the roles of each cells during OTM is critical and use of the transgenic mouse with each cell type-specific gene deletion can be a great tool for these studies.

2.3. Intracellular Signaling Pathways Stimulated by Mechanical Force

In OTM, various signaling pathways are activated, which mediate the response of mechanosensory cells that modulate bone resorption and formation. The function of Wnt/ β -Catenin signaling, and Yes-associated protein and transcriptional coactivator with PDZ-binding motif (YAP/TAZ) signaling participate in bone remodeling in tooth movement.

Wnt/ β -catenin signaling is critical for bone homeostasis [49,50]. β -catenin is a transcription factor that is activated by canonical Wnt signaling and translocates to the nucleus in osteoblasts lineage cells subjected to mechanical stimulation [90]. During OTM, Wnt/ β -catenin signaling modulate expression of osteogenesis- and osteoclastogenesis-related factors in response to mechanotransduction [91–93]. Mice with global loss-of-function Lrp5, a Wnt receptor, have low bone mineral density and impaired osteogenic response to mechanical loading [94]. Conversely, mice with gain-of function mutations in the Lrp5 gene have significantly increase bone mineral density and bone mass in response to mechanical forces [95,96]. In OTM, a gain-of-function mutation in Lrp5 decreases orthodontic tooth movement by reducing osteoclast- mediated bone resorption and increasing alveolar bone mass [97]. Consistent with this, constitutive Wnt signaling increases osteogenic gene expression and reduces RANKL expression and osteoclast activity [98]. Conversely, viral transduction of DKK1, a Wnt inhibitor, increases osteoclast activity and reduces osteogenic markers, resulting in increased PDL width [98]. In a rat OTM model, the expression of Wnt3a, Wnt10b, and β -catenin is stronger on the tension side, consistent with Wnt induced bone formation observed under tension. In contrast, Dkk-1 levels are much higher on the compression side, consistent with reduced Wnt signaling and greater bone resorption on the compression side [99].

Yes-associated protein (YAP) and transcriptional coactivator with PDZ-binding motif (TAZ) play a key role in the mechanotransduction process [63,100]. YAP senses extracellular mechanical signals and translocates into nucleus to function as the coactivator of other transcription factors [62]. During OTM, YAP/TAZ signaling is observed in osteoblasts, osteocytes, osteoclasts and PDL fibroblasts and increases proportionally with the degree of orthodontic force [62,63]. Conditional deletion of YAP in PDL mesenchymal stem cells decreases osteoclast formation by 80% on the compression side and reduces tooth movement by half. In vitro cyclic stretch stimulates proliferation of PDL fibroblasts and osteoblast differentiation via YAP activation [62,101]. YAP knockdown suppresses mechanical forced-induced osteogenesis while overexpression of YAP enhances osteogenesis in PDL fibroblasts [62].

3. Possible Mechanosensors

Cells sense their mechanical environment through cell-cell or cell-matrix adhesions during physiologic growth and development and during mechanical loading. Mechanosensing occurs by mechanical force-induced conformational changes in cellular molecules, including force-activated cytoskeleton, integrins, ion channels and cell-cell adhesions, consequently affecting cellular gene expression and its function and regulating orthodontic bone remodeling (Figure 2).

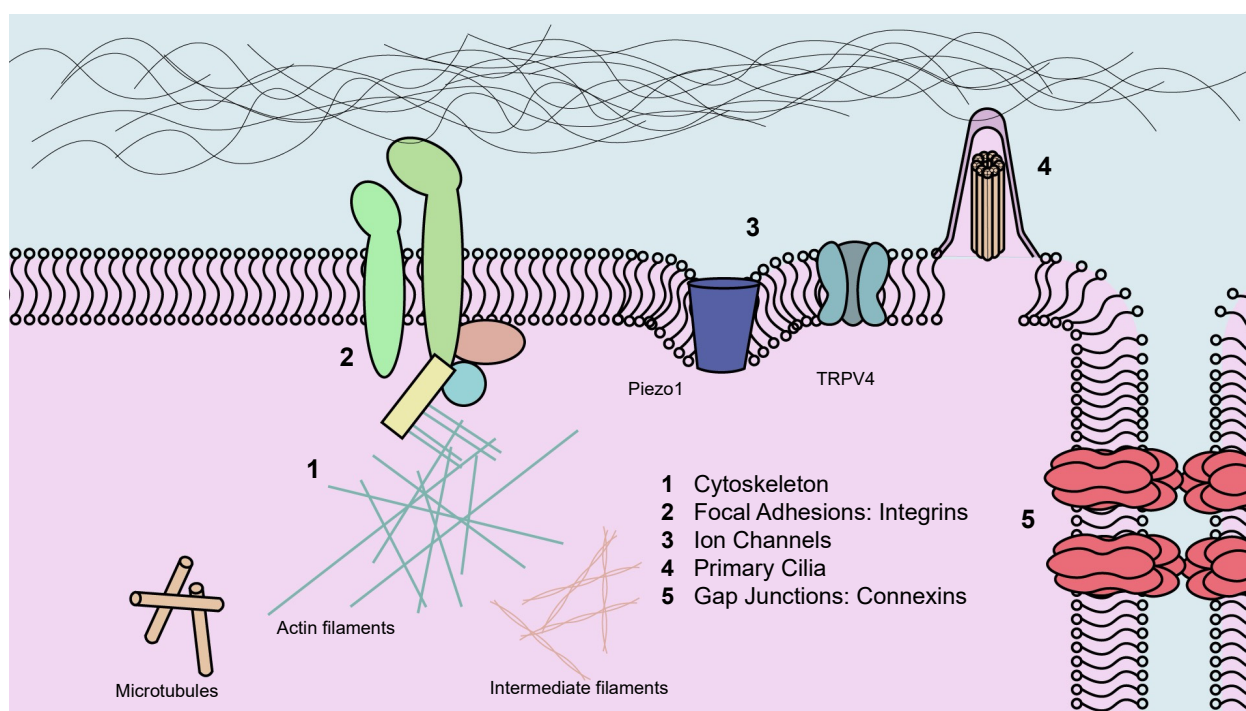


Figure 2. Possible Mechanosensors in Orthodontic Tooth Movement. (1) Cytoskeletons, (2) Focal adhesions: integrins, (3) Ion channels, (4) Primary cilia, and (5) Gap Junctions: connexins. TRPV4: transient receptor potential cation channel subfamily V member 4.

3.1. Cytoskeleton

Cellular cytoskeletons provide structural frameworks for the cell and are largely comprised of microtubules, actin, and intermediate filaments [102]. Cytoskeletons play a role in the response to mechanical force and are responsible for cell motility [103]. For example, cilia and flagella are mainly composed of microtubules and move as a result of microtubules sliding. In OTM, PDL and alveolar bone cells are reconstructed and their cellular cytoskeleton changes stimulate the elaboration of multiple cytokines and growth factors, mediating the cell morphology, differentiation, and proliferation [102,104,105]. On the tension side, cytoskeletal reorganization influences the differentiation of osteoprogenitors to osteoblasts and bone formation, stressing the critical role of cytoskeleton to influence both compression and tension sides during OTM [106].

3.2. Focal Adhesions (FAs)

Focal adhesions are integrin-associated proteins that connect intracellular actin filaments and extracellular matrix proteins [51,107]. Orthodontic force-induced stress on the extracellular matrix can be transmitted to cells through focal adhesions to induce proliferation and differentiation of several cells in the PDL and alveolar bone, leading to the balanced bone remodeling in response to the applied force [104]. Focal adhesions are involved in mechanosensing and downstream signaling through focal adhesion kinase in osteoblasts [108] and osteocytes [109,110]. Gene deletion that results in loss of focal

adhesions in osteoblasts reduce mechanical responses to fluid flow [108]. Mechanical forces through focal adhesion kinases stimulate Wnt/ β -catenin signaling in osteocytes [109].

3.3. Primary Cilia

Primary cilia are non-motile protruding organelles from the cell membrane and are observed in chondrocytes, mesenchymal stem cells, osteoblasts and osteocytes as mechanosensors [111,112]. Changes in fluid flow stimulate numerous cells via primary cilia [113], which may be important in OTM. Blocking primary cilia formation inhibits the expression of osteopontin, prostaglandins and cyclooxygenase-2 in osteoblasts or osteocytes and reduces their response to fluid flow. Tensile forces promote the osteogenic differentiation and proliferation of PDL mesenchymal stem cells via primary cilia that are needed for osteoblast differentiation and bone formation [114]. Lineage-specific deletion of key ciliary proteins including the IFT80, IFT88, Kif3a, Evc and polycystin in osteoblasts or osteoblast precursors leads to cilia loss, impairs osteoblast differentiation, reduces osteoid formation, and inhibits bone mineralization in response to mechanical loading in vivo [114–116]. On this basis, it may have a role in bone formation on tension side during OTM.

A calcium channel complex composed of the polycystin-1 and polycystin-2 is located at the base of primary cilium and mediates the effect of cilia bending [117]. When the primary cilium is bent by dynamic fluid flow, a Ca^{2+} signal is transduced proportional to the degree of distortion. This bending motion opens Ca^{2+} -permeable ion channels and stimulates formation of inositol (1,3,5)-trisphosphate (IP3) that is transmitted through gap junctions, thereby transmitting the ciliary signal to neighboring cells [4,118–120]. Loss of polycystin-1 function in vivo leads to reduced formation of osteoblasts, a reduced anabolic response to mechanical loading and the development of osteopenia [121]. Conditional deletion of polycystin-1 under the control of a regulatory element of the Wnt1 promoter has been used in OTM studies [122]. Conditional polycystin-1 deletion blocks the tooth movement with reduced osteoclast formation on the compression side. This study demonstrates that the calcium channels in primary cilia play an important role in the transduction of mechanical signals to induce bone resorption.

3.4. Gap Junctions: Connexins

Connexins are gap junction proteins that connect two neighboring cells [123,124]. Connexin 43 (Cx43) is the most abundant connexin in bone and modulates bone resorption and formation activity by regulating osteoprotegerin and sclerostin levels [74,125]. During OTM, Cx43 is strongly expressed in osteoclasts and PDL cells on the compression side and in osteoblasts and osteocytes on the tension side in vivo [124]. In vitro studies with PDL fibroblasts report that mechanical tension increases Cx43, up-regulating the expression of Runx2 and osterix, and down-regulating RANKL expression [126]. Suppression of Cx43 reduces the induction of osteogenic markers but promotes RANKL expression [126,127]. Given its function in regulating the response of osteoblasts and osteocytes to mechanical forces, it is reasonable to speculate that connexins play a role in OTM.

3.5. Ion Channels

Ion channels are pore-forming membrane proteins that facilitate direct ion passage through the cell membrane [51]. Mechanical force-activated ion channels increase membrane permeability and trigger the influx of extracellular calcium, demonstrating their role in mechanotransduction in osteocytes and PDL fibroblasts [51,128,129]. Piezo1 ion channel and transient receptor potential cation channel subfamily V member 4 (TRPV4) are key factors in the mechanotransduction of osteocytes and PDL fibroblasts under mechanical loading. Conditional deletion of Piezo1 in osteoblasts and osteocytes significantly reduced bone mass and strength in mice [130]. Conversely, administration of a Piezo1 agonist to adult mice increased bone mass in a way that mimicked the effects of mechanical loading, demonstrating that Piezo1 is a mechanosensitive ion channel by which osteoblast lineage cells sense and respond to changes in mechanical load. In vitro mechanical stimulation

of mature osteocytes activates Piezo1, which rapidly activates Akt and down-regulates sclerostin [131]. Piezo1 and TRPV4 increase their expression 8 h after mechanical loading, followed by the increased expression of M-CSF, RANKL and COX2 [128]. However, pretreatment with the inhibitors of Piezo1 and TRPV4 suppressed the related cytokine expression. Fluid shear stress on osteocytes activates TRPV4 to rapidly increase intracellular Ca^{2+} levels, which activates Ca^{2+} /calmodulin-dependent kinase (CaMK) II and down-regulates sclerostin [132,133]. This is functionally important as shown by in vivo and in vitro studies that conditional deletion of Piezo1 in osteoblasts and osteocytes reduces bone mass and strength [130], while administration of a Piezo1 agonist increases bone mass, mimicking the effects of mechanical loading. It is likely that ion channel proteins are important in OTM.

4. Conclusions

Orthodontic tooth movement is a highly coordinated process in which various cells, cytokines, and complex mechanisms are involved. To date, numbers of OTM studies have been performed, but many are in vitro studies or examined the global deletion of a specific gene or cell type. Transgenic animal studies with the cell type-specific gene deletion can provide the insight into the key cellular and molecular mechanisms in OTM by establishing the cause and effect relationships. Findings from those studies could be applied for our daily orthodontic practice in the future, accelerating osteoclastogenesis and reducing treatment time. Conversely, blocking osteoclastogenesis can be applied to prevent orthodontic relapse. In addition, increasing osteogenesis can greatly help the maxillary expansion procedure, reducing the retention period of 5 to 6 months. The RANKL gene transfer to expedite the OTM is just one example. Furthermore, the findings from the transgenic animal studies can contribute to the development of precision orthodontics in the future so that we can provide patient-specific orthodontic treatment.

One of the limitations of this review is that animal studies that specifically examined mechanosensors are rare and many of them were conducted in vitro. Mechanosensors play a critical role in the mechanotransduction process and further investigation is needed. In addition, several OTM studies used slightly different amount of orthodontic force and time points. The use of standardized OTM methods would greatly help compare the outcomes from multiple animal OTM studies. Lastly, applying the findings from rodent studies to humans does warrant some modification considering the species differences, for example when considering the time periods in OTM.

Author Contributions: Conceptualization, H.H.J.; writing—original draft preparation, H.H.J.; writing—review and editing, H.H.J., H.T. and A.T. All authors have read and agreed to the published version of the manuscript

Funding: This research was supported by the Schoenleber Pilot Grant from the University of Pennsylvania School of Dental Medicine (HHJ) and the Orthodontic Faculty Development Fellowship Award from the American Association of Orthodontists Foundation (HHJ).

Institutional Review Board Statement: Not applicable.

Informed Consent Statement: Not applicable.

Data Availability Statement: Not applicable.

Acknowledgments: We greatly appreciate Dana Graves for his helpful discussion and guidance.

Conflicts of Interest: The authors declare no conflict of interest.

References

1. Reitan, K. Clinical and histologic observations on tooth movement during and after orthodontic treatment. *Am. J. Orthod.* **1967**, *53*, 721–745. [[CrossRef](#)]
2. Profit, W.R.; Fields, H.W.; Larson, B.E.; Sarver, D.M. *Contemporary Orthodontics*, 6th ed.; Mosby: Maryland Heights, MO, USA, 2018.
3. von Bohl, M.; Kuijpers-Jagtman, A.M. Hyalinization during orthodontic tooth movement: A systematic review on tissue reactions. *Eur. J. Orthod.* **2009**, *31*, 30–36. [[CrossRef](#)]

4. Temiyasathit, S.; Jacobs, C.R. Osteocyte primary cilium and its role in bone mechanotransduction. *Ann. N. Y. Acad. Sci.* **2010**, *1192*, 422–428. [[CrossRef](#)]
5. Uematsu, S.; Mogi, M.; Deguchi, T. Interleukin (IL)-1 beta, IL-6, tumor necrosis factor-alpha, epidermal growth factor, and beta 2-microglobulin levels are elevated in gingival crevicular fluid during human orthodontic tooth movement. *J. Dent. Res.* **1996**, *75*, 562–567. [[CrossRef](#)] [[PubMed](#)]
6. Ren, Y.; Hazemeijer, H.; de Haan, B.; Qu, N.; de Vos, P. Cytokine profiles in crevicular fluid during orthodontic tooth movement of short and long durations. *J. Periodontol.* **2007**, *78*, 453–458. [[CrossRef](#)]
7. Garlet, T.P.; Coelho, U.; Silva, J.S.; Garlet, G.P. Cytokine expression pattern in compression and tension sides of the periodontal ligament during orthodontic tooth movement in humans. *Eur. J. Oral Sci.* **2007**, *115*, 355–362. [[CrossRef](#)]
8. Rubartelli, A.; Lotze, M.T.; Latz, E.; Manfredi, A. Mechanisms of sterile inflammation. *Front. Immunol.* **2013**, *4*, 398. [[CrossRef](#)]
9. Klein, Y.; Fleissig, O.; Polak, D.; Barenholz, Y.; Mandelboim, O.; Chaushu, S. Immunorthodontics: In vivo gene expression of orthodontic tooth movement. *Sci. Rep.* **2020**, *10*, 8172. [[CrossRef](#)]
10. Meikle, M.C. The tissue, cellular, and molecular regulation of orthodontic tooth movement: 100 years after Carl Sandstedt. *Eur. J. Orthod.* **2006**, *28*, 221–240. [[CrossRef](#)]
11. Kang, Y.G.; Nam, J.H.; Kim, K.H.; Lee, K.S. FAK pathway regulates PGE(2) production in compressed periodontal ligament cells. *J. Dent. Res.* **2010**, *89*, 1444–1449. [[CrossRef](#)] [[PubMed](#)]
12. Krishnan, V.; Davidovitch, Z. On a path to unfolding the biological mechanisms of orthodontic tooth movement. *J. Dent. Res.* **2009**, *88*, 597–608. [[CrossRef](#)]
13. Yamaguchi, M. RANK/RANKL/OPG during orthodontic tooth movement. *Orthod. Craniofac. Res.* **2009**, *12*, 113–119. [[CrossRef](#)] [[PubMed](#)]
14. Glantschnig, H.; Fisher, J.E.; Wesolowski, G.; Rodan, G.A.; Reszka, A.A. M-CSF, TNFalpha and RANK ligand promote osteoclast survival by signaling through mTOR/S6 kinase. *Cell Death Differ.* **2003**, *10*, 1165–1177. [[CrossRef](#)] [[PubMed](#)]
15. Garlet, T.P.; Coelho, U.; Repeke, C.E.; Silva, J.S.; Cunha Fde, Q.; Garlet, G.P. Differential expression of osteoblast and osteoclast chemoattractants in compression and tension sides during orthodontic movement. *Cytokine* **2008**, *42*, 330–335. [[CrossRef](#)] [[PubMed](#)]
16. Cho, A.; Haruyama, N.; Kulkarni, A.B. Generation of transgenic mice. *Curr. Protoc. Cell Biol.* **2009**, *19*, 11. [[CrossRef](#)]
17. Elefteriou, F.; Yang, X. Genetic mouse models for bone studies—strengths and limitations. *Bone* **2011**, *49*, 1242–1254. [[CrossRef](#)]
18. Kim, T.; Handa, A.; Iida, J.; Yoshida, S. RANKL expression in rat periodontal ligament subjected to a continuous orthodontic force. *Arch. Oral Biol.* **2007**, *52*, 244–250. [[CrossRef](#)] [[PubMed](#)]
19. Otero, L.; Garcia, D.A.; Wilches-Buitrago, L. Expression and Presence of OPG and RANKL mRNA and Protein in Human Periodontal Ligament with Orthodontic Force. *Gene Regul. Syst. Biol.* **2016**, *10*, 15–20. [[CrossRef](#)] [[PubMed](#)]
20. Yan, Y.; Liu, F.; Kou, X.; Liu, D.; Yang, R.; Wang, X.; Song, Y.; He, D.; Gan, Y.; Zhou, Y. T Cells Are Required for Orthodontic Tooth Movement. *J. Dent. Res.* **2015**, *94*, 1463–1470. [[CrossRef](#)]
21. Yang, C.Y.; Jeon, H.H.; Alshabab, A.; Lee, Y.J.; Chung, C.H.; Graves, D.T. RANKL deletion in periodontal ligament and bone lining cells blocks orthodontic tooth movement. *Int. J. Oral Sci.* **2018**, *10*, 3. [[CrossRef](#)]
22. Shoji-Matsunaga, A.; Ono, T.; Hayashi, M.; Takayanagi, H.; Moriyama, K.; Nakashima, T. Osteocyte regulation of orthodontic force-mediated tooth movement via RANKL expression. *Sci. Rep.* **2017**, *7*, 8753. [[CrossRef](#)]
23. Nishijima, Y.; Yamaguchi, M.; Kojima, T.; Aihara, N.; Nakajima, R.; Kasai, K. Levels of RANKL and OPG in gingival crevicular fluid during orthodontic tooth movement and effect of compression force on releases from periodontal ligament cells in vitro. *Orthod. Craniofac. Res.* **2006**, *9*, 63–70. [[CrossRef](#)]
24. Ren, Y.; Vissink, A. Cytokines in crevicular fluid and orthodontic tooth movement. *Eur. J. Oral Sci.* **2008**, *116*, 89–97. [[CrossRef](#)]
25. Meeran, N.A. Biological response at the cellular level within the periodontal ligament on application of orthodontic force—An update. *J. Orthod. Sci.* **2012**, *1*, 2–10. [[CrossRef](#)]
26. Li, C.; Chung, C.J.; Hwang, C.J.; Lee, K.J. Local injection of RANKL facilitates tooth movement and alveolar bone remodelling. *Oral Dis.* **2019**, *25*, 550–560. [[CrossRef](#)] [[PubMed](#)]
27. Kanzaki, H.; Chiba, M.; Arai, K.; Takahashi, I.; Haruyama, N.; Nishimura, M.; Mitani, H. Local RANKL gene transfer to the periodontal tissue accelerates orthodontic tooth movement. *Gene Ther.* **2006**, *13*, 678–685. [[CrossRef](#)] [[PubMed](#)]
28. Chang, J.H.; Chen, P.J.; Arul, M.R.; Dutra, E.H.; Nanda, R.; Kumbar, S.G.; Yadav, S. Injectable RANKL sustained release formulations to accelerate orthodontic tooth movement. *Eur. J. Orthod.* **2020**, *42*, 317–325. [[CrossRef](#)]
29. Iglesias-Linares, A.; Moreno-Fernandez, A.M.; Yanez-Vico, R.; Mendoza-Mendoza, A.; Gonzalez-Moles, M.; Solano-Reina, E. The use of gene therapy vs. corticotomy surgery in accelerating orthodontic tooth movement. *Orthod. Craniofac. Res.* **2011**, *14*, 138–148. [[CrossRef](#)]
30. Li, Y.; Jacox, L.A.; Little, S.H.; Ko, C.C. Orthodontic tooth movement: The biology and clinical implications. *Kaohsiung J. Med. Sci.* **2018**, *34*, 207–214. [[CrossRef](#)] [[PubMed](#)]
31. Odagaki, N.; Ishihara, Y.; Wang, Z.; Ei Hsu Hlaing, E.; Nakamura, M.; Hoshijima, M.; Hayano, S.; Kawanabe, N.; Kamioka, H. Role of Osteocyte-PDL Crosstalk in Tooth Movement via SOST/Sclerostin. *J. Dent. Res.* **2018**, *97*, 1374–1382. [[CrossRef](#)] [[PubMed](#)]
32. Morse, A.; McDonald, M.M.; Kelly, N.H.; Melville, K.M.; Schindeler, A.; Kramer, I.; Kneissel, M.; van der Meulen, M.C.; Little, D.G. Mechanical load increases in bone formation via a sclerostin-independent pathway. *J. Bone Miner. Res.* **2014**, *29*, 2456–2467. [[CrossRef](#)]

33. Wijenayaka, A.R.; Kogawa, M.; Lim, H.P.; Bonewald, L.F.; Findlay, D.M.; Atkins, G.J. Sclerostin stimulates osteocyte support of osteoclast activity by a RANKL-dependent pathway. *PLoS ONE* **2011**, *6*, e25900. [[CrossRef](#)] [[PubMed](#)]
34. Galea, G.L.; Lanyon, L.E.; Price, J.S. Sclerostin's role in bone's adaptive response to mechanical loading. *Bone* **2017**, *96*, 38–44. [[CrossRef](#)]
35. Shu, R.; Bai, D.; Sheu, T.; He, Y.; Yang, X.; Xue, C.; He, Y.; Zhao, M.; Han, X. Sclerostin Promotes Bone Remodeling in the Process of Tooth Movement. *PLoS ONE* **2017**, *12*, e0167312. [[CrossRef](#)]
36. Lu, W.; Zhang, X.; Firth, F.; Mei, L.; Yi, J.; Gong, C.; Li, H.; Zheng, W.; Li, Y. Sclerostin injection enhances orthodontic tooth movement in rats. *Arch. Oral Biol.* **2019**, *99*, 43–50. [[CrossRef](#)] [[PubMed](#)]
37. Robling, A.G.; Niziolek, P.J.; Baldridge, L.A.; Condon, K.W.; Allen, M.R.; Alam, I.; Mantila, S.M.; Gluhak-Heinrich, J.; Bellido, T.M.; Harris, S.E.; et al. Mechanical stimulation of bone in vivo reduces osteocyte expression of Sost/sclerostin. *J. Biol. Chem.* **2008**, *283*, 5866–5875. [[CrossRef](#)] [[PubMed](#)]
38. Kamiya, N.; Mishina, Y. New insights on the roles of BMP signaling in bone-A review of recent mouse genetic studies. *Biofactors* **2011**, *37*, 75–82. [[CrossRef](#)]
39. Gao, Y.; Zhang, M.; Tian, X.; Wang, M.; Zhang, F. Experimental animal study on BMP-3 expression in periodontal tissues in the process of orthodontic tooth movement. *Exp. Ther. Med.* **2019**, *17*, 193–198. [[CrossRef](#)]
40. Iglesias-Linares, A.; Yanez-Vico, R.M.; Moreno-Fernandez, A.M.; Mendoza-Mendoza, A.; Solano-Reina, E. Corticotomy-assisted orthodontic enhancement by bone morphogenetic protein-2 administration. *J. Oral Maxillofac. Surg.* **2012**, *70*, e124–e132. [[CrossRef](#)] [[PubMed](#)]
41. Manokawinchoke, J.; Pavasant, P.; Sawangmake, C.; Limjeerajarus, N.; Limjeerajarus, C.N.; Egusa, H.; Osathanon, T. Intermittent compressive force promotes osteogenic differentiation in human periodontal ligament cells by regulating the transforming growth factor-beta pathway. *Cell Death Dis.* **2019**, *10*, 761. [[CrossRef](#)]
42. Quinn, J.M.; Itoh, K.; Udagawa, N.; Hausler, K.; Yasuda, H.; Shima, N.; Mizuno, A.; Higashio, K.; Takahashi, N.; Suda, T.; et al. Transforming growth factor beta affects osteoclast differentiation via direct and indirect actions. *J. Bone Miner. Res.* **2001**, *16*, 1787–1794. [[CrossRef](#)]
43. Itonaga, I.; Sabokbar, A.; Sun, S.G.; Kudo, O.; Danks, L.; Ferguson, D.; Fujikawa, Y.; Athanasou, N.A. Transforming growth factor-beta induces osteoclast formation in the absence of RANKL. *Bone* **2004**, *34*, 57–64. [[CrossRef](#)]
44. Wang, L.L.; Zhu, H.; Liang, T. Changes of transforming growth factor beta 1 in rat periodontal tissue during orthodontic tooth movement. *Chin. J. Dent. Res.* **2000**, *3*, 19–22.
45. Uematsu, S.; Mogi, M.; Deguchi, T. Increase of transforming growth factor-beta 1 in gingival crevicular fluid during human orthodontic tooth movement. *Arch. Oral Biol.* **1996**, *41*, 1091–1095. [[CrossRef](#)]
46. Nagai, M.; Yoshida, A.; Sato, N.; Wong, D.T. Messenger RNA level and protein localization of transforming growth factor-beta1 in experimental tooth movement in rats. *Eur. J. Oral Sci.* **1999**, *107*, 475–481. [[CrossRef](#)] [[PubMed](#)]
47. Van Schepdael, A.; Vander Sloten, J.; Geris, L. A mechanobiological model of orthodontic tooth movement. *Biomech. Model. Mechanobiol.* **2013**, *12*, 249–265. [[CrossRef](#)] [[PubMed](#)]
48. Masella, R.S.; Meister, M. Current concepts in the biology of orthodontic tooth movement. *Am. J. Orthod. Dentofac. Orthop.* **2006**, *129*, 458–468. [[CrossRef](#)]
49. Qin, L.; Liu, W.; Cao, H.; Xiao, G. Molecular mechanosensors in osteocytes. *Bone Res.* **2020**, *8*, 23. [[CrossRef](#)]
50. Huang, H.; Yang, R.; Zhou, Y.H. Mechanobiology of Periodontal Ligament Stem Cells in Orthodontic Tooth Movement. *Stem Cells Int.* **2018**, *2018*, 6531216. [[CrossRef](#)]
51. Klein-Nulend, J.; Bakker, A.D.; Bacabac, R.G.; Vatsa, A.; Weinbaum, S. Mechanosensation and transduction in osteocytes. *Bone* **2013**, *54*, 182–190. [[CrossRef](#)]
52. Mabuchi, R.; Matsuzaka, K.; Shimono, M. Cell proliferation and cell death in periodontal ligaments during orthodontic tooth movement. *J. Periodontal Res.* **2002**, *37*, 118–124. [[CrossRef](#)] [[PubMed](#)]
53. Seo, B.M.; Miura, M.; Gronthos, S.; Bartold, P.M.; Batouli, S.; Brahim, J.; Young, M.; Robey, P.G.; Wang, C.Y.; Shi, S. Investigation of multipotent postnatal stem cells from human periodontal ligament. *Lancet* **2004**, *364*, 149–155. [[CrossRef](#)]
54. Zheng, J.; Chen, S.; Albiero, M.L.; Vieira, G.H.A.; Wang, J.; Feng, J.Q.; Graves, D.T. Diabetes Activates Periodontal Ligament Fibroblasts via NF-kappaB In Vivo. *J. Dent. Res.* **2018**, *97*, 580–588. [[CrossRef](#)]
55. Dacquin, R.; Starbuck, M.; Schinke, T.; Karsenty, G. Mouse alpha1(I)-collagen promoter is the best known promoter to drive efficient Cre recombinase expression in osteoblast. *Dev. Dyn.* **2002**, *224*, 245–251. [[CrossRef](#)]
56. Giannopoulou, C.; Cimasoni, G. Functional characteristics of gingival and periodontal ligament fibroblasts. *J. Dent. Res.* **1996**, *75*, 895–902. [[CrossRef](#)]
57. Basdra, E.K.; Komposch, G. Osteoblast-like properties of human periodontal ligament cells: An in vitro analysis. *Eur. J. Orthod.* **1997**, *19*, 615–621. [[CrossRef](#)]
58. Hyeran Helen Jeon, C.-Y.Y.; Shin, M.K.; Wang, J.; Patel, J.H.; Chung, C.; Graves, D.T. Osteoblast lineage cells and periodontal ligament fibroblasts regulate orthodontic tooth movement that is dependent on Nuclear Factor-kappa B (NF-kB) activation. *Angle Orthod.* **2021**, in press.
59. Men, Y.; Wang, Y.; Yi, Y.; Jing, D.; Luo, W.; Shen, B.; Stenberg, W.; Chai, Y.; Ge, W.P.; Feng, J.Q.; et al. Gli1+ Periodontium Stem Cells Are Regulated by Osteocytes and Occlusal Force. *Dev. Cell* **2020**, *54*, 639–654 e636. [[CrossRef](#)] [[PubMed](#)]

60. Liu, A.Q.; Zhang, L.S.; Chen, J.; Sui, B.D.; Liu, J.; Zhai, Q.M.; Li, Y.J.; Bai, M.; Chen, K.; Jin, Y.; et al. Mechanosensing by Gli1(+) cells contributes to the orthodontic force-induced bone remodelling. *Cell Prolif.* **2020**, *53*, e12810. [[CrossRef](#)]
61. Dupont, S.; Morsut, L.; Aragona, M.; Enzo, E.; Giulitti, S.; Cordenonsi, M.; Zanconato, F.; Le Dıgabel, J.; Forcato, M.; Bicciato, S.; et al. Role of YAP/TAZ in mechanotransduction. *Nature* **2011**, *474*, 179–183. [[CrossRef](#)] [[PubMed](#)]
62. Yang, Y.; Wang, B.K.; Chang, M.L.; Wan, Z.Q.; Han, G.L. Cyclic Stretch Enhances Osteogenic Differentiation of Human Periodontal Ligament Cells via YAP Activation. *Biomed. Res. Int.* **2018**, *2018*, 2174824. [[CrossRef](#)]
63. Sun, B.; Wen, Y.; Wu, X.; Zhang, Y.; Qiao, X.; Xu, X. Expression pattern of YAP and TAZ during orthodontic tooth movement in rats. *J. Mol. Histol.* **2018**, *49*, 123–131. [[CrossRef](#)] [[PubMed](#)]
64. Zhang, L.; Liu, W.; Zhao, J.; Ma, X.; Shen, L.; Zhang, Y.; Jin, F.; Jin, Y. Mechanical stress regulates osteogenic differentiation and RANKL/OPG ratio in periodontal ligament stem cells by the Wnt/beta-catenin pathway. *Biochim. Biophys. Acta* **2016**, *1860*, 2211–2219. [[CrossRef](#)]
65. Pelaez, D.; Acosta Torres, Z.; Ng, T.K.; Choy, K.W.; Pang, C.P.; Cheung, H.S. Cardiomyogenesis of periodontal ligament-derived stem cells by dynamic tensile strain. *Cell Tissue Res.* **2017**, *367*, 229–241. [[CrossRef](#)]
66. Chen, J.; Zhang, W.; Backman, L.J.; Kelk, P.; Danielson, P. Mechanical stress potentiates the differentiation of periodontal ligament stem cells into keratocytes. *Br. J. Ophthalmol.* **2018**, *102*, 562–569. [[CrossRef](#)]
67. Liu, F.; Wen, F.; He, D.; Liu, D.; Yang, R.; Wang, X.; Yan, Y.; Liu, Y.; Kou, X.; Zhou, Y. Force-Induced H2S by PDLSCs Modifies Osteoclastic Activity during Tooth Movement. *J. Dent. Res.* **2017**, *96*, 694–702. [[CrossRef](#)] [[PubMed](#)]
68. He, D.; Liu, F.; Cui, S.; Jiang, N.; Yu, H.; Zhou, Y.; Liu, Y.; Kou, X. Mechanical load-induced H2S production by periodontal ligament stem cells activates M1 macrophages to promote bone remodeling and tooth movement via STAT1. *Stem Cell Res. Ther.* **2020**, *11*, 112. [[CrossRef](#)] [[PubMed](#)]
69. Huang, H.; Williams, R.C.; Kyrkanides, S. Accelerated orthodontic tooth movement: Molecular mechanisms. *Am. J. Orthod. Dentofac. Orthop.* **2014**, *146*, 620–632. [[CrossRef](#)] [[PubMed](#)]
70. Florencio-Silva, R.; Sasso, G.R.; Sasso-Cerri, E.; Simoes, M.J.; Cerri, P.S. Biology of Bone Tissue: Structure, Function, and Factors That Influence Bone Cells. *Biomed. Res. Int.* **2015**, *2015*, 421746. [[CrossRef](#)]
71. Dallas, S.L.; Prideaux, M.; Bonewald, L.F. The osteocyte: An endocrine cell ... and more. *Endocr. Rev.* **2013**, *34*, 658–690. [[CrossRef](#)]
72. Gluhak-Heinrich, J.; Ye, L.; Bonewald, L.F.; Feng, J.Q.; MacDougall, M.; Harris, S.E.; Pavlin, D. Mechanical loading stimulates dentin matrix protein 1 (DMP1) expression in osteocytes in vivo. *J. Bone Miner. Res.* **2003**, *18*, 807–817. [[CrossRef](#)]
73. Moin, S.; Kalajzic, Z.; Utreja, A.; Nihara, J.; Wadhwa, S.; Uribe, F.; Nanda, R. Osteocyte death during orthodontic tooth movement in mice. *Angle Orthod.* **2014**, *84*, 1086–1092. [[CrossRef](#)]
74. Bivi, N.; Condon, K.W.; Allen, M.R.; Farlow, N.; Passeri, G.; Brun, L.R.; Rhee, Y.; Bellido, T.; Plotkin, L.I. Cell autonomous requirement of connexin 43 for osteocyte survival: Consequences for endocortical resorption and periosteal bone formation. *J. Bone Miner. Res.* **2012**, *27*, 374–389. [[CrossRef](#)]
75. Kogianni, G.; Mann, V.; Noble, B.S. Apoptotic bodies convey activity capable of initiating osteoclastogenesis and localized bone destruction. *J. Bone Miner. Res.* **2008**, *23*, 915–927. [[CrossRef](#)]
76. Xiong, J.; Onal, M.; Jilka, R.L.; Weinstein, R.S.; Manolagas, S.C.; O’Brien, C.A. Matrix-embedded cells control osteoclast formation. *Nat. Med.* **2011**, *17*, 1235–1241. [[CrossRef](#)]
77. Nakashima, T.; Hayashi, M.; Fukunaga, T.; Kurata, K.; Oh-Hora, M.; Feng, J.Q.; Bonewald, L.F.; Kodama, T.; Wutz, A.; Wagner, E.F.; et al. Evidence for osteocyte regulation of bone homeostasis through RANKL expression. *Nat. Med.* **2011**, *17*, 1231–1234. [[CrossRef](#)]
78. Matsumoto, T.; Iimura, T.; Ogura, K.; Moriyama, K.; Yamaguchi, A. The role of osteocytes in bone resorption during orthodontic tooth movement. *J. Dent. Res.* **2013**, *92*, 340–345. [[CrossRef](#)]
79. Tatsumi, S.; Ishii, K.; Amizuka, N.; Li, M.; Kobayashi, T.; Kohno, K.; Ito, M.; Takeshita, S.; Ikeda, K. Targeted ablation of osteocytes induces osteoporosis with defective mechanotransduction. *Cell Metab.* **2007**, *5*, 464–475. [[CrossRef](#)]
80. Kassem, M.; Abdallah, B.M.; Saeed, H. Osteoblastic cells: Differentiation and trans-differentiation. *Arch. Biochem. Biophys.* **2008**, *473*, 183–187. [[CrossRef](#)]
81. Matic, I.; Matthews, B.G.; Wang, X.; Dymont, N.A.; Worthley, D.L.; Rowe, D.W.; Grcevic, D.; Kalajzic, I. Quiescent Bone Lining Cells Are a Major Source of Osteoblasts During Adulthood. *Stem Cells* **2016**, *34*, 2930–2942. [[CrossRef](#)]
82. Kohli, S.S.; Kohli, V.S. Role of RANKL-RANK/osteoprotegerin molecular complex in bone remodeling and its immunopathologic implications. *Indian J. Endocrinol. Metab.* **2011**, *15*, 175–181. [[CrossRef](#)] [[PubMed](#)]
83. Wang, L.; Li, J.Y.; Zhang, X.Z.; Liu, L.; Wan, Z.M.; Li, R.X.; Guo, Y. Involvement of p38MAPK/NF-kappaB signaling pathways in osteoblasts differentiation in response to mechanical stretch. *Ann. Biomed. Eng.* **2012**, *40*, 1884–1894. [[CrossRef](#)]
84. Matsuo, K.; Irie, N. Osteoclast-osteoblast communication. *Arch. Biochem. Biophys.* **2008**, *473*, 201–209. [[CrossRef](#)]
85. Zhang, S.; Wang, X.; Li, G.; Chong, Y.; Zhang, J.; Guo, X.; Li, B.; Bi, Z. Osteoclast regulation of osteoblasts via RANKRANKL reverse signal transduction in vitro. *Mol. Med. Rep.* **2017**, *16*, 3994–4000. [[CrossRef](#)] [[PubMed](#)]
86. Boyce, B.F.; Xing, L. The RANKL/RANK/OPG pathway. *Curr. Osteoporos. Rep.* **2007**, *5*, 98–104. [[CrossRef](#)]
87. Holland, R.; Bain, C.; Utreja, A. Osteoblast differentiation during orthodontic tooth movement. *Orthod. Craniofac. Res.* **2019**, *22*, 177–182. [[CrossRef](#)]

88. Uribe, F.; Kalajzic, Z.; Bibko, J.; Nanda, R.; Olson, C.; Rowe, D.; Wadhwa, S. Early effects of orthodontic forces on osteoblast differentiation in a novel mouse organ culture model. *Angle Orthod.* **2011**, *81*, 284–291. [[CrossRef](#)] [[PubMed](#)]
89. Ibrahim Disha, S.; Furlani, B.; Drevensek, G.; Plut, A.; Yanagisawa, M.; Hudoklin, S.; Prodan Zitnik, I.; Marc, J.; Drevensek, M. The role of endothelin B receptor in bone modelling during orthodontic tooth movement: A study on ETB knockout rats. *Sci. Rep.* **2020**, *10*, 14226. [[CrossRef](#)] [[PubMed](#)]
90. Premaraj, S.; Souza, I.; Premaraj, T. Mechanical loading activates beta-catenin signaling in periodontal ligament cells. *Angle Orthod.* **2011**, *81*, 592–599. [[CrossRef](#)] [[PubMed](#)]
91. Kramer, I.; Halleux, C.; Keller, H.; Pegurri, M.; Gooi, J.H.; Weber, P.B.; Feng, J.Q.; Bonewald, L.F.; Kneissel, M. Osteocyte Wnt/beta-catenin signaling is required for normal bone homeostasis. *Mol. Cell. Biol.* **2010**, *30*, 3071–3085. [[CrossRef](#)]
92. Chen, B.; Li, X.D.; Liu, D.X.; Wang, H.; Xie, P.; Liu, Z.Y.; Hou, G.Q.; Chang, B.; Du, S.X. Canonical Wnt signaling is required for Panax notoginseng saponin-mediated attenuation of the RANKL/OPG ratio in bone marrow stromal cells during osteogenic differentiation. *Phytomedicine* **2012**, *19*, 1029–1034. [[CrossRef](#)]
93. Fu, H.D.; Wang, B.K.; Wan, Z.Q.; Lin, H.; Chang, M.L.; Han, G.L. Wnt5a mediated canonical Wnt signaling pathway activation in orthodontic tooth movement: Possible role in the tension force-induced bone formation. *J. Mol. Histol.* **2016**, *47*, 455–466. [[CrossRef](#)] [[PubMed](#)]
94. Sawakami, K.; Robling, A.G.; Ai, M.; Pitner, N.D.; Liu, D.; Warden, S.J.; Li, J.; Maye, P.; Rowe, D.W.; Duncan, R.L.; et al. The Wnt co-receptor LRP5 is essential for skeletal mechanotransduction but not for the anabolic bone response to parathyroid hormone treatment. *J. Biol. Chem.* **2006**, *281*, 23698–23711. [[CrossRef](#)] [[PubMed](#)]
95. Cui, Y.; Niziolek, P.J.; MacDonald, B.T.; Zylstra, C.R.; Alenina, N.; Robinson, D.R.; Zhong, Z.; Matthes, S.; Jacobsen, C.M.; Conlon, R.A.; et al. Lrp5 functions in bone to regulate bone mass. *Nat. Med.* **2011**, *17*, 684–691. [[CrossRef](#)]
96. Niziolek, P.J.; Warman, M.L.; Robling, A.G. Mechanotransduction in bone tissue: The A214V and G171V mutations in Lrp5 enhance load-induced osteogenesis in a surface-selective manner. *Bone* **2012**, *51*, 459–465. [[CrossRef](#)] [[PubMed](#)]
97. Holland, R.; Bain, C.; Alrasheed, R.S.; Robling, A.G.; Utreja, A. The effect of overexpression of Lrp5 on orthodontic tooth movement. *Orthod. Craniofac. Res.* **2020**. [[CrossRef](#)] [[PubMed](#)]
98. Lim, W.H.; Liu, B.; Mah, S.J.; Yin, X.; Helms, J.A. Alveolar bone turnover and periodontal ligament width are controlled by Wnt. *J. Periodontol.* **2015**, *86*, 319–326. [[CrossRef](#)] [[PubMed](#)]
99. Lu, J.; Duan, Y.; Zhang, M.; Wu, M.; Wang, Y. Expression of Wnt3a, Wnt10b, beta-catenin and DKK1 in periodontium during orthodontic tooth movement in rats. *Acta Odontol. Scand.* **2016**, *74*, 217–223. [[CrossRef](#)] [[PubMed](#)]
100. Pocaterra, A.; Romani, P.; Dupont, S. YAP/TAZ functions and their regulation at a glance. *J. Cell Sci.* **2020**, *133*, jcs230425. [[CrossRef](#)]
101. Huelter-Hassler, D.; Tomakidi, P.; Steinberg, T.; Jung, B.A. Orthodontic strain affects the Hippo-pathway effector YAP concomitant with proliferation in human periodontal ligament fibroblasts. *Eur. J. Orthod.* **2017**, *39*, 251–257. [[CrossRef](#)]
102. Klein-Nulend, J.; Bacabac, R.G.; Bakker, A.D. Mechanical loading and how it affects bone cells: The role of the osteocyte cytoskeleton in maintaining our skeleton. *Eur. Cells Mater.* **2012**, *24*, 278–291. [[CrossRef](#)]
103. Feller, L.; Khammissa, R.A.; Schechter, I.; Thomadakis, G.; Fourie, J.; Lemmer, J. Biological Events in Periodontal Ligament and Alveolar Bone Associated with Application of Orthodontic Forces. *Sci. World J.* **2015**, *2015*, 876509. [[CrossRef](#)]
104. Feller, L.; Khammissa, R.A.; Schechter, I.; Moodley, A.; Thomadakis, G.; Lemmer, J. Periodontal Biological Events Associated with Orthodontic Tooth Movement: The Biomechanics of the Cytoskeleton and the Extracellular Matrix. *Sci. World J.* **2015**, *2015*, 894123. [[CrossRef](#)]
105. McBeath, R.; Pirone, D.M.; Nelson, C.M.; Bhadriraju, K.; Chen, C.S. Cell shape, cytoskeletal tension, and RhoA regulate stem cell lineage commitment. *Dev. Cell* **2004**, *6*, 483–495. [[CrossRef](#)]
106. Pan, J.; Wang, T.; Wang, L.; Chen, W.; Song, M. Cyclic strain-induced cytoskeletal rearrangement of human periodontal ligament cells via the Rho signaling pathway. *PLoS ONE* **2014**, *9*, e91580. [[CrossRef](#)] [[PubMed](#)]
107. Geiger, B.; Bershadsky, A.; Pankov, R.; Yamada, K.M. Transmembrane crosstalk between the extracellular matrix–cytoskeleton crosstalk. *Nat. Rev. Mol. Cell Biol.* **2001**, *2*, 793–805. [[CrossRef](#)]
108. Young, S.R.; Gerard-O’Riley, R.; Kim, J.B.; Pavalko, F.M. Focal adhesion kinase is important for fluid shear stress-induced mechanotransduction in osteoblasts. *J. Bone Miner. Res.* **2009**, *24*, 411–424. [[CrossRef](#)] [[PubMed](#)]
109. Santos, A.; Bakker, A.D.; Zandieh-Doulabi, B.; de Blicke-Hogervorst, J.M.; Klein-Nulend, J. Early activation of the beta-catenin pathway in osteocytes is mediated by nitric oxide, phosphatidylinositol-3 kinase/Akt, and focal adhesion kinase. *Biochem. Biophys. Res. Commun.* **2010**, *391*, 364–369. [[CrossRef](#)]
110. Chen, C.S.; Tan, J.; Tien, J. Mechanotransduction at cell-matrix and cell-cell contacts. *Annu. Rev. Biomed. Eng.* **2004**, *6*, 275–302. [[CrossRef](#)] [[PubMed](#)]
111. Yuan, X.; Yang, S. Cilia/Ift protein and motor-related bone diseases and mouse models. *Front. Biosci.* **2015**, *20*, 515–555. [[CrossRef](#)]
112. Song, J.; Wang, L.; Fan, F.; Wei, J.; Zhang, J.; Lu, Y.; Fu, Y.; Wang, S.; Juncos, L.A.; Liu, R. Role of the Primary Cilia on the Macula Densa and Thick Ascending Limbs in Regulation of Sodium Excretion and Hemodynamics. *Hypertension* **2017**, *70*, 324–333. [[CrossRef](#)] [[PubMed](#)]
113. Whitfield, J.F. Primary cilium—is it an osteocyte’s strain-sensing flowmeter? *J. Cell Biochem.* **2003**, *89*, 233–237. [[CrossRef](#)]
114. Yuan, X.; Yang, S. Primary Cilia and Intraflagellar Transport Proteins in Bone and Cartilage. *J. Dent. Res.* **2016**, *95*, 1341–1349. [[CrossRef](#)] [[PubMed](#)]

115. Yang, S.; Wang, C. The intraflagellar transport protein IFT80 is required for cilia formation and osteogenesis. *Bone* **2012**, *51*, 407–417. [[CrossRef](#)]
116. Qiu, N.; Xiao, Z.; Cao, L.; Buechel, M.M.; David, V.; Roan, E.; Quarles, L.D. Disruption of Kif3a in osteoblasts results in defective bone formation and osteopenia. *J. Cell Sci.* **2012**, *125*, 1945–1957. [[CrossRef](#)] [[PubMed](#)]
117. Nauli, S.M.; Alenghat, F.J.; Luo, Y.; Williams, E.; Vassilev, P.; Li, X.; Elia, A.E.; Lu, W.; Brown, E.M.; Quinn, S.J.; et al. Polycystins 1 and 2 mediate mechanosensation in the primary cilium of kidney cells. *Nat. Genet.* **2003**, *33*, 129–137. [[CrossRef](#)]
118. Wang, P.; Tang, C.; Wu, J.; Yang, Y.; Yan, Z.; Liu, X.; Shao, X.; Zhai, M.; Gao, J.; Liang, S.; et al. Pulsed electromagnetic fields regulate osteocyte apoptosis, RANKL/OPG expression, and its control of osteoclastogenesis depending on the presence of primary cilia. *J. Cell Physiol.* **2019**, *234*, 10588–10601. [[CrossRef](#)] [[PubMed](#)]
119. Delaine-Smith, R.M.; Sittichokechaiwut, A.; Reilly, G.C. Primary cilia respond to fluid shear stress and mediate flow-induced calcium deposition in osteoblasts. *FASEB J.* **2014**, *28*, 430–439. [[CrossRef](#)]
120. Malone, A.M.; Anderson, C.T.; Tummala, P.; Kwon, R.Y.; Johnston, T.R.; Stearns, T.; Jacobs, C.R. Primary cilia mediate mechanosensing in bone cells by a calcium-independent mechanism. *Proc. Natl. Acad. Sci. USA* **2007**, *104*, 13325–13330. [[CrossRef](#)]
121. Xiao, Z.; Zhang, S.; Mahlios, J.; Zhou, G.; Magenheimer, B.S.; Guo, D.; Dallas, S.L.; Maser, R.; Calvet, J.P.; Bonewald, L.; et al. Cilia-like structures and polycystin-1 in osteoblasts/osteocytes and associated abnormalities in skeletogenesis and Runx2 expression. *J. Biol. Chem.* **2006**, *281*, 30884–30895. [[CrossRef](#)]
122. Shalish, M.; Will, L.A.; Fukai, N.; Hou, B.; Olsen, B.R. Role of polycystin-1 in bone remodeling: Orthodontic tooth movement study in mutant mice. *Angle Orthod.* **2014**, *84*, 885–890. [[CrossRef](#)] [[PubMed](#)]
123. Riquelme, M.A.; Cardenas, E.R.; Xu, H.; Jiang, J.X. The Role of Connexin Channels in the Response of Mechanical Loading and Unloading of Bone. *Int. J. Mol. Sci.* **2020**, *21*, 1146. [[CrossRef](#)]
124. Su, M.; Borke, J.L.; Donahue, H.J.; Li, Z.; Warshawsky, N.M.; Russell, C.M.; Lewis, J.E. Expression of connexin 43 in rat mandibular bone and periodontal ligament (PDL) cells during experimental tooth movement. *J. Dent. Res.* **1997**, *76*, 1357–1366. [[CrossRef](#)] [[PubMed](#)]
125. Plotkin, L.I.; Stains, J.P. Connexins and pannexins in the skeleton: Gap junctions, hemichannels and more. *Cell. Mol. Life Sci.* **2015**, *72*, 2853–2867. [[CrossRef](#)]
126. Li, S.; Zhang, H.; Li, S.; Yang, Y.; Huo, B.; Zhang, D. Connexin 43 and ERK regulate tension-induced signal transduction in human periodontal ligament fibroblasts. *J. Orthop. Res.* **2015**, *33*, 1008–1014. [[CrossRef](#)]
127. Xu, C.; Fan, Z.; Shan, W.; Hao, Y.; Ma, J.; Huang, Q.; Zhang, F. Cyclic stretch influenced expression of membrane connexin 43 in human periodontal ligament cell. *Arch. Oral Biol.* **2012**, *57*, 1602–1608. [[CrossRef](#)]
128. Shen, Y.; Pan, Y.; Guo, S.; Sun, L.; Zhang, C.; Wang, L. The roles of mechanosensitive ion channels and associated downstream MAPK signaling pathways in PDLC mechanotransduction. *Mol. Med. Rep.* **2020**, *21*, 2113–2122. [[CrossRef](#)] [[PubMed](#)]
129. Jin, Y.; Li, J.; Wang, Y.; Ye, R.; Feng, X.; Jing, Z.; Zhao, Z. Functional role of mechanosensitive ion channel Piezo1 in human periodontal ligament cells. *Angle Orthod.* **2015**, *85*, 87–94. [[CrossRef](#)] [[PubMed](#)]
130. Li, X.; Han, L.; Nookaew, I.; Mannen, E.; Silva, M.J.; Almeida, M.; Xiong, J. Stimulation of Piezo1 by mechanical signals promotes bone anabolism. *Elife* **2019**, *8*. [[CrossRef](#)]
131. Sasaki, F.; Hayashi, M.; Mouri, Y.; Nakamura, S.; Adachi, T.; Nakashima, T. Mechanotransduction via the Piezo1-Akt pathway underlies Sost suppression in osteocytes. *Biochem. Biophys. Res. Commun.* **2020**, *521*, 806–813. [[CrossRef](#)]
132. Pei, F.; Liu, J.; Zhang, L.; Pan, X.; Huang, W.; Cen, X.; Huang, S.; Jin, Y.; Zhao, Z. The functions of mechanosensitive ion channels in tooth and bone tissues. *Cell. Signal.* **2021**, *78*, 109877. [[CrossRef](#)] [[PubMed](#)]
133. Lyons, J.S.; Joca, H.C.; Law, R.A.; Williams, K.M.; Kerr, J.P.; Shi, G.; Khairallah, R.J.; Martin, S.S.; Konstantopoulos, K.; Ward, C.W.; et al. Microtubules tune mechanotransduction through NOX2 and TRPV4 to decrease sclerostin abundance in osteocytes. *Sci. Signal.* **2017**, *10*, eaan5748. [[CrossRef](#)] [[PubMed](#)]

Osteoblast lineage cells and periodontal ligament fibroblasts regulate orthodontic tooth movement that is dependent on Nuclear Factor-kappa B (NF- κ B) activation

Hyeran Helen Jeon^a; Chia-Ying Yang^b; Min Kyung Shin^c; Jingyi Wang^d; Juhin Hiren Patel^e; Chun-Hsi Chung^e; Dana T. Graves^f

ABSTRACT

Objectives: To investigate the role of NF- κ B in osteoblast lineage cells and periodontal ligament (PDL) fibroblasts during orthodontic tooth movement (OTM).

Materials and Methods: Transgenic mice that expressed a dominant negative mutant of the inhibitor of κ B kinase (IKK-DN) with lineage specific expression in osteoblastic cells and PDL fibroblasts driven by a response element in the collagen1 α 1 promoter and matched wild-type (WT) mice were examined. A 10-12 g force was applied by a NiTi coil and maintained for 5 or 12 days. OTM distance, PDL width, and bone volume fraction were measured using micro computed tomography. Osteoclast numbers were counted in tartrate-resistant acid phosphatase-stained sections. Activation of nuclear factor kappa B (NF- κ B) was assessed by nuclear localization of p65, and the receptor activator of nuclear factor- κ B ligand (RANKL) was measured by immunofluorescence and compared to control specimens with no orthodontic force.

Results: OTM-induced NF- κ B activation (p65 nuclear localization) in WT mice was largely blocked in transgenic (TG) mice. OTM was significantly reduced in the TG mice compared to WT mice along with reduced osteoclastogenesis, narrower PDL width, higher bone volume fraction, and reduced RANKL expression.

Conclusions: Osteoblast lineage cells and PDL fibroblasts are key contributors to alveolar bone remodeling in OTM through IKK β dependent NF- κ B activation. (*Angle Orthod.* 0000;00:000–000.)

KEY WORDS: Osteoblast lineage cells; Periodontal ligament (PDL); Fibroblast; Nuclear Factor-kappa B (NF- κ B); Orthodontic tooth movement; Mechanical force

INTRODUCTION

Bone remodeling in orthodontic tooth movement (OTM) is a highly regulated process that coordinates bone resorption by osteoclasts and new bone formation by osteoblasts.¹ OTM has three phases: (1) initial

tooth tipping within periodontal ligament (PDL), (2) a lag phase, where the hyalinization area is observed on the compression side and osteoclasts mediate bone resorption, and (3) the post-lag phase, where rapid tooth movement occurs.² Osteoclasts are essential in

^a Assistant Professor, Department of Orthodontics, School of Dental Medicine, University of Pennsylvania, Philadelphia, PA, USA.

^b Former Orthodontic Resident, Department of Orthodontics, School of Dental Medicine, University of Pennsylvania, Philadelphia, PA, USA.

^c Dental Student, School of Dental Medicine, University of Pennsylvania, Philadelphia, PA, USA.

^d Orthodontic Resident, Department of Orthodontics, School of Dental Medicine, University of Pennsylvania, Philadelphia, PA, USA.

^e Associate Professor and Chauncey M. F. Egel Endowed Chair and Director, Department of Orthodontics, School of Dental Medicine, University of Pennsylvania, Philadelphia, PA, USA.

^f Professor, Vice Dean of Scholarship and Research, Director of Doctor of Science in Dentistry Program, Department of Periodontics, School of Dental Medicine, University of Pennsylvania, Philadelphia, PA, USA.

Corresponding author: Hyeran Helen Jeon, DDS, MSD, DScD, University of Pennsylvania School of Dental Medicine, 240 South 40th Street, Philadelphia, PA 19104-6030 (e-mail: hjeon@upenn.edu)

Accepted: February 2021. Submitted: March 2020.

Published Online: April 14, 2021

© 0000 by The EH Angle Education and Research Foundation, Inc.

bone maintenance, repair, and remodeling of bones. On mechanical loading, the cells around the tooth induce osteoclastogenesis through upregulation of the receptor activator of nuclear factor- κ B ligand (RANKL).³ When osteoclasts resorb alveolar bone next to the hyalinized tissue, PDL spaces are widened, and the tooth starts to move in the direction of the mechanical force. To date, the underlying mechanisms of main cell types in OTM and how they regulate this process remain unclear.

OTM involves the close interaction of several cell types that produce RANKL to induce osteoclastogenesis.⁴ Osteoblast lineage cells including osteoblasts and osteocytes stimulate bone resorption by expression of RANKL and contribute to bone formation.⁵ Osteocytes are the major mechanosensor in bone and play an essential role in inducing osteoclastogenesis during OTM.⁶ PDL is the fibrous tissue between cementum and alveolar bone that maintains a tooth in the bony socket and PDL fibroblasts transmit mechanical signals in the PDL.⁷ Recently, it was reported that RANKL from PDL fibroblasts and bone lining cells were essential in OTM and osteoclastogenesis in response to mechanical loading.⁴ Interestingly, PDL fibroblasts have several characteristics similar to those of osteoblasts and exhibit promoter activity regulated by a 2.3 kb response element in the Col1 α 1 promoter, exhibit high alkaline phosphatase activity and have other bone-associated markers.⁸ The 2.3 kb Col1 α 1-Cre transgenic mice are widely used in mechanistic studies to examine promoter activity and gene expression in osteoblasts, osteocytes, and PDL fibroblasts.^{9–11} In previous studies, this regulatory element was used to generate transgenic mice that expressed a lineage specific dominant negative mutant of an inhibitor of κ B kinase (IKK-DN) in osteoblast lineage cells and PDL fibroblasts.^{1,9,11–14}

NF- κ B is a master regulator of inflammation, induces osteoclastogenesis and inhibits new bone formation.^{15,16} The members of NF- κ B are RelA (p65), p50, p52, RelB and c-Rel. The p65/p50 heterodimeric complex, canonical NF- κ B, is the most common isoform of NF- κ B in mammalian cells. The canonical NF- κ B pathway is activated by pro-inflammatory stimuli such as tumor necrosis factor (TNF) and IL-1, while the alternative NF- κ B pathway is activated by a small subset of TNF family members. When NF- κ B is inactive, it is combined with inhibitors of NF- κ B (I κ B) and exists in the cytoplasm. When the inhibitor of κ B kinase (IKK) is activated, it causes I κ B degradation and NF- κ B translocates to the nucleus, stimulating pro-inflammatory gene transcription. Conversely, inhibition or deletion of IKK prevents activation NF- κ B.^{9,11,17–19} Previous studies reported that NF- κ B affected bone remodeling predominantly by inducing osteoclast

formation and activity.^{20–22} Although the role of IKK/NF- κ B signaling in periodontitis is well established,^{9,11} its role in the mechanical force-induced bone remodeling has not been reported.

The goal of this study was to examine the effect of IKK/NF- κ B signaling in osteoblast lineage cells and PDL fibroblasts during OTM, examining transgenic mice with a dominant negative inhibitor of NF- κ B under the control of a 2.3 kb collagen 1 α 1 promoter. It was found that OTM was significantly reduced with less osteoclastogenesis, narrower PDL space, higher bone volume fraction, and less RANKL expression in experimental IKK-DN mice. This study demonstrated the importance of NF- κ B activation in osteoblast lineage cells and PDL fibroblasts in transducing mechanical forces during OTM.

MATERIALS AND METHODS

Animal Model

The mouse experiments were approved by the University of Pennsylvania Institutional Animal Care and Use Committee. Transgenic IKK-DN mice (TG) were generated that expressed a dominant negative IKK under the control of a 2.3 kb element of the collagen 1 α 1 promoter that restricts activation of NF- κ B to osteoblast lineage cells and PDL fibroblasts.^{1,9,12,21} Experiments were performed with adult mice 12–13 weeks old ($n = 8$ per group). C57BL/6 mice were used as a control group (wild-type, age and gender matched). Two to five mice were housed per cage under standard conditions with a 14-hour light/10-hour dark cycle. All the animals were closely monitored and fed a diet of powdered food, DietGel (ClearH₂O, Westbrook, ME) and water ad libitum throughout the experimental period.

Application of Orthodontic Force

OTM experiments were performed as previously described.⁴ Briefly, mice were anesthetized by intraperitoneal administration of ketamine (80 mg/kg), xylazine (5 mg/kg), and acepromazine (1 mg/kg). Orthodontic force of 10–12 g was applied to move the upper right first molar for 5 and 12 days with a 0.006 \times 0.030-inch NiTi coil spring (Ultimate Wireforms, Inc., Bristol, CT). OTM mouse models typically apply forces between 10 g and 50 g.^{4,23–25} It has been reported that the higher level of force causes minor tissue damage and root resorption was observed with 0.50 N (51 g).²³ Therefore, lighter forces (10–12 g) were used, which have been successfully tested in several publications.^{4,24,25} Self-etching primer and light-cured dental adhesive resin (Transbond XT; 3M Unitek, Monrovia, CA) were applied on maxillary incisors to prevent

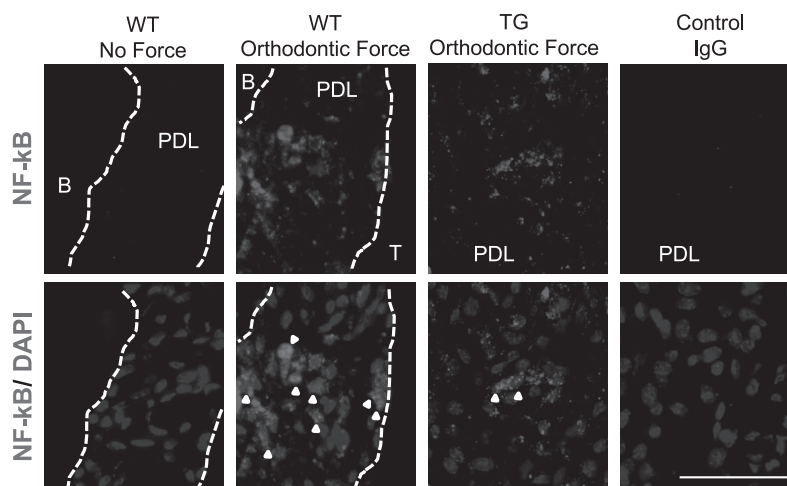


Figure 1. Nuclear NF- κ B expression was significantly increased on the compression side in WT mice but this increase was blocked in TG mice. Sagittal sections from wild-type (WT) and transgenic (TG) mice were treated by immunofluorescence stain with anti-NF- κ B p65 antibody. Nuclear translocation of NF- κ B p65 (arrowheads), indicative of NF- κ B activation, was examined on the compression side. Bar = 50 μ m. B indicates alveolar bone; PDL, periodontal ligament; T, tooth.

detachment of a spring. The left side was used as a control. Mice were checked every day to assess their general conditions and euthanized on days 5 and 12 after orthodontic force loading.

Micro-CT

Samples were fixed in 4% paraformaldehyde in phosphate-buffered saline (PBS) at 4°C for 24 hours and then scanned using a micro-CT (MicroCT35; SCANCO Medical, Bassersdorf, Switzerland) at 55 kVp and 145 μ A intensity with an integration time 200 ms. Maxillary molar areas were scanned at a 20 μ m isotropic voxel size. After reconstruction, all images were converted to Digital Imaging and Communications in Medicine files and then imported to OsiriX (Pixmeo SARL, Bernex, Switzerland) for analysis. The OTM distance was measured as the minimum distance between the maxillary right first and second molar crowns in relation to the same measurements for the unloaded left side. Bone density was examined by assessing bone volume/total volume (BV/TV) without or with orthodontic forces as previously described.²⁶ A 250 \times 250 \times 250 μ m³ cube on the compression side of the coronal one-third of the distobuccal root of the maxillary first molar was selected for analysis. The average PDL width was measured from the coronal to the apical portion of the PDL on the compression side of the distobuccal root of the maxillary first molar as previously described.⁴ OsiriX (Pixmeo SARL, Bernex, Switzerland) and Image Pro Plus (Media Cybernetics, Inc., Rockville, MD) software was used for 3D image reconstruction and quantitative image analysis.

Histology and TRAP stain

Specimens were decalcified in 10% ethylenediamine tetraacetic acid for 5 weeks, paraffin-embedded, and sectioned with 4- μ m thickness. Tartrate-resistant acid phosphatase (TRAP) staining with hematoxylin counterstaining was performed according to the manufacturer's instructions (Sigma-Aldrich, Saint Louis, MO). TRAP-positive multinucleated cells were counted on the alveolar bone surfaces on the compression sides of the distobuccal root of the maxillary first molar under 10 \times and 20 \times objectives. Image analysis of TRAP-stained sections was performed with NIS-elements image analysis software (Nikon, Melville, NY).

Immunofluorescence stain

Immunofluorescence was performed as previously described with the following primary antibodies:⁴ RANKL (ab216484; Abcam, Cambridge, MA) and NF- κ B p65 (ab16502; Abcam) and compared to matched control antibody. Image analysis was performed at 40 \times magnification using NIS-Element software (Nikon) to examine the NF- κ B p65 nuclear localization and measure the number of RANKL positive cells on the compression side of the distobuccal root of the maxillary first molar.

Statistics

Statistical analysis between WT and TG mice was performed using two-tailed Student's *t*-test and differences among multiple groups was established by analysis of variance with Scheffé's post-hoc test. Results were expressed as the mean \pm SEM. *P* < .05 was considered statistically significant.

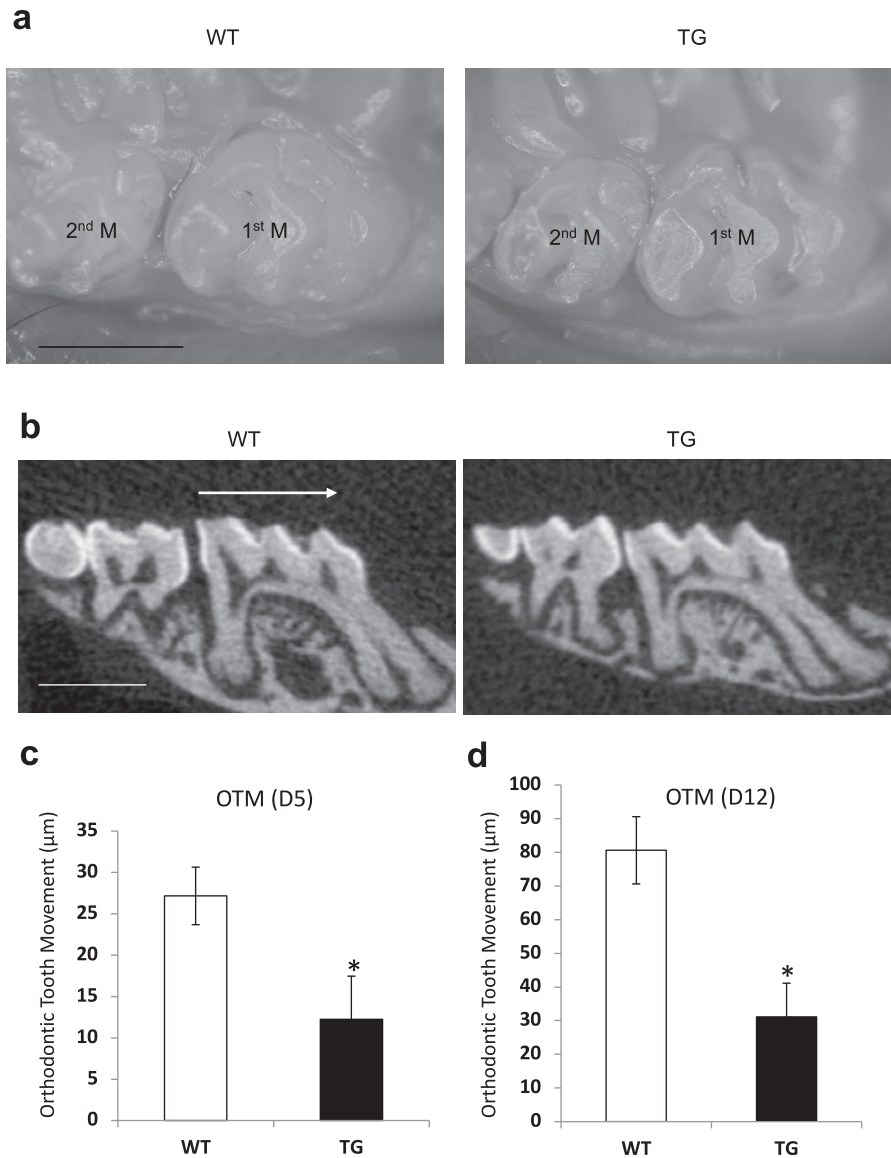


Figure 2. NF- κ B inhibition in osteoblast lineage cells and PDL fibroblasts decreased orthodontic tooth movement. (a) Digital photos. Bar, 1 mm. (b) Orthodontic tooth movement was measured as the minimum distance between the most distal point of the maxillary right first molar crown and the most mesial point of the maxillary right second molar crown. Bar, 1 mm. (c) The amount of tooth movement on days 5 and 12. Each in vivo value is the mean \pm SEM for $n = 8$ mice per group. * $P < .05$ vs WT mice group.

RESULTS

Application of orthodontic force increased NF- κ B activation in wild-type but not experimental mice. NF- κ B activation was assessed by p65 nuclear localization by immunofluorescence. Nuclear p65 immunopositive cells were substantially increased on the compression side in WT mice compared to the control side with no mechanical loading. The nuclear localization of p65 was largely blocked in experimental mice (Figure 1).

Inhibition of NF- κ B in osteoblast lineage cells and PDL fibroblasts prevented OTM. Orthodontic tooth movement was examined in WT and experimental TG mice by measuring the minimum distance between the

maxillary right first and second molar crowns (Figure 2a,b). On day 5, the teeth in the WT group moved $27.16 \pm 3.48 \mu\text{m}$ and, on day 12, moved $80.6 \pm 18.57 \mu\text{m}$ ($P < .05$, Figure 1c,d). The OTM amount decreased by 55% in the TG ($12.24 \pm 5.22 \mu\text{m}$) on day 5 ($P < .05$) and, by 61% in the TG ($31.13 \pm 13.34 \mu\text{m}$) compared with WT mice on day 12 ($P < .05$). There was no significant difference between groups on the unloaded control side ($P > .05$, data not shown).

Inhibition of NF- κ B in osteoblast lineage cells and PDL fibroblasts showed higher bone volume fraction compared with WT mice after orthodontic force application. The bone volume fraction (BV/TV) was examined on the compression side of the coronal one-

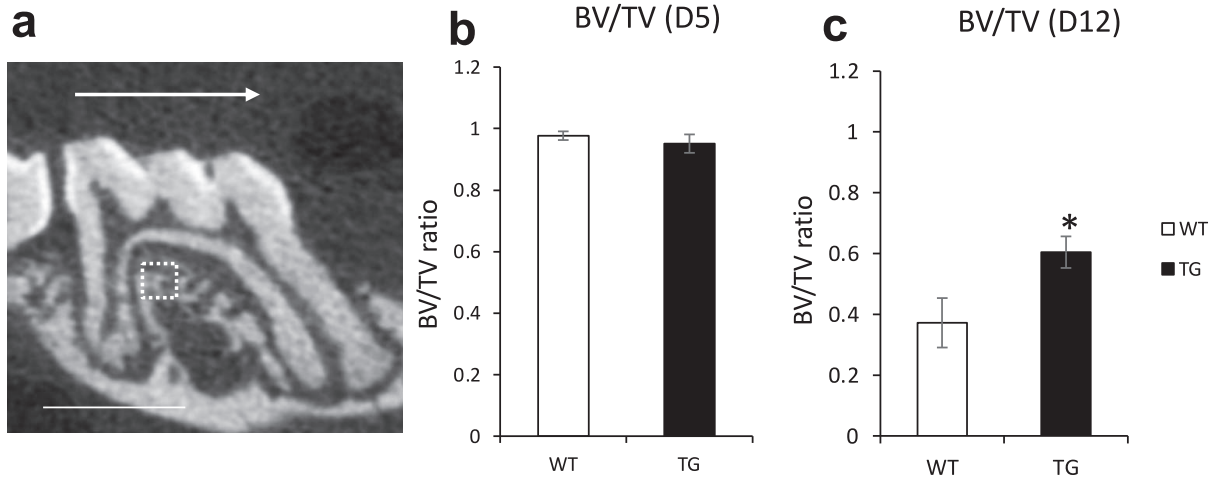


Figure 3. Inhibition of NF-κB in osteoblast lineage cells and PDL fibroblasts showed higher bone volume fraction after orthodontic force loading. (a) ROI: a 250 × 250 × 250 μm³ cube on the compression side of the coronal one-third of the distobuccal root of the maxillary first molar. Bar, 1 mm. (b and c) bone volume fraction (BV/TV) on days 5 and 12. Each in vivo value is the mean ± SEM for n = 8 mice per group. * P < .05 vs WT mice group.

third of the distobuccal root of the maxillary first molar (Figure 3a). MicroCT analysis revealed similar values on day 5 in the WT and experimental groups ($P > .05$, Figure 3b). On day 12, WT mice had a 63% decrease (0.37 ± 0.08) in bone volume fraction with orthodontic force compared to the unloaded side, which was almost twice the loss of bone density seen in TG mice ($P < .05$, Figure 3c).

Inhibition of NF-κB in osteoblast lineage cells and PDL fibroblasts showed narrower PDL width after orthodontic force application. The average PDL width on the compression side of the distobuccal root of the maxillary first molar was examined with microCT. As the bone on the compression side was resorbed by

osteoclasts, the PDL space was widened. The PDL width increased by 200% in WT mice after orthodontic force loading ($60.13 \pm 7.46 \mu\text{m}$) compared to the unloaded control side ($29.88 \pm 1.45 \mu\text{m}$) (Figure 4, $P < .05$). Conversely, there was no increase on the compression side in the TG mice ($36.88 \pm 5.31 \mu\text{m}$). The PDL width in the TG mice after mechanical force loading was significantly less than the WT mice ($P < .05$).

Inhibition of NF-κB in osteoblast lineage cells and PDL fibroblasts showed less osteoclast numbers and RANKL expression after orthodontic force application. Osteoclast formation was examined along the bone surface on the compression side of the distobuccal root of the maxillary first molar using the TRAP-stained sections. On mechanical force loading, the number of osteoclasts greatly increased in the WT mice and less in the TG mice (Figure 5a). On day 5, the osteoclast number was 86% less in the TG mice ($1.34 \pm 0.41/\text{mm}$) compared to the WT mice ($9.42 \pm 1.85/\text{mm}$) ($P < .05$; Figure 5b). There was no difference between groups on the unloaded control side ($P > .05$). On day 12, TG mice ($7.18 \pm 1.84/\text{mm}$) had half the number of osteoclasts compared to the WT mice ($14.56 \pm 2.67/\text{mm}$) ($P < .05$; Figure 5c).

To further investigate the potential mechanisms, RANKL expression was examined on the compression side by immunofluorescence. Mechanical loading caused an 8.7-fold increase in RANKL expression in WT mice ($440.74 \pm 163.79/\text{mm}^2$) compared with the control side ($50.49 \pm 26.10/\text{mm}^2$) on day 5, whereas this increase was significantly reduced in experimental TG mice ($31.98 \pm 20.99/\text{mm}^2$) ($P < .05$; Figure 6).

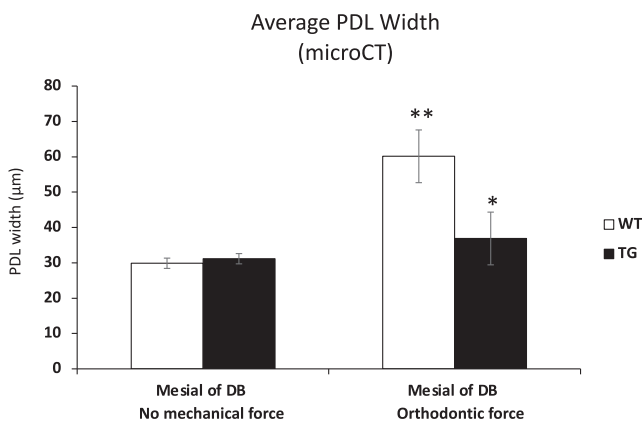


Figure 4. Inhibition of NF-κB in osteoblast lineage cells and PDL fibroblasts showed narrower PDL width after orthodontic force application (microCT). The average PDL width was measured on a sagittal section on the compression side of the distobuccal root of the maxillary right first molars. Each in vivo value is the mean ± SEM for n = 8 mice per group. * P < .05 vs WT mice group. ** P < .05 vs no mechanical force-matched mice group.

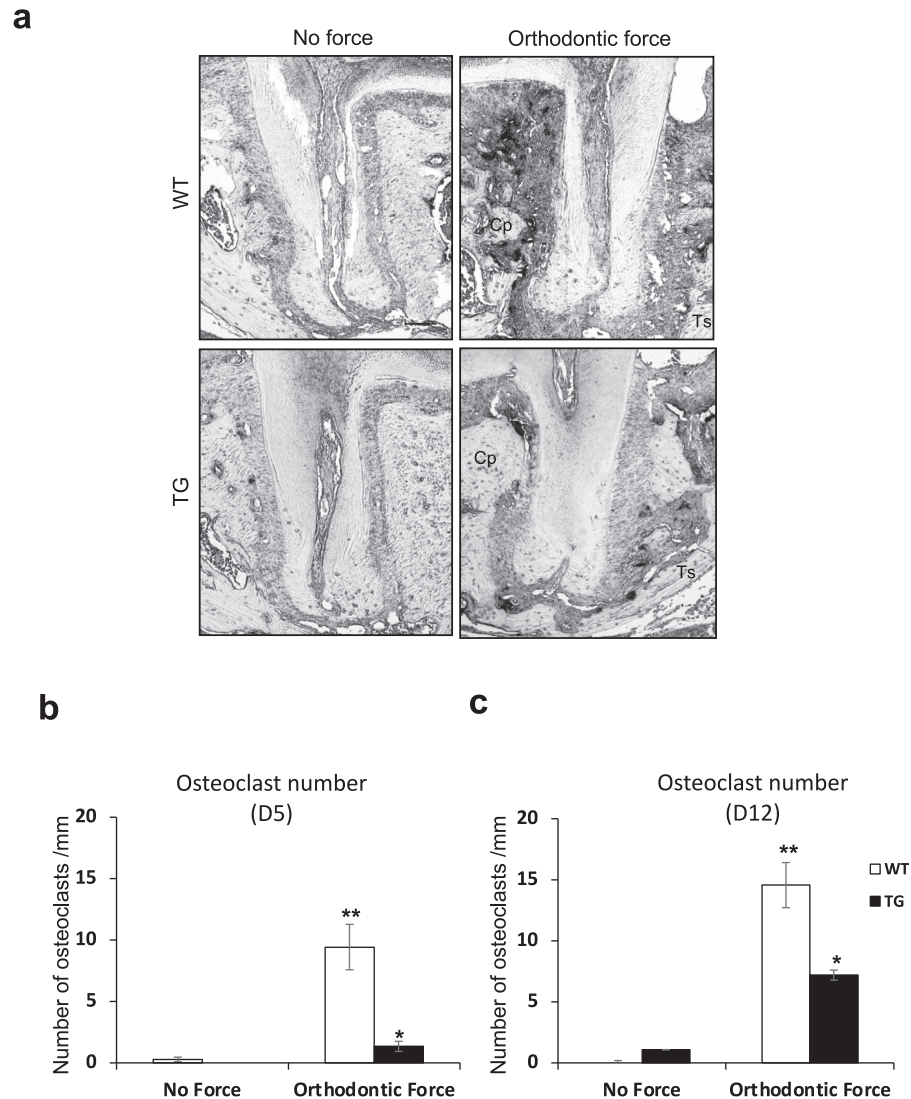


Figure 5. NF- κ B inhibition in osteoblast lineage cells and PDL fibroblasts decreased osteoclast formation on the compression side of orthodontic force (TRAP stain). (a) Representative images of TRAP-stained sections (100 \times original magnification, distobuccal root). Bar, 100 μ m. Cp, compression side; Ts: tension side. (b and c) Quantification of osteoclasts on days 5 and 12. Each in vivo value is the mean \pm SEM for $n = 7-8$ mice per group. * $P < .05$ vs WT mice group. ** $P < .05$ vs no mechanical force matched mice group.

DISCUSSION

This study demonstrated for the first time that inhibition of NF- κ B activation in osteoblast lineage cells and PDL fibroblasts significantly reduced OTM. This finding was further supported by less osteoclast formation, narrower PDL width, higher bone volume fraction, and reduced RANKL expression in experimental TG mice compared to WT mice. The results established the importance of osteoblast lineage cells and PDL fibroblasts in OTM in response to orthodontic forces mediated by NF- κ B regulation in these cells.

The NF- κ B signaling pathway plays important roles in physiological and pathological bone remodeling.^{27,28} Zuo et al. reported that NF- κ B was produced rapidly, mainly in osteoclasts, in response to orthodontic force

and NF- κ B activation was essential in RANKL-induced osteoclast differentiation in OTM.²⁹ A recent study demonstrated that vibration combined with orthodontic force increased the NF- κ B activation and RANKL expression in osteocytes in vivo and in vitro.³⁰ Similarly, continuous orthodontic force with high-frequency vibration increased osteoclastogenesis and accelerated OTM via NF- κ B activation in osteoblasts, osteocytes, and osteoclasts.³¹ However, this was the first study to examine the effect of NF- κ B on mechanical force-induced bone remodeling using lineage specific deletion models. NF- κ B activation was observed on the compression side in WT mice, which was considerably less in experimental TG mice, leading to significantly reduced OTM.

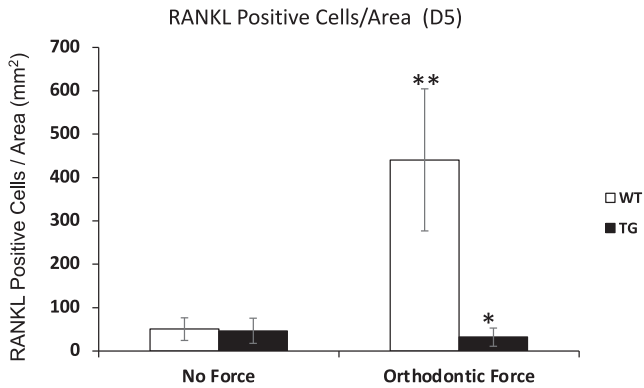


Figure 6. NF- κ B inhibition in osteoblast lineage cells and PDL fibroblasts decreased RANKL expression on the compression side of orthodontic force. Sagittal sections from wild-type (WT) and transgenic (TG) mice were treated by immunofluorescence stain with anti-RANKL antibody. The number of RANKL immunopositive cells per area was counted on the compression side. Each in vivo value is the mean \pm SEM for $n = 5-6$ mice per group. * $P < .05$ vs WT mice group. ** $P < .05$ vs no mechanical force matched mice group.

The roles of NF- κ B on RANKL-induced osteoclastogenesis are well understood.^{20,22,32} Inhibition of NF- κ B prevents precursor cell differentiation into osteoclasts by TNF and RANKL, clearly demonstrating that NF- κ B pathways are necessary for osteoclast differentiation and activity.³³ NF- κ B p50 and p52 double deficient mice demonstrate lack of osteoclasts.³⁴ Inversely, Otero et al. found that constitutive activation of NF- κ B was capable of inducing osteoclast differentiation in the absence of RANK or RANKL.³⁵ In the current study, both osteoclast formation and RANKL expression were found to be much less in TG mice with the NF- κ B inhibition in osteoblast lineage cells and PDL fibroblasts, compared with WT mice. The same transgenic mice were previously examined in a periodontitis model, demonstrating that nuclear localization of the NF- κ B, indicative of NF- κ B activation, in osteoblast lineage cells and PDL fibroblasts, was suppressed in experimental TG mice and that inhibition of NF- κ B activation blocked bone loss in normoglycemic and diabetic mice.^{9,11} Thus, osteoblastic cells and PDL fibroblasts activated by NF- κ B play a key role in bone remodeling in inflammatory periodontitis and in response to mechanical orthodontic forces.

The large number of PDL fibroblasts and osteoblast lineage cells, and their close proximity to alveolar bone, are consistent with their essential role in transducing mechanical forces that lead to bone resorption in response to orthodontic force. PDL fibroblasts constitute 50% to 60% of the total PDL cellularity,³⁶ are an important source of RANKL,^{4,9} and have been shown to stimulate osteoclast progenitor cells.³⁷ In addition, NF- κ B activation in osteoblasts is induced by mechanical force³⁸ and the inhibition of NF- κ B in osteoblast lineage

cells reduces bone resorption and enhances coupled bone formation to reduce periodontal bone loss.¹¹ Osteocytes, comprising >90% of all bone cells, show high levels of RANKL expression and support osteoclastogenesis in vitro³⁹ and in alveolar bone remodeling during OTM.⁶

In summary, it was demonstrated for the first time that osteoblast lineage cells and PDL fibroblasts play an essential role in OTM through NF- κ B regulation. Blocking NF- κ B activation in those cells significantly reduced osteoclastogenesis and RANKL expression in response to mechanical force and prevented tooth movement, indicating that the IKK/NF- κ B signaling pathway in these cells is needed to mediate OTM. These studies provide new understanding about the biologic response to mechanical force and suggest the clinical benefits of using NF- κ B activation/inhibition in clinical orthodontics.

CONCLUSIONS

- Inhibition of NF- κ B in osteoblast lineage cells and PDL fibroblasts significantly blocked OTM with significantly less osteoclast formation and PDL width, higher bone volume fraction, and less RANKL expression on the compression side in TG mice compared to WT mice, demonstrating the importance of osteoblast lineage cells and PDL fibroblasts in osteoclastogenesis during OTM via NF- κ B regulation.

ACKNOWLEDGMENTS

We thank Jiahui Madelaine Li for her help with sample staining procedure. This work was supported by NIDCR grants R01DE017732 and R01 AR0600 (DTG), the Schoenleber Pilot Grant from the University of Pennsylvania School of Dental Medicine (CHC) and the Orthodontic Faculty Development Fellowship Award from the American Association of Orthodontists Foundation (HHJ).

REFERENCES

1. Chang J, Wang Z, Tang E, et al. Inhibition of osteoblastic bone formation by nuclear factor-kappaB. *Nat Med*. 2009; 15(6):682–689.
2. Reitan K. Clinical and histologic observations on tooth movement during and after orthodontic treatment. *Am J Orthod*. 1967;53(10):721–745.
3. Yamaguchi M. RANK/RANKL/OPG during orthodontic tooth movement. *Orthod Craniofac Res*. 2009;12(2):113–119.
4. Yang CY, Jeon HH, Alshabab A, Lee YJ, Chung CH, Graves DT. RANKL deletion in periodontal ligament and bone lining cells blocks orthodontic tooth movement. *Int J Oral Sci*. 2018;10(1):3.
5. Takayanagi H. Osteoimmunology: shared mechanisms and crosstalk between the immune and bone systems. *Nat Rev Immunol*. 2007;7(4):292–304.

6. Shoji-Matsunaga A, Ono T, Hayashi M, Takayanagi H, Moriyama K, Nakashima T. Osteocyte regulation of orthodontic force-mediated tooth movement via RANKL expression. *Sci Rep*. 2017;7(1):8753.
7. Mabuchi R, Matsuzaka K, Shimono M. Cell proliferation and cell death in periodontal ligaments during orthodontic tooth movement. *J Periodontal Res*. 2002;37(2):118–124.
8. Giannopoulou C, Cimasoni G. Functional characteristics of gingival and periodontal ligament fibroblasts. *J Dent Res*. 1996;75(3):895–902.
9. Zheng J, Chen S, Albiero ML, et al. Diabetes activates periodontal ligament fibroblasts via NF-kappaB in vivo. *J Dent Res*. 2018;97(5):580–588.
10. Dacquin R, Starbuck M, Schinke T, Karsenty G. Mouse alpha1(I)-collagen promoter is the best known promoter to drive efficient Cre recombinase expression in osteoblast. *Dev Dyn*. 2002;224(2):245–251.
11. Pacios S, Xiao W, Mattos M, et al. Osteoblast lineage cells play an essential role in periodontal bone loss through activation of Nuclear Factor-Kappa B. *Sci Rep*. 2015;5:16694.
12. Mina M, Braut A. New insight into progenitor/stem cells in dental pulp using Col1a1-GFP transgenes. *Cells Tissues Organs*. 2004;176(1-3):120–133.
13. Braut A, Kollar EJ, Mina M. Analysis of the odontogenic and osteogenic potentials of dental pulp in vivo using a Col1a1-2.3-GFP transgene. *Int J Dev Biol*. 2003;47(4):281–292.
14. Kalajzic I, Kalajzic Z, Kaliterna M, et al. Use of type I collagen green fluorescent protein transgenes to identify subpopulations of cells at different stages of the osteoblast lineage. *J Bone Miner Res*. 2002;17(1):15–25.
15. Ting AY, Endy D. Signal transduction. Decoding NF-kappaB signaling. *Science*. 2002;298(5596):1189–1190.
16. Lin TH, Gibon E, Loi F, et al. Decreased osteogenesis in mesenchymal stem cells derived from the aged mouse is associated with enhanced NF-kappaB activity. *J Orthop Res*. 2017;35(2):281–288.
17. Krum SA, Chang J, Miranda-Carboni G, Wang CY. Novel functions for NFkappaB: inhibition of bone formation. *Nat Rev Rheumatol*. 2010;6(10):607–611.
18. Chang J, Liu F, Lee M, et al. NF-kappaB inhibits osteogenic differentiation of mesenchymal stem cells by promoting beta-catenin degradation. *Proc Natl Acad Sci U S A*. 2013;110(23):9469–9474.
19. Sui Y, Liu Z, Park SH, et al. IKKbeta is a beta-catenin kinase that regulates mesenchymal stem cell differentiation. *JCI Insight*. 2018;3(2).
20. Boyce BF, Yao Z, Xing L. Functions of nuclear factor kappaB in bone. *Ann N Y Acad Sci*. 2010;1192:367–375.
21. Abu-Amer Y. NF-kappaB signaling and bone resorption. *Osteoporos Int*. 2013;24(9):2377–2386.
22. Boyce BF, Xiu Y, Li J, Xing L, Yao Z. NF-kappaB-mediated regulation of osteoclastogenesis. *Endocrinol Metab (Seoul)*. 2015;30(1):35–44.
23. Taddei SR, Moura AP, Andrade I Jr, et al. Experimental model of tooth movement in mice: a standardized protocol for studying bone remodeling under compression and tensile strains. *J Biomech*. 2012;45(16):2729–2735.
24. Olson C, Uribe F, Kalajzic Z, et al. Orthodontic tooth movement causes decreased promoter expression of collagen type 1, bone sialoprotein and alpha-smooth muscle actin in the periodontal ligament. *Orthod Craniofac Res*. 2012;15(1):52–61.
25. Yadav S, Assefnia A, Gupta H, et al. The effect of low-frequency mechanical vibration on retention in an orthodontic relapse model. *Eur J Orthod*. 2016;38(1):44–50.
26. An J, Li Y, Liu Z, Wang R, Zhang B. A micro-CT study of microstructure change of alveolar bone during orthodontic tooth movement under different force magnitudes in rats. *Exp Ther Med*. 2017;13(5):1793–1798.
27. Novack DV. Role of NF-kappaB in the skeleton. *Cell Res*. 2011;21(1):169–182.
28. Luo JL, Kamata H, Karin M. IKK/NF-kappaB signaling: balancing life and death—a new approach to cancer therapy. *J Clin Invest*. 2005;115(10):2625–2632.
29. Zuo J, Archer LA, Cooper A, Johnson KL, Holliday LS, Dolce C. Nuclear factor kappaB p65 phosphorylation in orthodontic tooth movement. *J Dent Res*. 2007;86(6):556–559.
30. Sakamoto M, Fukunaga T, Sasaki K, et al. Vibration enhances osteoclastogenesis by inducing RANKL expression via NF-kappaB signaling in osteocytes. *Bone*. 2019;123:56–66.
31. Takano-Yamamoto T, Sasaki K, Fatemeh G, et al. Synergistic acceleration of experimental tooth movement by supplementary high-frequency vibration applied with a static force in rats. *Sci Rep*. 2017;7(1):13969.
32. Ruocco MG, Maeda S, Park JM, et al. I{kappa}B kinase (IKK){beta}, but not IKK{alpha}, is a critical mediator of osteoclast survival and is required for inflammation-induced bone loss. *J Exp Med*. 2005;201(10):1677–1687.
33. Luo G, Li F, Li X, Wang ZG, Zhang B. TNFalpha and RANKL promote osteoclastogenesis by upregulating RANK via the NFkappaB pathway. *Mol Med Rep*. 2018;17(5):6605–6611.
34. Iotsova V, Caamano J, Loy J, Yang Y, Lewin A, Bravo R. Osteopetrosis in mice lacking NF-kappaB1 and NF-kappaB2. *Nat Med*. 1997;3(11):1285–1289.
35. Otero JE, Dai S, Alhawagri MA, Darwech I, Abu-Amer Y. IKKbeta activation is sufficient for RANK-independent osteoclast differentiation and osteolysis. *J Bone Miner Res*. 2010;25(6):1282–1294.
36. McCulloch CA, Bordin S. Role of fibroblast subpopulations in periodontal physiology and pathology. *J Periodontal Res*. 1991;26(3 Pt 1):144–154.
37. Sokos D, Everts V, de Vries TJ. Role of periodontal ligament fibroblasts in osteoclastogenesis: a review. *J Periodontal Res*. 2015;50(2):152–159.
38. Granet C, Boutahar N, Vico L, Alexandre C, Lafage-Proust MH. MAPK and SRC-kinases control EGR-1 and NF-kappa B inductions by changes in mechanical environment in osteoblasts. *Biochem Biophys Res Commun*. 2001;284(3):622–631.
39. Nakashima T, Hayashi M, Fukunaga T, et al. Evidence for osteocyte regulation of bone homeostasis through RANKL expression. *Nat Med*. 2011;17(10):1231–1234.

Original Article

Clinical application of a FOXO1 inhibitor improves connective tissue healing in a diabetic minipig model

Hyeran H Jeon^{1,2*}, Quan Yu^{2,7*}, Lukasz Witek^{4*}, Yongjian Lu^{2,5}, Tianshou Zhang^{2,6}, Olga Stepanchenko², Victoria J Son², Evelyn Spencer², Temitope Oshilaja², Min K Shin², Faizan Alawi³, Paulo G Coelho^{4,8}, Dana T Graves²

*Departments of ¹Orthodontics, ²Periodontics, ³Basic & Translational Sciences, School of Dental Medicine, University of Pennsylvania, Philadelphia, PA, USA; ⁴Biomaterials and Biomimetics, College of Dentistry, New York University, New York, NY, USA; ⁵Department of Stomatology, Xinhua Hospital, School of Medicine, Shanghai Jiao Tong University, Shanghai, China; ⁶Department of Implantology, School and Hospital of Stomatology, Jilin University, Changchun, China; ⁷Department of Orthodontics, Ninth People's Hospital, School of Medicine, Shanghai Jiao Tong University, Shanghai, China; ⁸Hansjörg Wyss Department of Plastic Surgery, Langone Medical Center, New York University, New York, NY, USA. *Equal contributors.*

Received August 21, 2020; Accepted December 1, 2020; Epub February 15, 2021; Published February 28, 2021

Abstract: The forkhead box O1 (FOXO1) transcription factor plays a key role in wound healing process. Recently it has been reported that lineage-specific genetic ablation of FOXO1 significantly improves diabetic wound healing in a mouse model. To investigate the clinical usefulness of these findings, translational preclinical studies with a large animal model are needed. We report for the first time that the local application of a FOXO1 inhibitor (AS1842856) significantly improves connective tissue healing in a preclinical T2DM minipig model, reflected by increased collagen matrix formation, increased myofibroblast numbers, improved angiogenesis, and a shift in cell populations from pro-inflammatory (IL-1 β ⁺, TNF- α ⁺ and iNOS⁺) to pro-healing (CD163⁺). Our results set up the basis for the clinical application of a FOXO1 antagonist in early diabetic wounds where there is impaired connective tissue healing.

Keywords: Wound healing, forkhead box O1 (FOXO1), diabetes, hyperglycemia, minipig, inflammation skin

Introduction

According to the 2020 National Diabetes Statistics Report, 34.2 million people, 10.5% of the US population had diabetes in 2018 and the total estimated cost of diagnosed diabetes in the US in 2017 was \$327 billion [1]. One of the biggest diabetes-related complications is the delayed wound healing which increases the risk of infections and other serious complications [2]. The initial cause of impaired healing is due to complex factors such as an altered host response, increased and prolonged inflammation, a reduced rate of re-epithelialization, and a failure to form sufficient extracellular matrix [2]. Transcription factors coordinate the complex series of events needed for wound healing. The forkhead box O1 (FOXO1) transcription factor plays a key role in activating keratinocytes to participate in the wound healing process.

Lineage-specific FOXO1 deletion in keratinocytes interferes with keratinocyte migration, angiogenesis, and connective tissue formation in normal skin and mucosal wounds [3, 4] whereas FOXO1 haploinsufficiency accelerates the healing at normal skin wounds [5]. Interestingly, FOXO1 deletion in keratinocytes in diabetic wounds has the opposite effect, significantly improving the healing response [4, 6]. Despite the important roles of FOXO1 in the treatment of diabetic wounds, translational preclinical trials using a large animal model have not been carried out. Furthermore, no studies on the effect of FOXO1 in a T2DM model have been performed.

The minipig is frequently used as a preclinical large animal model for cutaneous wound healing and diabetes research [7, 8]. In both porcine and human skin, the relative thickness of the

epidermis and dermis, the epidermis' turnover time, and the immune cells in the skin are similar and the porcine wound healing model closely approximates the healing process in humans. In contrast to humans, rodents have a thin epidermis and a higher density of epidermal appendages and their healing occurs largely by contraction [9]. Furthermore, T2DM minipig models show similar metabolic abnormalities to humans including hyperglycemia, hyperlipidemia, insulin resistance, and a pro-inflammatory state [8]. In this study we demonstrate for the first time that the local application of a FOXO1 inhibitor significantly improved several parameters of connective tissue healing in a preclinical T2DM female minipig model, reflected by increased collagen formation, increased myofibroblast numbers, and improved angiogenesis. Mechanistically, FOXO1 inhibitor treatment reversed an anti-wound healing, pro-inflammatory environment as shown by reduced numbers of cells that express IL-1 β , TNF- α , and iNOS and a shift to increased numbers of CD163⁺ cells.

Materials and methods

T2DM minipig model

The following study was performed in accordance with the guidelines of the Institutional Animal Care and Use Committee (IACUC #: #17PCDI-001). Ten female Göttingen minipigs (3.0 \pm 0.6 years of age) were acquired and allowed to acclimate for 7 days. To induce T2DM the pigs were fed (2 times/day) a high-fat diet and subsequent low-dosage administration of streptozotocin (STZ) as previously described [10]. The cafeteria diet consisted of highly saturated hydrogenated fats, cholesterol, and sugar while the control pigs were fed with a "normal" low-fat standard diet (MH500, Test Diet, NJ, USA). The cohort of minipigs was randomly assigned to the DM group (n=5) and injected with a streptozotocin (STZ; Enzo Life Sciences, Raamsdonksveer, Netherlands) (20 mg/kg in 0.1-mol/L sodium citrate, pH 4.5) to induce the diabetic condition [10]. The DM group minipigs were treated with 25 g of glucose during STZ treatment to prevent hypoglycemia. Animal weight (initial weight, 8 weeks, 14 weeks and subsequently every 2 weeks until termination), complete blood count (CBC), and HOMA2-IR

value (calculated using fasting glucose and fasting insulin by HOMA calculator) were recorded. Fasting glucose was monitored weekly using Glucomen LX (A. Menarini Diagnostics, Berlin, Germany). The plasma cortisol and insulin levels were evaluated with the Porcine Insulin ELISA kit (Mercodia, Uppsala, Sweden) and Radioimmunoassay Coat-a-Count Cortisol (Siemens Healthcare Diagnostics, Los Angeles, CA). Blood assays were performed 6 weeks after STZ treatment.

Porcine skin wounding procedure

Skin wound procedures were performed as previously described [11]. Under general anesthesia, the full-thickness dorsal skin wounds were bilaterally approximately 3 cm from the midline starting at the level of the first thoracic vertebra (T1) using a 1-cm punch (depth: 1.2-cm, Acuderm inc., Fort Lauderdale, FL). FOXO1 inhibitor (AS1842856) was purchased from EMD Millipore (Billerica, Massachusetts) [12]. 10 mg of FOXO1 inhibitor was dissolved in 1.5 ml DMSO and diluted 100x in sterile PBS (2.0 mM) just prior to injection and the control was 1% DMSO in PBS. FOXO1 inhibitor or vehicle control was injected at six sites around each wound with 10 μ l per injection at the time of wounding and every other day. The last injection was performed 2 days before euthanization. Injections were performed at the level of the dermis (three on the upper half and another three on the lower half of the wound). One operator was responsible for all injections and was not blinded to the procedure as it was a split side design. On day 8 and 15 after surgery tissue was collected at the time of euthanasia with the use of a 3 cm biopsy punch to take the wound site and surrounding tissue.

Histology

Specimens were fixed in 4% paraformaldehyde in phosphate-buffered saline (PBS) for 24 h. Wounds were bisected at the center of the wound with the use of a dissecting microscope and embedded in paraffin. Five μ m paraffin sections were stained with H&E or Masson's trichrome in one batch and histomorphometric analysis was performed with NIS-elements image analysis software (Nikon, Melville, NY) at the center/edges of each lesion. Total 30-40

FOXO1 inhibitor improves diabetic connective tissue healing

Table 1. T2DM minipig models

	Normal	Diabetes	P value	
Weight (kg)	31.9±0.9	73.6±3.4	< 0.001	
Glucose (mg/dL)	70.4±3.0	153.8±13.9	0.001	
Cortisol (ug/dL)	5.41±1.3	11.1±1.6	0.01	
Insulin (uIU/mL)	5.41±1.3	9.2±1.2	0.03	
HOMA2-IR	% B	120±15.6	49±12.2	0.006
	% S	182.6±33.4	72.4±17.2	0.025
	IR	0.67±0.2	1.6±0.2	0.0008

images were taken with a 20× objective from the middle (10) and the two edges of the wound (10-15 per each) and combined using the Image Composite Editor (Microsoft, Redmond, WA). Images were examined by a double-blinded examiner and the results were confirmed with a second examiner.

Immunohistochemistry in histological sections

Immunofluorescence was performed as previously described [11] with the following primary antibodies: α-SMA (ab21027; Abcam, Cambridge, MA), CD31 (ab28364; Abcam), TNF-α (ab6671; Abcam), IL-1β (sc-7884; Santa Cruz, Dallas, TX), FOXO1 (ab70382; Abcam), iNOS (ABIN 615202, antibodies-online Inc., Limerick, PA) and CD163 (ABIN 2478731; antibodies-online Inc.). Image analysis was performed using NIS-Element software (Nikon). The number of immunopositive cells divided by the area was compared among different groups for each measured antibody. Blood vessels were described as small or moderate vessels depending on the number of endothelial cells associated with the vessel as previously described [13]. Images were examined by a double-blinded examiner and the results were confirmed with a second examiner.

Statistics

Statistical analysis with multiple groups was performed using ANOVA with Scheffe's posthoc test or non-parametric Kruskal-Wallis test with Dunn test. Statistical analysis between diabetic vehicle and diabetic FOXO1 inhibitor groups was performed using a 2-tailed paired t-test or non-parametric Wilcoxon matched-pairs signed-rank test. Results were expressed as the mean ± SEM. P < 0.05 was considered statistically significant.

Results

Establishment of T2DM minipig models

Eight months of full high-fat high-energy feeding and subsequent STZ injection resulted in an increase in body weight of 230% compared to control normal minipigs with the abnormalities in glucose tolerance and insulin sensitivity, characterized by hyperglycemia, compensatory hyperinsulinemia, and increased Homeostatic Model

Assessment 2 of Insulin Resistance (HOMA2-IR) value (P < 0.05, **Table 1**) [10].

FOXO1 inhibitor increases the collagen formation and the number of myofibroblasts in diabetic minipig wounds but does not have a significant effect on epithelial healing

Histologic examination of the H&E and Masson's trichrome-stained tissue sections showed open wounds at a mid-stage of healing with granulation tissue in the center of the wound and more mature healing at the wound edges. The edges and center of the wounds were examined separately. On day 8 we found that the epithelial gap and mean epithelial thickness were similar in both diabetic vehicle and FOXO1 inhibitor groups (P > 0.05, **Figure 1A-C**). Therefore, we focused on the connective tissue healing next. The production of collagen assessed with Masson's trichrome stain was decreased by 28-60% in diabetic wounds compared to wounds in normoglycemic minipigs. Local application of a FOXO1 inhibitor reversed the effect of T2DM, increasing the amount of collagen by 150-230% (P < 0.05, **Figure 1D, 1E**).

To probe the potential mechanisms, we examined the formation of myofibroblasts, which are crucial for extracellular matrix production and wound maturation [14]. Diabetes reduced the number of myofibroblasts by 43% compared with normal wounds. This reduction was rescued by treatment with FOXO1 inhibitor (P < 0.05, **Figure 2A-C**) so that the number of myofibroblasts rose to normal levels. In addition, we examined the wound samples at day 15 and found both FOXO1 inhibitor- and vehicle-treated group showed the complete re-epithelialization and similar collagen percentage at day 15 (data not shown).

FOXO1 inhibitor improves diabetic connective tissue healing

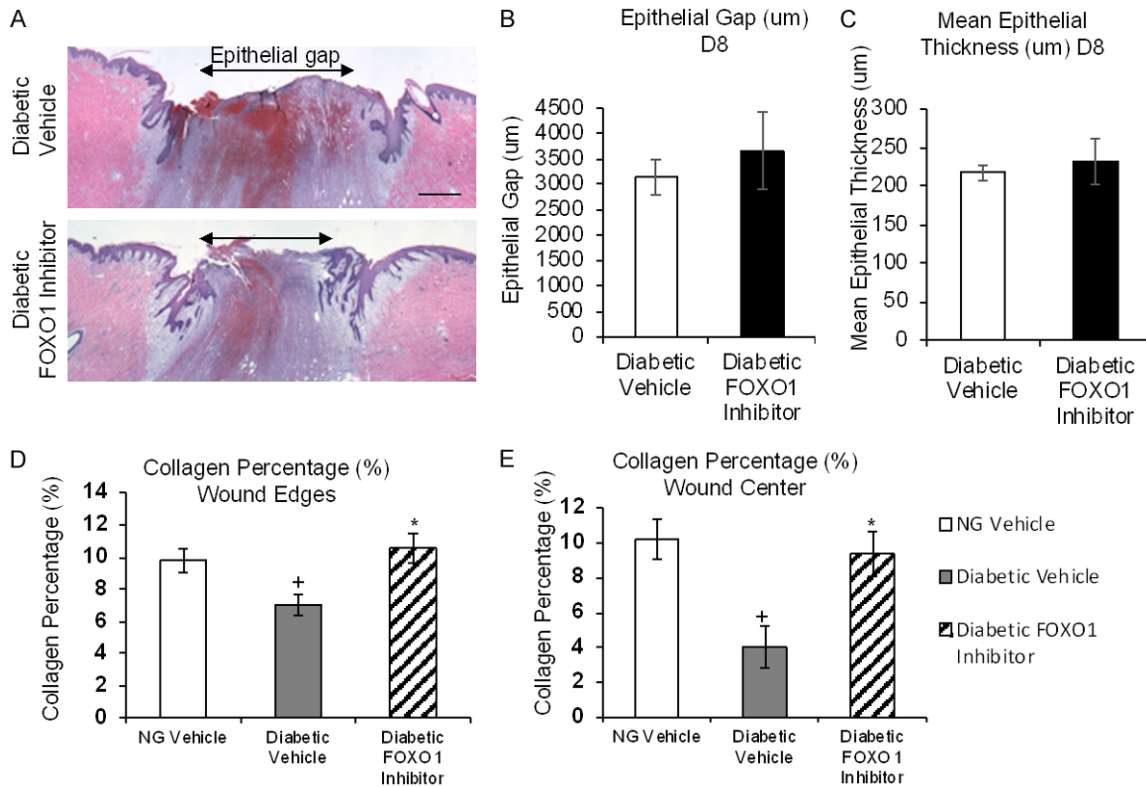


Figure 1. Local application of a FOXO1 inhibitor improves connective tissue by not epithelial healing in a preclinical T2DM minipig model. A. H&E stained sections (2 \times), bar =1000 μ m. B. Epithelial gap (μ m). C. Mean epithelial thickness (μ m). D, E. Quantitative analyses of newly formed collagen at the wound edges and center measured in Masson's trichrome stained sections. Each *in vivo* value is the mean \pm SEM for n=5 minipigs per group. *, P < 0.05 versus diabetic vehicle group; †, P < 0.05 versus normal vehicle group. Bar, 50 μ m.

FOXO1 inhibitor improves the wound angiogenesis in diabetic minipig wounds

We examined the wound angiogenesis using an endothelial cell marker, CD31, which is expressed in immature microvascular endothelial cells as well as mature endothelial cells in small to moderate-sized vessels [13]. Diabetes reduced the number of CD31-immunopositive single cells and moderate-sized vessels by 34-54% compared with normal wounds, which was rescued by 157-198% by FOXO1 inhibitor at the wound edge (P < 0.05, **Figure 3A-C**). We did not observe the statistically significant difference in small-sized vessels and wound centers (P > 0.05, data not shown).

FOXO1 inhibitor causes a shift in cell populations

Since inflammation has been shown to impair diabetic wound healing [15], we examined IL-1 β and TNF- α levels in diabetic wounds. A patholo-

gist (FA, co-author) determined that the cell types which express IL-1 β and TNF- α were largely leukocytes, endothelial cells, and fibroblastic cells as supported by other studies [16]. Immunopositive cells were counted at both the wound edges and wound center. IL-1 β immunopositive cells increased by ~10 fold and TNF- α levels increased by 4-22 fold in diabetic wounds compared with normoglycemic wounds (P < 0.05, **Figure 4A-F**). Treatment with a FOXO1 inhibitor rescued the high numbers of IL-1 β ⁺ and TNF- α ⁺ caused by diabetes (P < 0.05, **Figure 4A-F**). We also investigated inducible nitric oxide synthase (iNOS) and CD163 expressing cells. The number of iNOS⁺ cells increased by 5-11 folds in diabetic wounds compared with normoglycemic wounds, whereas FOXO1 inhibition blocked this increase (P < 0.05, **Figure 4G**). In contrast, the number of CD163⁺ cells, positively associated with enhanced wound healing, decreased by 76-83% in diabetic wounds compared with normoglycemic

FOXO1 inhibitor improves diabetic connective tissue healing

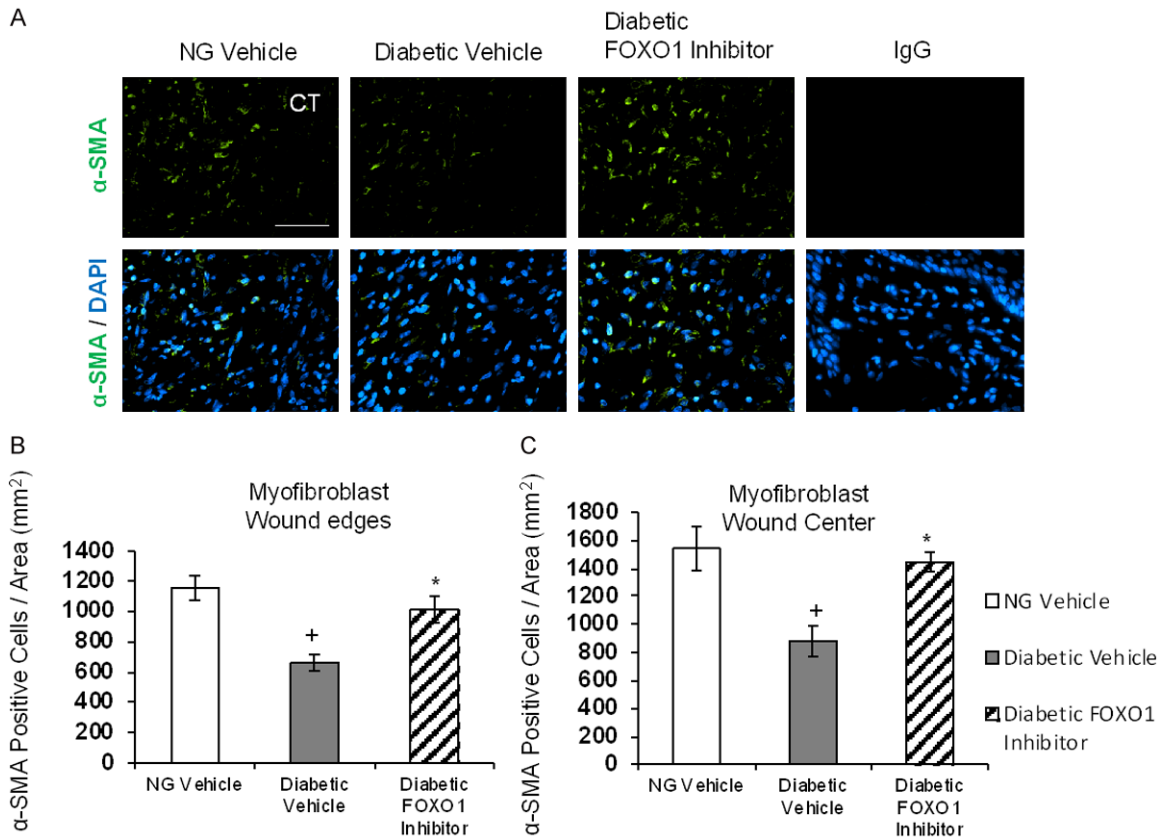


Figure 2. Local application of a FOXO1 inhibitor significantly improves myofibroblast numbers in a preclinical T2DM minipig model. A-C. α -SMA immunofluorescence analyses (40 \times). EPI, epithelium; CT, connective tissue. Each *in vivo* value is the mean \pm SEM for n=5 minipigs per group. *, P < 0.05 versus diabetic vehicle group; +, P < 0.05 versus normal vehicle group. Bar, 50 μ m.

wounds, and treatment of diabetic wounds with a FOXO1 inhibitor reversed this decline, increasing CD163⁺ cells by 4-5 fold in diabetic minipigs (P < 0.05, **Figure 4H**).

Discussion

Data presented here demonstrate that the application of a FOXO1 inhibitor improves connective tissue healing in T2DM minipig dermal wounds. The improved healing was reflected by greater production of connective tissue matrix, enhanced myofibroblast formation, and greater angiogenesis in diabetic wounds. Mechanistic studies indicate that the FOXO1 reduced the formation of a pro-inflammatory environment that is known to interfere with the healing process in diabetic wounds [15]. These studies were carried out in a large animal minipig model, which is needed for a pre-clinical study to expand the validity and translational applicability [17]. Studies in pigs show a much higher

concordance with human studies (78%) compared with small laboratory animals (53%) and *in vitro* results (57%) [18]. In addition, results presented here show for the first time that FOXO1 inhibition can improve connective tissue healing in type-2 diabetic wounds, demonstrating its translational value.

Several aspects of wound healing were improved by FOXO1 inhibition in the type-2 diabetic minipigs. This is reflected by greater production of connective tissue matrix, enhanced myofibroblast formation, and greater angiogenesis in diabetic wounds. A distinctive feature of diabetic wound healing is increased and prolonged inflammation [19]. Pro-inflammatory mediators such as TNF- α and IL-1 β and enzymes that produce reactive oxygen species are increased in diabetes and contribute to diabetic complications, including deficient wound angiogenesis and prolonged inflammation [19-21]. Increased levels of TNF- α may limit the

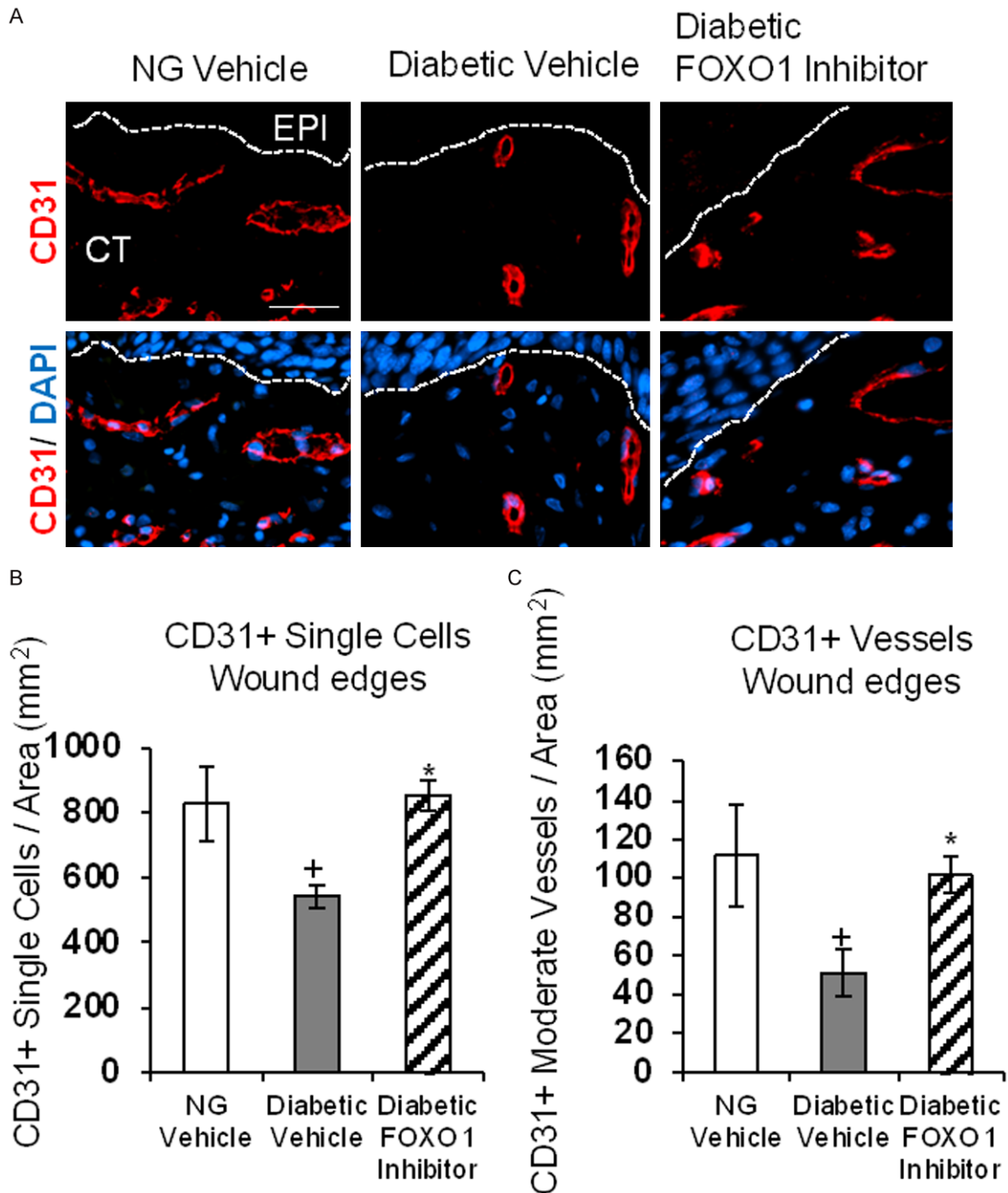
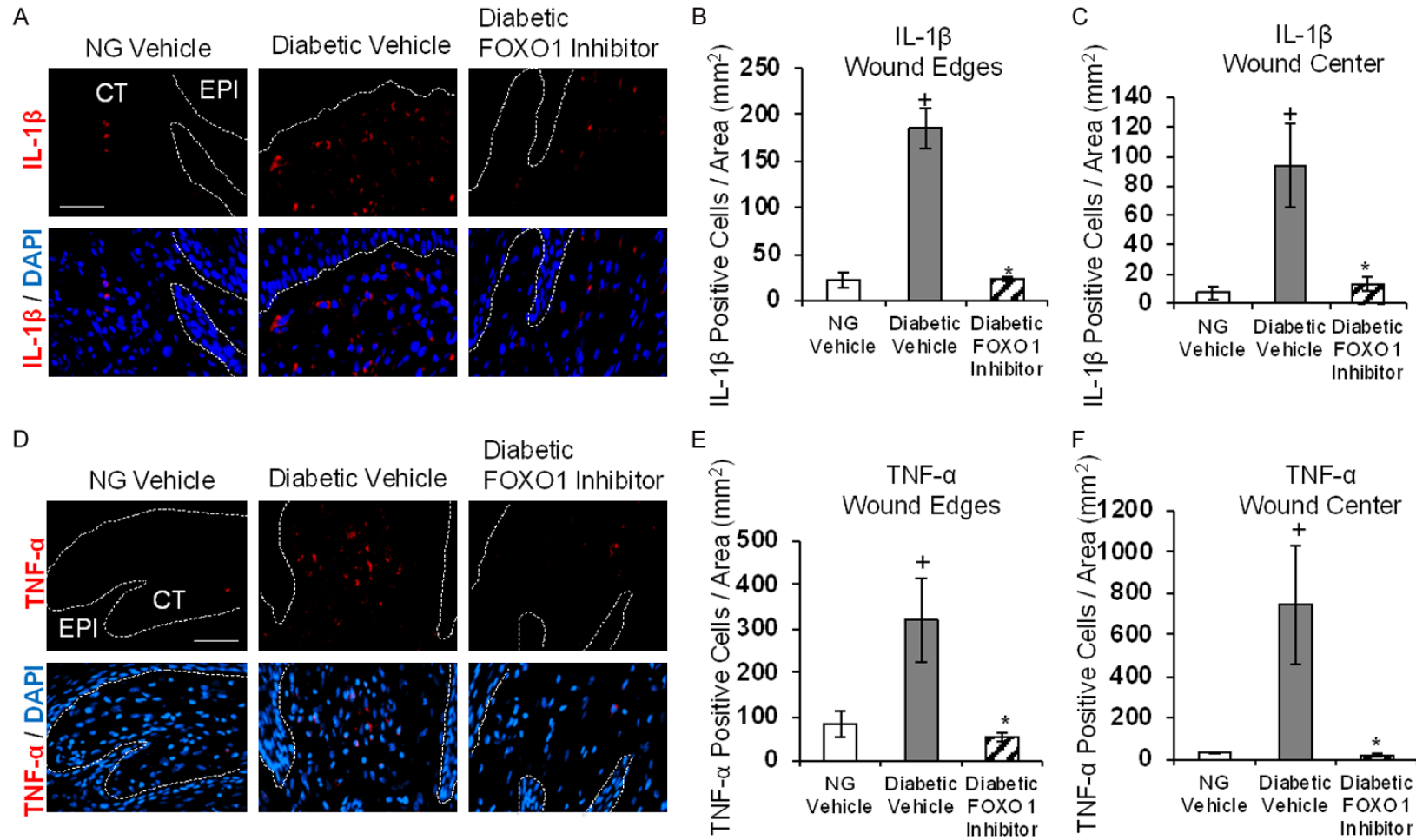


Figure 3. Local application of a FOXO1 inhibitor significantly improves wound angiogenesis. A. CD31 immunofluorescence (40 \times). IgG control was negative (data not shown). B, C. Quantitative analyses of CD31 immuno-positive single cells and moderate-sized vessels at the wound edge. EPI, epithelium; CT, connective tissue. Each *in vivo* value is the mean \pm SEM for n=5 minipigs per group. *, P < 0.05 versus diabetic vehicle group; ⁺, P < 0.05 versus normal vehicle group. Bar, 50 μ m.

capacity of diabetics to downregulate other inflammatory genes [15, 18, 22]. In this study, we found that FOXO1 inhibition reduced the number of cells that expressed IL-1 β , TNF- α ,

and iNOS. This is important since reducing prolonged inflammation improves the healing of wounds in T2DM animals [15, 22] and consistent with reports that FOXO1 promotes IL-1 β

FOXO1 inhibitor improves diabetic connective tissue healing



FOXO1 inhibitor improves diabetic connective tissue healing

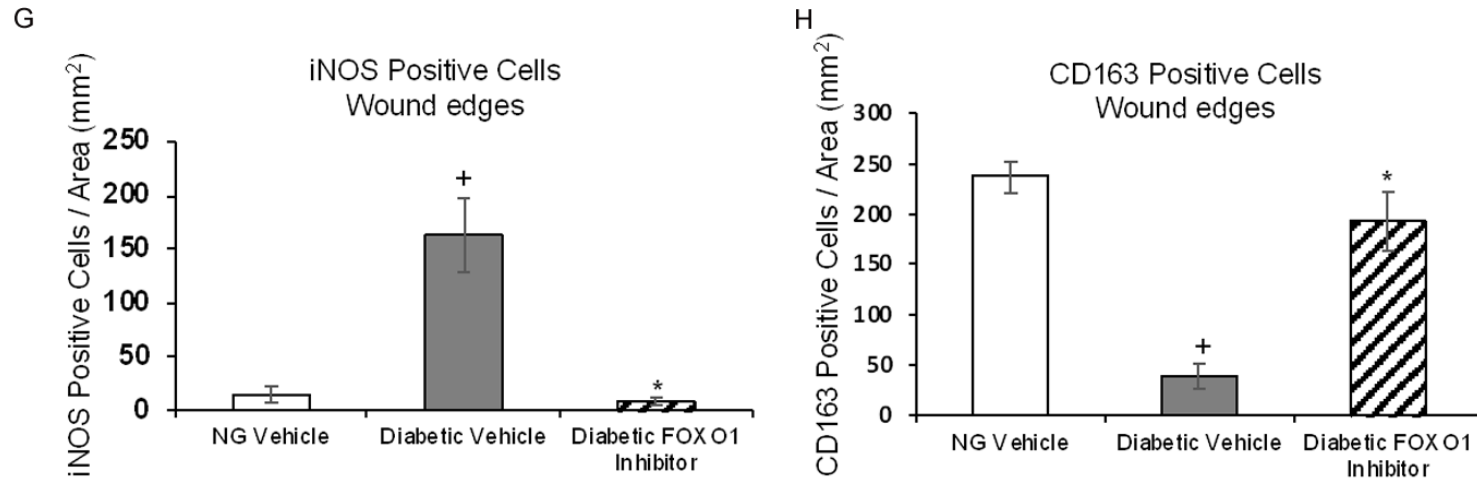


Figure 4. Local application of a FOXO1 inhibitor reduces the number of inflammatory cells and increases the number of CD163⁺ cells in diabetic wounds. A. IL-1 β immunofluorescence (40 \times). B, C. Quantitative analyses of IL-1 β immunopositive cells at the wound edge and center area. D. TNF- α immunofluorescence (40 \times). E, F. Quantitative analyses of TNF- α immunopositive cells at wound edge and center area. G, H. Quantitative analyses of iNOS and CD163 immunopositive cells at wound edge. EPI, epithelium; CT, connective tissue. Each *in vivo* value is the mean \pm SEM for n=5 minipigs per group. *, P < 0.05 versus diabetic vehicle group; +, P < 0.05 versus normal vehicle group. Bar, 50 μ m.

FOXO1 inhibitor improves diabetic connective tissue healing

production [23]. Moreover, previous studies support the effect of the FOXO1 inhibition in diabetic wounds, consistent with our results. IL-6 is an important proinflammatory cytokine during wound healing and its dysregulation is a hallmark of diabetes [24, 25]. FOXO1 activation triggered by TNF- α has been reported to increase the expression of IL-6 through direct binding of FOXO1 to its promoter, while FOXO1 knockdown inhibited IL-6 expression [26]. In addition, high glucose increases FOXO1 interactions with consensus FOXO1 response elements in CCL20, IL-36 γ , MMP9, and SERPINB2 promoters, which increase transcription in a FOXO1-dependent manner [4, 6, 27]. High levels of CCL20, IL-36 γ , MMP9, and SERPINB2 in diabetic conditions interfere with keratinocyte migration, which leads to the impaired wound healing. Given that high glucose stimulates FOXO1 binding to promoter regions of proinflammatory genes [3, 4, 6], FOXO1 may be a key factor that leads to greater inflammation under hyperglycemic conditions. We also examined CD163, which is associated with a pro-wound healing environment [28]. Diabetes reduced CD163⁺ cells and the FOXO1 inhibitor largely reversed this effect of diabetes. The improved wound healing environment is also reflected by the increased angiogenesis, which was improved by the application of a FOXO1 inhibitor. The angiogenic balance is modulated by multiple factors, such as hyperglycemia-induced oxidative stress, cytokines, and inflammatory factors [29]. Lim et al. reported that the inflammation plays a major role in diabetes-impaired angiogenesis in fracture healing through its effect on microvascular endothelial cells through a FOXO1 dependent mechanism [13]. High levels of TNF- α , high glucose, and advanced glycation endproducts (AGEs) reduced proliferation and enhanced apoptosis of microvascular endothelial cells mediated by FOXO1. Therefore, the reduction of inflammation by a FOXO1 inhibition can be an important factor in the improvement of the diabetic wound healing process as reflected by increased angiogenesis.

Interestingly, we did not observe the clear effect of a FOXO1 inhibition on the epithelial healing in diabetic minipig wounds whereas we previously found that the keratinocyte-specific FOXO1 deletion improved the keratinocyte migration and wound healing accordingly in dia-

betic mouse models. This discrepancy might be due to the different animal models [9]. Healing in pig wounds is more comparable to humans with similar epidermal/dermal ratios, epidermal turnover time, types of keratinous proteins, the composition of lipids in the skin, blood vessel size, and circulation. An alternative explanation is that the genetic model with lineage specific FOXO1 deletion in keratinocytes may more effectively impact re-epithelialization compared to the use of an inhibitor, due to pharmacokinetics and biodistribution of the inhibitor.

Our results focused on an early phase of wound healing. We also examined a second-time point, day 15, and found no differences between FOXO1 inhibitor- and vehicle-treated groups (data not shown). Thus, we conclude that the primary benefit of FOXO1 inhibition is during the early phases. This is consistent with the major effect of FOXO1 contributing to an inflammatory environment under diabetic conditions that delays healing [4, 15]. Thus, FOXO1 in diabetic wounds may interfere with the resolution of inflammation to delay wound healing. Inhibition of FOXO1 in diabetic wounds may facilitate early healing by reducing inflammation and improving connective tissue formation and angiogenesis.

Acknowledgements

We thank Jayden Kwak, Issam Ghaben, Marie-Elena Cronin, Jiahui Madelaine Li and Pooja Patel for their help with sample processing and image analysis. This work was supported by a grant R01DE019108 from the NIDCR and ITI grant #926-2013.

Disclosure of conflict of interest

None.

Address correspondence to: Dana T Graves, Department of Periodontics, School of Dental Medicine, University of Pennsylvania, 240 South 40th Street, Philadelphia 19104-6030, PA, USA. Tel: 215-573-8818; Fax: 215-573-8071; E-mail: dtgraves@upenn.edu

References

- [1] Prevention CfDca. National Diabetes Statistics Report. Atlanta, GA: Centers for Disease Control and Prevention, U.S. Dept of Health and Human Services, 2020.

FOXO1 inhibitor improves diabetic connective tissue healing

- [2] Eming SA, Martin P and Tomic-Canic M. Wound repair and regeneration: mechanisms, signaling, and translation. *Sci Transl Med* 2014; 6: 265sr266.
- [3] Zhang C, Lim J, Liu J, Ponugoti B, Alsadun S, Tian C, Vafa R and Graves DT. FOXO1 expression in keratinocytes promotes connective tissue healing. *Sci Rep* 2017; 7: 42834.
- [4] Xu F, Othman B, Lim J, Batres A, Ponugoti B, Zhang C, Yi L, Liu J, Tian C, Hameedalddeen A, Alsadun S, Tarapore R and Graves DT. Foxo1 inhibits diabetic mucosal wound healing but enhances healing of normoglycemic wounds. *Diabetes* 2015; 64: 243-256.
- [5] Mori R, Tanaka K, de Kerckhove M, Okamoto M, Kashiwama K, Tanaka K, Kim S, Kawata T, Komatsu T, Park S, Ikematsu K, Hirano A, Martin P and Shimokawa I. Reduced FOXO1 expression accelerates skin wound healing and attenuates scarring. *Am J Pathol* 2014; 184: 2465-2479.
- [6] Zhang C, Ponugoti B, Tian C, Xu F, Tarapore R, Batres A, Alsadun S, Lim J, Dong G and Graves DT. FOXO1 differentially regulates both normal and diabetic wound healing. *J Cell Biol* 2015; 209: 289-303.
- [7] Stricker-Krongrad A, Shoemake CR, Liu J, Brocksmith D and Bouchard G. The importance of minipigs in dermal safety assessment: an overview. *Cutan Ocul Toxicol* 2017; 36: 105-113.
- [8] Bellinger DA, Merricks EP and Nichols TC. Swine models of type 2 diabetes mellitus: insulin resistance, glucose tolerance, and cardiovascular complications. *ILAR J* 2006; 47: 243-258.
- [9] Dorsett-Martin WA. Rat models of skin wound healing: a review. *Wound Repair Regen* 2004; 12: 591-599.
- [10] Coelho PG, Pippenger B, Tovar N, Koopmans SJ, Plana NM, Graves DT, Engebretson S, van Beusekom HMM, Oliveira P and Dard M. Effect of obesity or metabolic syndrome and diabetes on osseointegration of dental implants in a miniature swine model: a pilot study. *J Oral Maxillofac Surg* 2018; 76: 1677-1687.
- [11] Jeon HH, Yu Q, Lu Y, Spencer E, Lu C, Milovanova T, Yang Y, Zhang C, Stepanchenko O, Vafa RP, Coelho PG and Graves DT. FOXO1 regulates VEGFA expression and promotes angiogenesis in healing wounds. *J Pathol* 2018; 245: 258-264.
- [12] Nagashima T, Shigematsu N, Maruki R, Urano Y, Tanaka H, Shimaya A, Shimokawa T and Shibasaki M. Discovery of novel forkhead box O1 inhibitors for treating type 2 diabetes: improvement of fasting glycemia in diabetic db/db mice. *Mol Pharmacol* 2010; 78: 961-970.
- [13] Lim JC, Ko KI, Mattos M, Fang M, Zhang C, Feinberg D, Sindi H, Li S, Alblowi J, Kayal RA, Einhorn TA, Gerstenfeld LC and Graves DT. TNF- α contributes to diabetes impaired angiogenesis in fracture healing. *Bone* 2017; 99: 26-38.
- [14] Hinz B, Phan SH, Thannickal VJ, Galli A, Bochaton-Piallat ML and Gabbiani G. The myofibroblast: one function, multiple origins. *Am J Pathol* 2007; 170: 1807-1816.
- [15] Siqueira MF, Li J, Chehab L, Desta T, Chino T, Krothpali N, Behl Y, Alikhani M, Yang J, Braasch C and Graves DT. Impaired wound healing in mouse models of diabetes is mediated by TNF- α dysregulation and associated with enhanced activation of forkhead box O1 (FOXO1). *Diabetologia* 2010; 53: 378-388.
- [16] Mast BA and Schultz GS. Interactions of cytokines, growth factors, and proteases in acute and chronic wounds. *Wound Repair Regen* 1996; 4: 411-420.
- [17] Epstein SE, Luger D and Lipinski MJ. Large animal model efficacy testing is needed prior to launch of a stem cell clinical trial: an evidence-lacking conclusion based on conjecture. *Circ Res* 2017; 121: 496-498.
- [18] Sullivan TP, Eaglstein WH, Davis SC and Mertz P. The pig as a model for human wound healing. *Wound Repair Regen* 2001; 9: 66-76.
- [19] Wang Y and Graves DT. Keratinocyte function in normal and diabetic wounds and modulation by FOXO1. *J Diabetes Res* 2020; 2020: 3714704.
- [20] Graves DT and Kayal RA. Diabetic complications and dysregulated innate immunity. *Front Biosci* 2008; 13: 1227-1239.
- [21] Nikolajczyk BS, Jagannathan-Bogdan M, Shin H and Gyurko R. State of the union between metabolism and the immune system in type 2 diabetes. *Genes Immun* 2011; 12: 239-250.
- [22] Huang SM, Wu CS, Chiu MH, Wu CH, Chang YT, Chen GS and Lan CE. High glucose environment induces M1 macrophage polarization that impairs keratinocyte migration via TNF- α : an important mechanism to delay the diabetic wound healing. *J Dermatol Sci* 2019; 96: 159-167.
- [23] Su D, Coudriet GM, Hyun Kim D, Lu Y, Perdomo G, Qu S, Slusher S, Tse HM, Piganelli J, Gianoukakis N, Zhang J and Dong HH. FoxO1 links insulin resistance to proinflammatory cytokine IL-1 β production in macrophages. *Diabetes* 2009; 58: 2624-2633.
- [24] Lee EG, Lockett-Chastain LR, Calhoun KN, Frempah B, Bastian A and Gallucci RM. Interleukin 6 function in the skin and isolated keratinocytes is modulated by hyperglycemia. *J Immunol Res* 2019; 2019: 5087847.

FOXO1 inhibitor improves diabetic connective tissue healing

- [25] Nishikai-Yan Shen T, Kanazawa S, Kado M, Okada K, Luo L, Hayashi A, Mizuno H and Tanaka R. Interleukin-6 stimulates Akt and p38 MAPK phosphorylation and fibroblast migration in non-diabetic but not diabetic mice. *PLoS One* 2017; 12: e0178232.
- [26] Ito Y, Daitoku H and Fukamizu A. Foxo1 increases pro-inflammatory gene expression by inducing C/EBPbeta in TNF-alpha-treated adipocytes. *Biochem Biophys Res Commun* 2009; 378: 290-295.
- [27] Zhang C, Lim J, Jeon HH, Xu F, Tian C, Miao F, Hameedaldeen A and Graves DT. FOXO1 deletion in keratinocytes improves diabetic wound healing through MMP9 regulation. *Sci Rep* 2017; 7: 10565.
- [28] Ferreira DW, Ulecia-Moron C, Alvarado-Vazquez PA, Cunnane K, Moracho-Vilriales C, Grosick RL, Cunha TM and Romero-Sandoval EA. CD163 overexpression using a macrophage-directed gene therapy approach improves wound healing in ex vivo and in vivo human skin models. *Immunobiology* 2020; 225: 151862.
- [29] Cheng R and Ma JX. Angiogenesis in diabetes and obesity. *Rev Endocr Metab Disord* 2015; 16: 67-75.

Short-term and long-term effects of rapid maxillary expansion on the nasal soft and hard tissue: *A cone beam computed tomography study*

Cassie T. Truong^a; Hyeran H. Jeon^b; Puttipong Sripinun^c; Ann Tierney^d; Normand S. Boucher^e

ABSTRACT

Objectives: To evaluate nasal soft and hard tissue changes immediately post-rapid maxillary expansion (RME) and to assess the stability of these changes using cone beam computed tomography (CBCT).

Materials and Methods: A total of 35 treatment group (TG) patients (18 girls, 17 boys; 9.39 ± 1.4) had a pre-RME CBCT and a post-RME CBCT approximately 66 days after expansion, and 25 patients had a follow-up CBCT 2.84 years later. A total of 28 control group (CG; no RME) patients (16 girls, 12 boys; 8.81 ± 1.6) had an initial CBCT and a CBCT an average of 2.25 years later. Soft and hard tissue nasal landmarks were measured in transverse, sagittal, and coronal planes of space on CBCT scans. Differences within the same group were evaluated by paired *t*-tests or Wilcoxon signed-rank tests. Long-term comparisons between TG and CG were evaluated by independent-sample *t*-tests or Wilcoxon rank-sum tests.

Results: Immediately post-RME, there were statistically significant mean increases of 1.6 mm of alar base width, 1.77 mm of pyriform height, and 3.57 mm of pyriform width ($P < .05$). CG showed the significant increases over 2.25 years ($P < .001$). Compared with CG, the long-term evaluation of TG demonstrated only pyriform height and pyriform width showed a statistically significant difference ($P < .01$).

Conclusions: Although RME produced some significant increase on the nasal soft tissue immediately after expansion, it regressed to the mean of normal growth and development over time. However, long-term evaluation of TG compared with CG showed only pyriform height and pyriform width to be affected by RME. (*Angle Orthod.* 2021;91:46–53.)

KEY WORDS: Rapid maxillary expansion (RME); Nasal tissues; Long term; Short term

The first two authors contributed equally to this work.

^a Private Practice, Seattle, Wash, USA.

^b Assistant Professor, Department of Orthodontics, School of Dental Medicine, University of Pennsylvania, Philadelphia, Pa, USA.

^c Orthodontic Resident, Department of Orthodontics, School of Dental Medicine, University of Pennsylvania, Philadelphia, Pa, USA.

^d Biostatistician, Center for Clinical Epidemiology and Biostatistics, Perelman School of Medicine, University of Pennsylvania, Philadelphia, Pa, USA.

^e Associate Clinical Professor, Department of Orthodontics, School of Dental Medicine, University of Pennsylvania, Philadelphia, Pa, USA.

Corresponding author: Dr Normand S. Boucher, 333 W. Lancaster Ave., Wayne, PA 19087, USA
(e-mail: nsjboucher@gmail.com)

Accepted: July 2020. Submitted: February 2020.

Published Online: October 12, 2020

© 2021 by The EH Angle Education and Research Foundation, Inc.

INTRODUCTION

Rapid maxillary expansion (RME) is a common way to correct a narrow maxilla in adolescents. In addition, it helps eliminate mandibular shifts upon closure, provides more space for erupting maxillary teeth, and lessens dental arch distortion and potential tooth abrasion from dental interferences.^{1–4} The skeletal effects for the maxillary hard tissue changes are well documented, but there are fewer studies that examine RME effects on the nasal soft and hard tissue. Furthermore, the previous studies that have evaluated nasal tissue changes have been limited and contradictory, and utilized a variety of data intake modalities, making their findings unclear.

The earliest study was by Berger et al.⁵ in 1999, which analyzed photographic renderings of facial changes associated with maxillary expansion. They found an increase in nasal width post-orthopedic and

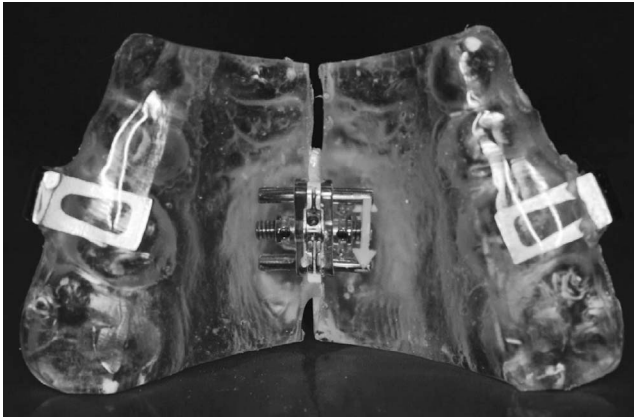


Figure 1. All patients of TG were delivered a bonded rapid maxillary expander extending from the primary or permanent canine to the permanent first molar.

surgical expansion that was maintained 1 year after treatment. Filho et al.⁶ also used facial analysis to assess nasal morphology in children following RME and found contradictory results to Berger et al.,⁵ concluding that RME had no impact on nasal morphology. Johnson et al.⁷ used a caliper and clinical measurements reporting significant increases of alar width (defined as greater alar cartilage) in the RME group in age groups 11 to 13 compared with a normative sample group, but this increase did not show a clinically significant effect. Santariello et al.⁸ analyzed nasal dimensions in pre-pubertal patients during clinical sessions similar to Johnson et al.⁷ and were in agreement that RME induced an increase in alar width. These studies used a variety of methods from photographic analysis to in-person clinical exams and were limited to only evaluating nasal changes immediately following RME. These methods can introduce various errors, including frontal photographic error, examiner bias, and patient movement during clinical exams. Studies that have employed a variety of traditional two-dimensional cephalometrics neglect structures lateral to the midline, cannot measure the transverse dimension, and have difficulty in reliably identifying soft tissue landmarks.

Recent cone beam computed tomography (CBCT) studies introduced a more accurate and reproducible method in evaluating in the transverse dimension. In 2012, Kim et al.⁹ was one of the first CBCT studies to evaluate nasal soft tissue changes. This was followed by Badreddine et al.^{10,11} in 2018, who studied changes in the noses of mouth-breathing patients using multi-slice computed tomography scans. These studies focused on the short-term nasal soft and hard tissue changes after expansion.

This is the first study to compare the long-term effect of RME on nasal tissue with a nontreatment control

group using CBCT. The goal of this study was to evaluate the short-term and long-term effects of RME on nasal soft and hard tissue and compare the effects with a control group using CBCT.

MATERIALS AND METHODS

The study consisted of 63 patients, of which 35 patients (18 girls, 17 boys; average age 9.39 ± 1.4) were diagnosed with a constricted maxilla, treated with RME, and placed in the treatment group (TG). The remaining 28 patients (16 girls, 12 boys; average age 8.81 ± 1.6) were only subjected to routine records and placed in the control group (CG). All patients were evaluated at the private practice office of Dr Boucher. Exclusionary factors included patients with severe skeletal asymmetries, craniofacial anomalies, and syndromic patients and patients with prior orthodontic treatment or any other surgeries in the craniofacial complex. This retrospective study was approved by the Institutional Review Board, University of Pennsylvania, under Institutional Review Board Protocol 829908.

After initial routine records, patients of the TG were delivered a full coverage bonded rapid palatal expander extending from the maxillary primary or permanent canine to the maxillary first molar (Figure 1). The expanders had four predrilled holes in the palatal acrylic prior to cementation to measure the extent of expansion. With a digital caliper, the distance between the anterior and posterior holes were measured and averaged. Patients and parents were instructed to perform two turns per day (0.2 mm/turn) until adequate expansion was reached.

A CBCT was taken as part of the initial (T1 and T1') records of all 63 patients (35 for TG and 28 for CG) on an I-CAT machine (Imaging Sciences International, Hatfield, Pa). For the patients of the TG, immediate post-RME CBCT images (T2) were taken approximately 66 days after initial delivery. A smaller window of exposure was taken at post-RME, decreasing the time from 20 to 10 seconds, halving the amount of radiation exposure to the patients. Fixed comprehensive orthodontic treatment, including wires and brackets, were only placed after post-RME. A subsequent progress CBCT was taken for 25 patients of the TG (T3) 2.84 years after post-RME. Generally, T3 CBCTs were taken for the phase II records when the secondary teeth had erupted, and it was clear that the malocclusion was not fully corrected during the phase I treatment. Progress records as part of phased treatment is the standard of care for most orthodontists and is advocated by the American Board of Orthodontics. One of the reasons for the attrition at T3 was that some patients required no additional treatment after palatal expansion.

Table 1. Definition of Soft and Hard Tissue Landmarks^a

Landmark	ST or HT	Definition
Alar	ST	Most lateral point of the contour of each nostril
Alar base	ST	Most lateral point of the base insertion of each nostril
Nasion soft tissue	ST	Soft tissue point of the most anterior aspect of the frontonasal suture
Pronasale	ST	Most anterior point of the nose soft tissue down the midsagittal plane
Subnasale	ST	Intersection of the nasal septum and upper lip that meet in the midsagittal plane
Nasion	HT	Most anterior aspect of the frontonasal suture
ANS	HT	Anterior tip of the nasal spine
PNS	HT	Most posterior aspect of the palatine bone
Superior pyriform aperture	HT	Most superior point of the bony anterior limitation of the nasal skeletal down the midsagittal plane
Inferior pyriform aperture	HT	Most inferior point of the bony anterior limitation of the nasal skeletal down the midsagittal plane

^a Landmarks placed in soft tissue (ST) or hard tissue (HT).

The CG consisted of a total of 28 patients who had visited from November 2006 to July 2016 and presented for an orthodontic consultation, where the clinical examination revealed a malocclusion, records were taken, and following the review of records, treatment was not initiated for 1 to 2 years. Some patients were referred to an otolaryngologist for a consultation related to hypertrophy of the adenoids and tonsils, several sought second opinions and returned later, and others postponed treatment for financial reasons. The control patients had skeletal Class 1 or mild to moderate Class 2 attributed to mandibular retrognathia. Most patients had anterior arch perimeter deficiencies. Of 28 patients, 6 had posterior crossbite. Updated records were taken at T3', an average of 2.25 years after T1'.

All CBCTs were anonymized, oriented, and standardized in Dolphin Imaging (version 11.9; Dolphin Imaging & Management Solutions, Chatsworth, Calif). Orientation was completed in three planes of space from the frontal and lateral views. From the frontal, inferior rims of the orbit were placed symmetrically and parallel to the floor. The midsagittal line was placed at the soft tissue of nasion, through the pronasale, to the middle of the chin. From the lateral views, the Frankfort horizontal line (inferior border of the orbital rim to porion) was oriented parallel to the floor. The coronal line was placed just posterior to the condyle. The right lateral view was turned to be superimposed as closely

as possible to the left lateral view without a cant. Soft and hard nasal tissue points were chosen as landmarks that would give accurate measurements of any changes that occurred in the nasal complex post-RME. They are shown and defined in Tables 1 and 2 and Figure 2a,b,c. The landmarks were measured in millimeters on the CBCTs in three dimensions in Dolphin Imaging.

Descriptive statistics of the data, including means (M), standard deviations (SD), and 95% confidential intervals, were calculated for T1, T2, and T3 for the treated group and T1' and T3' for the control group. Differences between timepoints and within a treatment group were evaluated by paired *t*-tests or Wilcoxon signed-rank tests. Long-term comparisons between treatment and control groups were evaluated by independent-sample *t*-tests or Wilcoxon rank-sum tests. Nonparametric tests were used when the Shapiro-Wilk test was statistically significant at a *P* value < .05. *P* values for the 40 pairwise comparisons were adjusted using Hochberg's step-up Bonferroni method and considered statistically significant when < .05. SAS version 9.4 (SAS Institute Inc, Cary, N.C.) was used for these analyses. To assess the reliability of the numerical measurements of all variables, all samples from both groups were repeatedly measured after 2 weeks by the same investigator (P.S.) according to Houston.¹² The power was calculated for detecting group differences in T1 to T3 change in alar base width. Using group sample sizes of 25 and 28 and pooled SDs of 0.879,¹³ there was an estimated 98% power to detect a 1-mm difference between groups.

Table 2. Description of Measurements

Measurement	Landmark
Alar width	Alar width right–alar width left
Alar base width	Alar base width right–alar base width left
Nasal length	Pronasale–Subnasale
Nasal height	Nasion soft tissue–Subnasale
Nasion–ANS height	Nasion–ANS
ANS–PNS length	ANS–PNS
Pyriform height	Superior pyriform aperture–inferior pyriform aperture
Pyriform width	Par=right pyriform aperture. Pal= left pyriform aperture

RESULTS

Immediate Post-RME Nasal Soft and Hard Tissue Changes

Table 3 shows the descriptive statistics of the soft and hard tissue variables for TG. Table 4 depicts the comparison of T1 and T2 values of the soft and hard nasal tissue variables of the TG. At the alar base width,

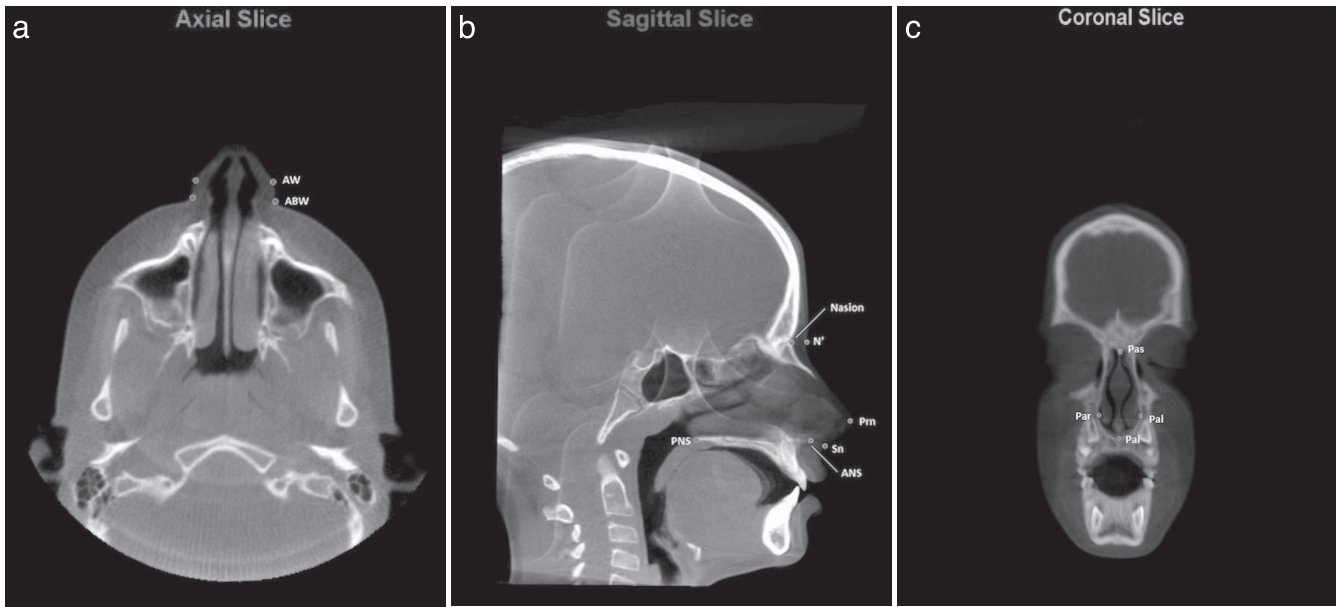


Figure 2. Landmarks in (a) axial, (b) sagittal, and (c) coronal slices. ABW, alar base width; ANS, anterior nasal spine; AW indicates alar width; N', nasion soft tissue; Pas, superior pyriform aperture; Pai, inferior pyriform aperture; Pal, left pyriform aperture; Par, right pyriform aperture; PNS, posterior nasal spine; Prn, pronasale; Sn, subnasale.

there was a mean increase of 1.60 mm ($P < .0001$). For alar width, nasal length, and nasal height, there was an increase of 0.65 mm, 0.14 mm and 0.34 mm, respectively ($P > .05$). With the skeletal tissues, there was an increase of pyriform height of 1.77 mm ($P < .0001$) and of pyriform width of 3.57 mm ($P < .0001$) when comparing T1 and T2 of the TG. For nasion–anterior nasal spine (ANS) height and ANS–posterior nasal spine (PNS) length, there were increases of 1.04 mm and 0.34 mm, respectively ($P > .05$).

Long-Term Post-RME Nasal Soft and Hard Tissue Changes

To evaluate the long-term effects of RME on the nasal tissue, T2 and T3 values of the TG were examined (Table 4). Of 35 at T1, there were 22 at T2 and 25 at T3. Alar base width and pyriform height measurements that significantly increased immediately post-RME remained stable during a span of 2.58 years

when compared with T3. There were increases in nasal height (+3.92 mm) and nasion–ANS height (+2.75 mm) and a decrease in pyriform width (–1.07 mm) ($P < .05$), possibly attributed to vertical growth and skeletal transverse relapse during the follow-up period.

Long-Term Comparison of TG vs CG

Table 5 shows the descriptive statistics of the soft and hard tissue variables for CG. Table 6 depicts the comparison of T1' and T3' values of the soft and hard nasal tissue variables of the CG. The control group showed significant differences regarding all measurements except pyriform width from T1' to T3', demonstrating the effect of growth (Table 6). The increase in pyriform width was 0.30 mm ($P = .056$). Table 7 illustrates the comparison of changes that occurred between T1 and T3 (TG) and T1' and T3' (CG). There was no significant difference in the nasal soft and hard

Table 3. Descriptive Statistics of the Soft and Hard Tissue Variables for TG^a

	T1	T2	T3
No. of sample	35	22	25
Alar width	31.03 ± 2.3	31.86 ± 2.5	33.76 ± 3.1
Alar base width	31.25 ± 2.2	32.89 ± 2.6	33.73 ± 2.9
Nasal length	14.93 ± 1.6	15.02 ± 1.8	16.32 ± 1.6
Nasal height	47.45 ± 3.6	47.90 ± 3.2	52.1 ± 3.6
Nasion–ANS height	44.65 ± 3.7	45.79 ± 4.0	49.06 ± 3.4
ANS–PNS length	48.47 ± 3.0	50.02 ± 2.8	48.50 ± 3.1
Pyriform height	36.64 ± 3.2	38.81 ± 3.5	40.37 ± 2.8
Pyriform width	22.38 ± 1.7	26.60 ± 1.6	24.74 ± 1.9

^a Values are mean ± SD. Measurements for parameters are shown in mm.

Table 4. Comparison of the Soft and Hard Tissue Variables for TG^a

Variables	T1 to T2 (n = 22)				T2 to T3 (n = 22)				T1 to T3 (n = 25)			
	Mean	SD	95% CI	P Value	Mean	SD	95% CI	P Value	Mean	SD	95% CI	P Value
Alar width	0.65	1.1	0.15 to 1.15	.166	1.08	1.7	0.02 to 2.13	.4138	2.17	2.0	1.33 to 3.02	.0005 ^{b*}
Alar base width	1.60	1.2	1.06 to 2.14	<.0001*	-0.21	0.7	-0.64 to 0.22	.7246	1.95	1.8	1.18 to 2.71	.0006 ^{b*}
Nasal length	0.14	1.5	-0.52 to 0.80	.7246	0.96	0.9	0.39 to 1.53	.0580	1.40	1.1	0.94 to 1.87	<.0001 ^{b*}
Nasal height	0.34	1.7	-0.44 to 1.12	.7246	3.92	1.4	2.99 to 4.85	<.0001*	4.39	1.9	3.62 to 5.16	<.0001 ^{c*}
Nasion-ANS height	1.04	1.7	0.29 to 1.80	.1195	2.75	1.8	1.51 to 3.98	.0107*	3.89	1.7	3.17 to 4.61	<.0001 ^{b*}
ANS-PNS length	0.34	1.2	-0.21 to 0.89	.7246 ^c	0.80	1.0	0.17 to 1.43	.1956	0.89	1.2	0.40 to 1.38	.0187 ^{b*}
Pyriform height	1.77	1.1	1.27 to 2.26	<.0001*	1.36	1.5	0.43 to 2.29	.1170	3.37	1.1	2.92 to 3.82	<.0001 ^{b*}
Pyriform width	3.57	1.2	3.04 to 4.10	<.0001*	-1.07	0.8	-1.60 to -0.53	.0192*	2.66	1.0	2.24 to 3.09	<.0001 ^{b*}

^a 95% CI indicates 95% confidence interval.

^b Paired *t*-test.

^c Wilcoxon rank-sum test.

* Statistically significant at Hochberg *P* values < .05.

tissue measurements except for pyriform height and pyriform width attributed to the RME (*P* < .05).

Intraexaminer Reliability

After all sample remeasurements by the same investigator (P.S.) at least 2 weeks apart, the intraclass correlation coefficients were calculated and ranged from 0.976 to 0.999, which assured the reproducibility of all measurements.

DISCUSSION

Based on the intimate relationship of the maxilla and the nasal cavity,¹⁴ there has been a growing interest for orthodontists to study the effect of expansion on the nasal anatomy and its impact on nasal physiology relative to the airway. In this study, the nasal soft and hard tissue changes after RME and the stability of these changes were examined. In addition, the use of CBCT scans was a more reliable way to diagnose and analyze the changes that occurred during expansion.

The short-term effect outcomes showed a 1.6 mm increase of the alar base width, which was closer to the underlying skeletal change. This was in agreement with previous studies showing less than 2 mm widening of the alar base.^{5,7,15} Studies that were reliant

on facial photographs and in-person clinical measurements reported various outcomes. Baysal et al.¹³ reported that alar base width was greater by approximately 1 mm in the RME treatment group after a 6-month retention period. Badreddine et al.¹¹ reported that, after RME, the alar base width, alar width, and height of the nasal soft tissues increased, whereas changes did not occur in the control group. Berger et al.⁵ reported a 2-mm increase in alar width, which was maintained 1 year after tooth-borne expansion. Johnson et al.⁷ reported that alar base width increased 1.98 mm in the treated group compared with the control group, but the difference might not be clinically significant on the impact to the whole face. On the contrary, Filho et al.⁶ showed no impact on nasal morphology using facial analysis, concluding that RME was incapable of influencing the nasal soft tissues. Torun reported no significant differences observed in soft tissue alar base, nostril width, nostril height, and nasolabial angle.¹⁶ Discrepancies in the extent of nasal soft tissue changes with RME may be attributable to different measurement methods, expansion protocols, age groups, and/or amounts of expansion. Another potential side effect after RME could be the development of a dorsal hump,^{5,17,18} which was not found in the patients in this study. The short-term nasal hard tissue change showed a significant increase in pyriform height and width, which was consistent with Badreddine et al.,^{10,11} Cordasco et al.,¹⁹ Palaisa et al.,²⁰ and Fastuca et al.²¹

For the long term, this study examined how RME affected patients' nasal growth in comparison with the nontreatment CG. The differences between T1 and T3 values in the TG (Δ T1-T3, average 2.84 years) was compared with the differences between T1' and T3' in the CG (Δ T1'-T3', average 2.25 years). There were no statistically significant differences across all measurements except for the nasal hard tissue pyriform height and pyriform width. This suggests that the significant soft tissue changes that occurred during expansion

Table 5. Descriptive Statistics of the Soft and Hard Tissue Variables for CG^a

	T1'	T3'
No. of sample	28	28
Alar width	30.80 ± 2.8	32.63 ± 3.1
Alar base width	31.44 ± 2.5	32.73 ± 2.9
Nasal length	14.90 ± 2.2	15.63 ± 2.1
Nasal height	46.81 ± 3.65	49.68 ± 4.4
Nasion-ANS height	44.25 ± 3.1	46.95 ± 3.9
ANS-PNS length	47.00 ± 3.0	48.09 ± 3.4
Pyriform height	36.38 ± 3.0	38.30 ± 3.3
Pyriform width	22.40 ± 2.0	22.70 ± 2.2

^a Values are mean ± SD. Measurements for parameter are shown in mm.

Table 6. Comparison of the Soft and Hard Tissue Variables for CG

	T1' to T3' (n = 28)			
	Mean	SD	95% CI	P Value
Alar width	1.83	1.5	1.26–2.40	<.0001 ^{a*}
Alar base width	1.29	1.4	0.76–1.81	.0006 ^{a*}
Nasal length	0.94	0.8	0.62–1.27	<.0001 ^{a*}
Nasal height	2.87	2.0	2.11–3.63	<.0001 ^{b*}
Nasion–ANS height	2.70	1.9	1.98–3.42	<.0001 ^{a*}
ANS–PNS length	1.10	1.3	0.61–1.58	<.0001 ^{b*}
Pyriform height	1.92	1.2	1.46–2.38	<.0001 ^{b*}
Pyriform width	0.30	0.5	0.11–0.49	.0558

^a Paired *t*-test.

^b Wilcoxon rank-sum test.

* Statistically significant at Hochberg *P* values < .05.

will, over time, regress to the mean of normal growth and development. In other words, the significant nasal soft tissue changes were immediate, and RME did not have a long-lasting impact on an adolescent's nasal soft tissue anatomy. This may be attributed to continuous growth of the nose and soft tissue elasticity. In the CG without RME (average age 8.81 ± 1.6), a significant increase over all nasal soft and hard tissue measurements except pyriform width ($P = .056$) was observed during the follow-up period, which was supported by other studies.^{22,23} The amount of change in pyriform height and pyriform width in TG showed a significant difference compared with CG, probably attributed to the RME effect. The long term RME effect on the nasal hard tissue is supported by previous studies. Long-term maintenance of a significant increase in nasal cavity width for 12 months²⁴ and 5 years²⁵ were reported in studies and a previous systematic review.²⁶

Immediate and long-term changes after RME in growing patients showed a significant increase in nasal cavity dimension and volume, reducing the resistance of nasal airflow.^{26–31} In this study, the RME group showed 3.57 ± 1.2 mm (immediate) and 2.66 ± 1.0 mm increases of pyriform width in 2.84 years, which were consistent with other studies.³² In a previous systemic review,³² RME increased nasal geometry and the increase in transverse nasal measurements ranged from 2 to 4 mm. RME increased the nasal cavity volume by about 0.10% of the pre-expansion volume.¹⁹ In addition, Izuka et al.³³ reported that RME positively impacted the quality of life of mouth-breathing patients with maxillary atresia by increasing the nasal cavity volume significantly and reducing subsequent respiratory symptoms. Interestingly, RME increased the mucociliary clearance in patients who had maxillary atresia, having positive effects on nasal physiology and increasing nasal cavity volume.¹⁴ On the other hand, Langer et al.³⁴ concluded that RME did not influence nasal resistance in their long-term evaluation. Itikawa et al.³⁵ and Matsumoto et al.³⁶ examined the effects of

Table 7. Long-Term Comparison of Changes of the Soft and Hard Tissue Variables Between T1 and T3 (TG) and T1' and T3' (CG)

	Changes, Mean \pm SD		
			P Value
	CG (n = 28)	TG (n = 25)	
Alar width	1.83 ± 1.5	2.17 ± 2.0	.7246 ^a
Alar base width	1.29 ± 1.4	1.95 ± 1.8	.7246 ^a
Nasal length	0.94 ± 0.8	1.40 ± 1.1	.7246 ^a
Nasal height	2.87 ± 2.0	4.39 ± 1.9	.0728 ^b
Nasion–ANS height	2.70 ± 1.9	3.89 ± 1.7	.2013 ^a
ANS–PNS length	1.10 ± 1.3	0.89 ± 1.2	.7246 ^b
Pyriform height	1.92 ± 1.2	3.37 ± 1.1	.0014 ^{a*}
Pyriform width	0.30 ± 0.5	2.66 ± 1.0	<.0001 ^{a*}

^a Independent-sample *t*-test.

^b Wilcoxon rank-sum test.

* Statistically significant at Hochberg *P* values < .05.

RME on nasal cavity dimensions of young children and observed a significant increase in nasal transverse bony width. However, no difference in nasal volume was detected as a result of mucosal compensation. Nasal bony expansion was followed by a mucosal compensation at a 3-month follow-up study using acoustic rhinometry and rhinomanometry.³⁷ In the current study, the change of nasal mucosal tissue could not be examined precisely using CBCT. Furthermore, the wide variability of the nasal mucosa, which is influenced by several factors such as nasal cycle, body posture, age, infection, exercise, medication, and ultradian rhythm, made it very difficult to compare.^{38–41} Therefore, the effect of RME on airway should be carefully interpreted, and RME cannot be indicated only for the improvement of nasal breathing because of the wide variability of individual responses.²⁸

CBCT is being widely used in orthodontic field for diagnosis and treatment planning, and it is considered as one of the most reliable methods for evaluating facial soft and hard tissue changes.^{9,42} It has several strengths including lower costs, lower radiation dose, shorter scanning time, and overall accuracy compared with conventional multislice computed tomography scans.^{43–46} In addition, CBCT allows the simultaneous evaluation of both skeletal and related soft tissue changes. Previously, studies used several different methods to evaluate nasal soft tissue changes, including photography,⁵ in-person clinical measurements,⁴⁷ three-dimensional facial scans,²¹ and tomography,¹⁶ showing the wide range of outcomes. For those reasons, CBCT was used to assess the changes in the nasal soft and hard tissue in this study.

This study had some limitations resulting from the retrospective design. There was attrition in T2 and T3. Not all treatment groups had T1, T2, and T3 records. Possible reasons for attrition were described in the Material and Methods section. In addition, the power analysis was based on soft tissue changes after RME

and not on the control group as the reference value for a control group was not found. However, the sample size was large enough to detect statistically significant findings.

CONCLUSIONS

- The results of this study suggest that, although RME produces some significant increase on the nasal soft tissue immediately after treatment, in the long-term this gain appears to be clinically similar to that observed in untreated control patients.
- The significant increase on the nasal hard tissue immediately after RME was maintained at long-term follow-up. There was a statistically significant difference in nasal hard tissue change between TG and CG at long-term follow-up attributed to the RME effect.
- A well-controlled future prospective study is recommended to overcome the current limitations from the retrospective study design.
- This is the first study to compare the long-term effect of RME on nasal tissue with a nontreatment CG using CBCT.

DISCLOSURE

This work was supported by the Orthodontic Faculty Development Fellowship Award from the American Association of Orthodontists Foundation (Dr Jeon).

ACKNOWLEDGMENTS

The authors thank Dr. Diana Carvel for assistance in the measurement of the scans.

REFERENCES

1. Haas AJ. The treatment of maxillary deficiency by opening the midpalatal suture. *Angle Orthod.* 1965;35:200–217.
2. Haas AJ. Palatal expansion: just the beginning of dentofacial orthopedics. *Am J Orthod.* 1970;57(3):219–255.
3. Haas AJ. Long-term posttreatment evaluation of rapid palatal expansion. *Angle Orthod.* 1980;50(3):189–217.
4. Lagravere MO, Major PW, Flores-Mir C. Long-term dental arch changes after rapid maxillary expansion treatment: a systematic review. *Angle Orthod.* 2005;75(2):155–161.
5. Berger JL, Pangrazio-Kulbersh V, Thomas BW, Kaczynski R. Photographic analysis of facial changes associated with maxillary expansion. *Am J Orthod Dentofacial Orthop.* 1999; 116(5):563–571.
6. Silva Filho OG, Lara TS, Ayub PV, Ohashi AS, Bertoz FA. Photographic assessment of nasal morphology following rapid maxillary expansion in children. *J Appl Oral Sci.* 2011; 19(5):535–543.
7. Johnson BM, McNamara JA, Bandeen RL, Baccetti T. Changes in soft tissue nasal widths associated with rapid maxillary expansion in prepubertal and postpubertal subjects. *Angle Orthod.* 2010;80(6):995–1001.
8. Santariello C, Nota A, Baldini A, Ballanti F, Cozza P. Analysis of rapid maxillary expansion effects on nasal soft tissues widths. *Minerva Stomatol.* 2014;63(9):307–314.
9. Kim KB AD, Araújo EA, Behrens RG. Evaluation of immediate soft tissue changes after rapid maxillary expansion. *Dental Press J Orthod.* 2012;17(5):157–164.
10. Badreddine FR, Fujita RR, Alves F, Cappellette M Jr. Rapid maxillary expansion in mouth breathers: a short-term skeletal and soft-tissue effect on the nose. *Braz J Otorhinolaryngol.* 2018;84(2):196–205.
11. Badreddine FR, Fujita RR, Cappellette M Jr. Short-term evaluation of tegumentary changes of the nose in oral breathers undergoing rapid maxillary expansion. *Braz J Otorhinolaryngol.* 2018;84(4):478–485.
12. Houston WJ. The analysis of errors in orthodontic measurements. *Am J Orthod.* 1983;83(5):382–390.
13. Baysal A, Ozturk MA, Sahan AO, Uysal T. Facial soft-tissue changes after rapid maxillary expansion analyzed with 3-dimensional stereophotogrammetry: a randomized, controlled clinical trial. *Angle Orthod.* 2016;86(6):934–942.
14. Babacan H, Doruk C, Uysal IO, Yuce S. Effects of rapid maxillary expansion on nasal mucociliary clearance. *Angle Orthod.* 2016;86(2):250–254.
15. Altindis S, Toy E, Basciftci FA. Effects of different rapid maxillary expansion appliances on facial soft tissues using three-dimensional imaging. *Angle Orthod.* 2016;86(4):590–598.
16. Torun GS. Soft tissue changes in the orofacial region after rapid maxillary expansion: a cone beam computed tomography study. *J Orofac Orthop.* 2017;78(3):193–200.
17. Haas AJ. Rapid expansion of the maxillary dental arch and nasal cavity by opening the midpalatal suture. *Angle Orthod* 1961;31(2):73–90.
18. Kilic N, Kiki A, Oktay H, Erdem A. Effects of rapid maxillary expansion on Holdaway soft tissue measurements. *Eur J Orthod.* 2008;30(3):239–243.
19. Cordasco G, Nucera R, Fastuca R, et al. Effects of orthopedic maxillary expansion on nasal cavity size in growing subjects: a low dose computer tomography clinical trial. *Int J Pediatr Otorhinolaryngol.* 2012;76(11):1547–1551.
20. Palaisa J, Ngan P, Martin C, Razmus T. Use of conventional tomography to evaluate changes in the nasal cavity with rapid palatal expansion. *Am J Orthod Dentofacial Orthop.* 2007;132(4):458–466.
21. Fastuca R, Campobasso A, Zecca PA, Caprioglio A. 3D facial soft tissue changes after rapid maxillary expansion on primary teeth: a randomized clinical trial. *Orthod Craniofac Res.* 2018;21(3):1–6.
22. Burke PH, Hughes-Lawson CA. Stereophotogrammetric study of growth and development of the nose. *Am J Orthod Dentofacial Orthop.* 1989;96(2):144–151.
23. Ferrario VF, Sforza C, Poggio CE, Schmitz JH. Three-dimensional study of growth and development of the nose. *Cleft Palate Craniofac J.* 1997;34(4):309–317.
24. Compadretti GC, Tasca I, Bonetti GA. Nasal airway measurements in children treated by rapid maxillary expansion. *Am J Rhinol.* 2006;20(4):385–393.
25. Baccetti T, Franchi L, Cameron CG, McNamara JA Jr. Treatment timing for rapid maxillary expansion. *Angle Orthod.* 2001;71(5):343–350.
26. Lagravere MO, Major PW, Flores-Mir C. Long-term skeletal changes with rapid maxillary expansion: a systematic review. *Angle Orthod.* 2005;75(6):1046–1052.

27. Lagravere MO, Heo G, Major PW, Flores-Mir C. Meta-analysis of immediate changes with rapid maxillary expansion treatment. *J Am Dent Assoc.* 2006;137(1):44–53.
28. Baratieri C, Alves M Jr, de Souza MM, de Souza Araujo MT, Maia LC. Does rapid maxillary expansion have long-term effects on airway dimensions and breathing? *Am J Orthod Dentofacial Orthop.* 2011;140(2):146–156.
29. Hershey HG, Stewart BL, Warren DW. Changes in nasal airway resistance associated with rapid maxillary expansion. *Am J Orthod.* 1976;69(3):274–284.
30. Basciftci FA, Mutlu N, Karaman AI, Malkoc S, Kucukkolbasi H. Does the timing and method of rapid maxillary expansion have an effect on the changes in nasal dimensions? *Angle Orthod.* 2002;72(2):118–123.
31. Wertz RA. Skeletal and dental changes accompanying rapid midpalatal suture opening. *Am J Orthod.* 1970;58(1):41–66.
32. Alyessary AS, Othman SA, Yap AUJ, Radzi Z, Rahman MT. Effects of non-surgical rapid maxillary expansion on nasal structures and breathing: a systematic review. *Int Orthod.* 2019;17(1):12–19.
33. Izuka EN, Feres MF, Pignatari SS. Immediate impact of rapid maxillary expansion on upper airway dimensions and on the quality of life of mouth breathers. *Dental Press J Orthod.* 2015;20(3):43–49.
34. Langer MR, Itikawa CE, Valera FC, Matsumoto MA, Anselmo-Lima WT. Does rapid maxillary expansion increase nasopharyngeal space and improve nasal airway resistance? *Int J Pediatr Otorhinolaryngol.* 2011;75(1):122–125.
35. Itikawa CE, Valera FC, Matsumoto MAN, Lima WTA. Effect of rapid maxillary expansion on the dimension of the nasal cavity and on facial morphology assessed by acoustic rhinometry and rhinomanometry. *Dental Press J Orthod.* 2012;17(4):129–133.
36. Matsumoto MA, Itikawa CE, Valera FC, Faria G, Anselmo-Lima WT. Long-term effects of rapid maxillary expansion on nasal area and nasal airway resistance. *Am J Rhinol Allergy.* 2010;24(2):161–165.
37. Enoki C, Valera FC, Lessa FC, Elias AM, Matsumoto MA, Anselmo-Lima WT. Effect of rapid maxillary expansion on the dimension of the nasal cavity and on nasal air resistance. *Int J Pediatr Otorhinolaryngol.* 2006;70(7):1225–1230.
38. Bazargani F, Magnuson A, Ludwig B. Effects on nasal airflow and resistance using two different RME appliances: a randomized controlled trial. *Eur J Orthod.* 2018;40(3):281–284.
39. Kahana-Zweig R, Geva-Sagiv M, Weissbrod A, Secundo L, Soroker N, Sobel N. Measuring and characterizing the human nasal cycle. *PLoS One.* 2016;11(10):e0162918.
40. Hasegawa M, Kern EB. The human nasal cycle. *Mayo Clin Proc.* 1977;52(1):28–34.
41. Gungor A, Moinuddin R, Nelson RH, Corey JP. Detection of the nasal cycle with acoustic rhinometry: techniques and applications. *Otolaryngol Head Neck Surg.* 1999;120(2):238–247.
42. Lee KC, Perrino M. Alar width changes due to surgically-assisted rapid palatal expansion: a meta-analysis. *J Orthod Sci.* 2017;6(4):115–122.
43. Palomo JM, Rao PS, Hans MG. Influence of CBCT exposure conditions on radiation dose. *Oral Surg Oral Med Oral Pathol Oral Radiol Endod.* 2008;105(6):773–782.
44. El H, Palomo JM. Measuring the airway in 3 dimensions: a reliability and accuracy study. *Am J Orthod Dentofacial Orthop.* 2010;137(4 suppl):S50 e51–e59; discussion S50–S52.
45. Kwong JC, Palomo JM, Landers MA, Figueroa A, Hans MG. Image quality produced by different cone-beam computed tomography settings. *Am J Orthod Dentofacial Orthop.* 2008;133(2):317–327.
46. Osorio F, Perilla M, Doyle DJ, Palomo JM. Cone beam computed tomography: an innovative tool for airway assessment. *Anesth Analg.* 2008;106(6):1803–1807.
47. de Assis DS, Duarte MA, Goncales ES. Clinical evaluation of the alar base width of patients submitted to surgically assisted maxillary expansion. *Oral Maxillofac Surg.* 2010;14(3):149–154.